AD-A052 710 DAVID W TAYLOR NAVAL SHIP RESEARCH AND DEVELOPMENT CE--ETC F/G 20/4
A REVIEW OF RESISTANCE PREDICTION AND DESIGN METHODS FOR STRUT---ETC(U)
MAR 78 P LAFRANCE

UNCLASSIFIED SPD-789-01 NL

1 OF 2
AD
A052710

DAVID W. TAYLOR NAVAL SHIP RESEARCH AND DEVELOPMENT CENTER

Bethesda, Md. 20084

12

A REVIEW OF RESISTANCE PREDICTION AND DESIGN METHODS FOR STRUT-POD INLETS

by

Pierre Lafrance

APPROVED FOR PUBLIC RELEASE: DISTRIBUTION UNLIMITED

SHIP PERFORMANCE DEPARTMENT

DEPARTMENTAL REPORT

March 1978

SPD-789-01

MAJOR DTNSRDC ORGANIZATIONAL COMPONENTS

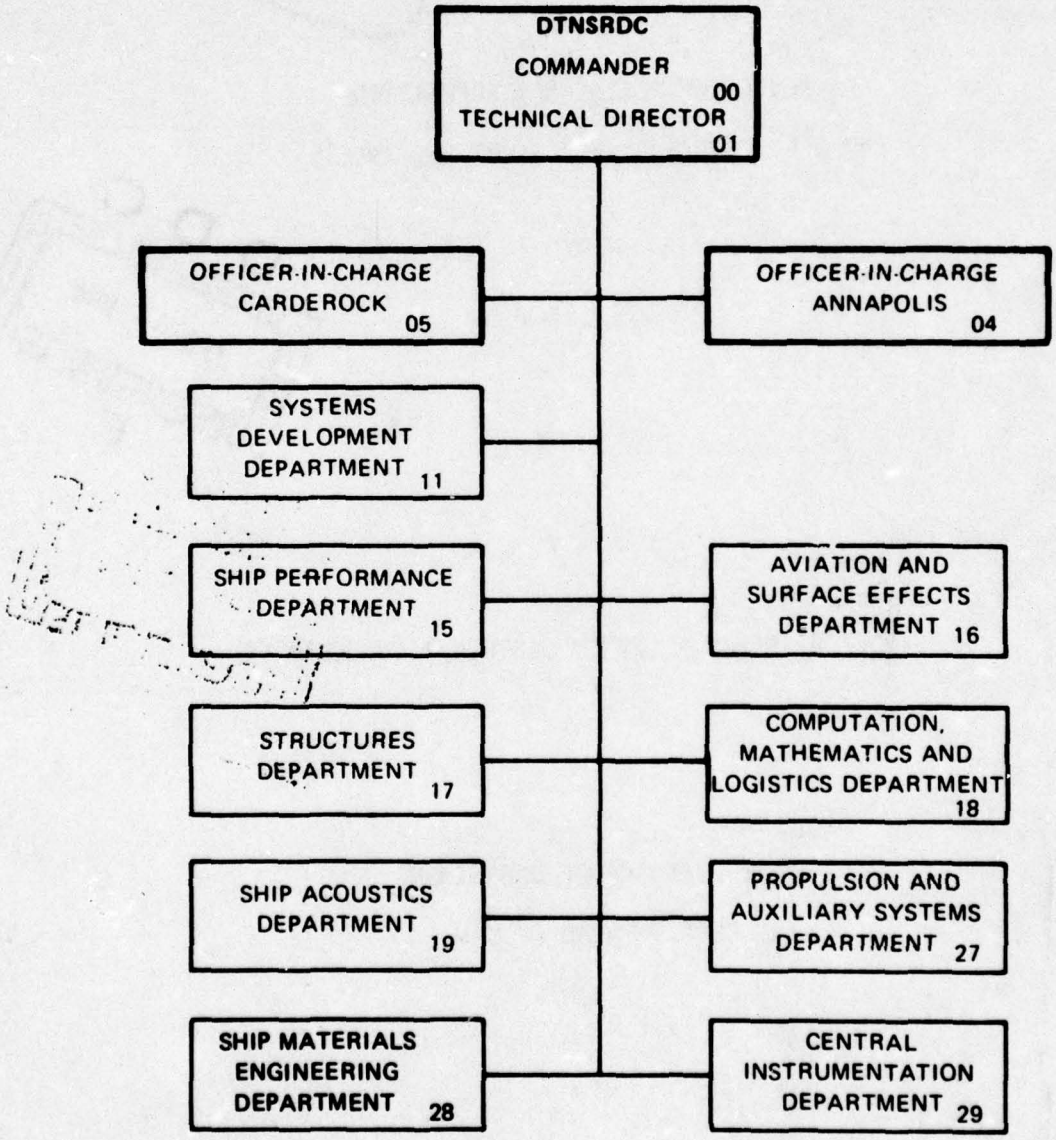

UNCLASSIFIED

SECURITY CLASSIFICATION OF THIS PAGE (When Data Entered)

REPORT DOCUMENTATION PAGE

READ INSTRUCTIONS BEFORE COMPLETING FORM

1. REPORT NUMBER: SPD-789-01
2. GOVT ACCESSION NO.
3. RECIPIENT'S CATALOG NUMBER

4. TITLE (and Subtitle): A REVIEW OF RESISTANCE PREDICTION AND DESIGN METHODS FOR STRUT-POD INLETS
5. TYPE OF REPORT & PERIOD COVERED
6. PERFORMING ORG. REPORT NUMBER

7. AUTHOR(s): Pierre Lafrance
8. CONTRACT OR GRANT NUMBER(s): F43432

9. PERFORMING ORGANIZATION NAME AND ADDRESS: David W. Taylor Naval Ship R&D Center, Bethesda, MD 20084
10. PROGRAM ELEMENT, PROJECT, TASK AREA & WORK UNIT NUMBERS: Element 62543N, Task 12501, Task Area SF 43432301

11. CONTROLLING OFFICE NAME AND ADDRESS: Naval Sea Systems Command, Washington, D.C. 20350
12. REPORT DATE: March 1978
13. NUMBER OF PAGES: 108

14. MONITORING AGENCY NAME & ADDRESS (if different from Controlling Office): 117p.
15. SECURITY CLASS. (of this report): UNCLASSIFIED
15a. DECLASSIFICATION/DOWNGRADING SCHEDULE

16. DISTRIBUTION STATEMENT (of this Report)

APPROVED FOR PUBLIC RELEASE: DISTRIBUTION UNLIMITED

17. DISTRIBUTION STATEMENT (of the abstract entered in Block 20, if different from Report)

18. SUPPLEMENTARY NOTES

19. KEY WORDS (Continue on reverse side if necessary and identify by block number)

Waterjet, Strut-Pod, Inlet, Drag

20. ABSTRACT (Continue on reverse side if necessary and identify by block number)

Two aspects of strut-pod waterjet inlet technology are reviewed in this report. First, hydrodynamic aspects of inlet design are discussed and various design methods are presented. Second, the subject of drag prediction is briefly reviewed, state-of-the-art drag prediction methods are presented and their predictive accuracy is compared.

For superhigh speed applications (≥100 kts), a variable area concept with auxiliary strut vanes is recommended. For speeds below 50 kts, fixed

DD FORM 1 JAN 73 1473 EDITION OF 1 NOV 65 IS OBSOLETE S/N 0102-LF-014-6601

approximately

20. Continued

area inlets should suffice. Intermediate speed applications should be investigated on a case-by-case basis to determine if auxiliary vanes are desirable.

TABLE OF CONTENTS

LIST OF FIGURES

LIST OF TABLES

NOMENCLATURE

Symbol	Meaning	Dimension
A, A_i	Area, inlet area	L^2
c	Chord	L
C_D	Drag coefficient	-
C_f	Skin friction coefficient	-
C_p	Pressure coefficient	-
C_R	Residuary drag coefficient	-
d	Inlet diameter	L
D	Drag	MLT^{-2}
f	Straight pipe friction factor	-
F	Fanning friction factor	-
g	Gravitational acceleration	LT^{-2}
H	Boundary layer shape factor	-
H_L	Inlet head losses	L
h_s	Submergence depth	L
IVR	Inlet velocity ratio = V_i/V_o	-
K_i	Inlet loss coefficient	-
K_T	Total head loss coefficient	-
ℓ, L	Body length	L
N_R	Reynolds number	-
p_o, p_i	Pressure, inlet pressure	$ML^{-1}T^{-2}$
q	Dynamic pressure	$ML^{-1}T^{-2}$
q_∞	Free stream stagnation pressure	$ML^{-1}T^{-2}$
Q	Volumetric flowrate	L^3T^{-1}
r	Radial coordinate	L

Symbol	Meaning	Dimension
r_o	Radial coordinate of a point on body	L
t	Strut thickness	L
u_∞	Free stream velocity	LT^{-1}
u	Streamwise velocity	LT^{-1}
u_s	Surface velocity	LT^{-1}
v	Fluid speed	LT^{-1}
V_i	Inlet flow speed	LT^{-1}
V_j	Jet flow speed	LT^{-1}
V_o	Craft speed	LT^{-1}
x	Coordinate measured along body	L
y	Coordinate measured normal to body	L
α	Diffuser expansion half-angle	-
δ	Boundary layer thickness, where $u = 0.99\, u_\infty$	L
δ^*	Boundary layer displacement thickness = $\int_0^\infty (1 - \frac{u}{u_\infty})\frac{r}{r_o}\, dy$	L
θ, δ_θ	Boundary layer momentum thickness = $\int_0^\infty (1 - \frac{u}{u_\infty})\, \frac{u}{u_\infty}\, \frac{r}{r_o}\, dy$	L
η	Jet propulsive efficiency	-
ν	Fluid kinematic viscosity	L^2T^{-1}
ρ	Fluid density	ML^{-3}
σ	Cavitation number	-
ψ_s	Stagnation streamline	-

ABSTRACT

Two aspects of strut-pod waterjet inlet technology are reviewed in this report. First, hydrodynamic aspects of inlet design are discussed and various design methods are presented. Second, the subject of drag prediction is briefly reviewed, state-of-the-art drag prediction methods are presented and their predictive accuracy is compared.

For superhigh speed applications (≃ 100 kts), a variable area concept with auxiliary strut vanes is recommended. For speeds below 50 kts, fixed area inlets should suffice. Intermediate speed applications should be investigated on a case-by-case basis to determine if auxiliary vanes are desirable.

ADMINISTRATIVE INFORMATION

This project was sponsored by the Naval Sea Systems Command, Code 0331G, Task Area SF 43432301, Task 12501, Element 62543N.

INTRODUCTION

The design of inlets for waterjet-propelled craft shares a common feature with many other technology-intensive fields. It has reached the stage where most of the knowledge is scattered throughout a multitute of reports and technical papers from which a comprehensive view is difficult to obtain. It would appear that a compendium of inlet design methodology would be a timely contribution. However, the very speed with which developments are being made in engineering and scientific fields touching on that area precludesthe present realization of a work of enduring value. However, it is safe to state that the major problems in inlet design, at least in the hydrodynamic sense, have been identified, and

that a document describing these problems and the various existing solutions is not out of place.

This report represents a step toward the establishment of an inlet design philosophy at DTNSRDC. Although a detailed mathematical description of the hydrodynamics pertaining to inlet design falls outside the scope of this report, the underlying physical principles are presented to give the reader an appreciation for the design methods which have evolved over the years.

The actual design of ram inlets is reviewed through the descriptions of several existing design methods. These descriptions are necessarily brief and are meant to be a short review of the state-of-the-art. The reader is led to the references for additional details.

Since the purpose of this study was to gather from the literature examples representative of the current state-of-the-art, some passages in this report have been transcribed almost verbatim from existing reports and papers. These are not identified as direct quotations, but the sources are all listed in the references.

DESIGN PHILOSOPHY

In principle, there is little difference between conventional propellers and waterjet propulsion systems. With the former, the actuator is situated in the external stream while with the latter, the stream is directed within the hull, where it is allowed to interact with the

actuator and is subsequently discharged astern in the form of a high speed jet. There, the shape of the ducting dictates the flow speed and hence can be advantageously used to increase static pressure at the pump, thereby retarding cavitation. Waterjet inlet design centers around the determination of ducting configurations which will adequately supply the pump while maintaining hydrodynamic losses at a minimum. The principal difference, from a designer's point of view, between propellers and waterjet propulsion is that with waterjets, one has more control over the incoming flow.

A waterjet propulsion system is built around a central element - the pump - whose purpose is to increase the momentum of the water stream flowing through it, resulting in a net thrust on the craft. A concise and lucid description of waterjet pumps was given by Wislicenus[1]*. Figure 1 schematically shows a typical waterjet propulsion unit utilizing a pod inlet. Pump performance is limited by cavitation. To operate properly, the pump must be supplied with the required flowrate at pressures which will not result in cavitation. In addition, the flow at the pump face should be uniform. Providing the pump with these flow conditions is accomplished by the conduit upstream of the pump face. This structure typically comprises the inlet, diffuser, turning vanes, ducting, and may include devices for varying the effective inlet area, such as auxiliary inlets or a retractable centerbody. These elements are housed within the nacelle and strut, as shown in Figure 2, and shall be referred to by the generic names of "waterjet inlet," or simply "inlet."

---

*List of references given on page 104

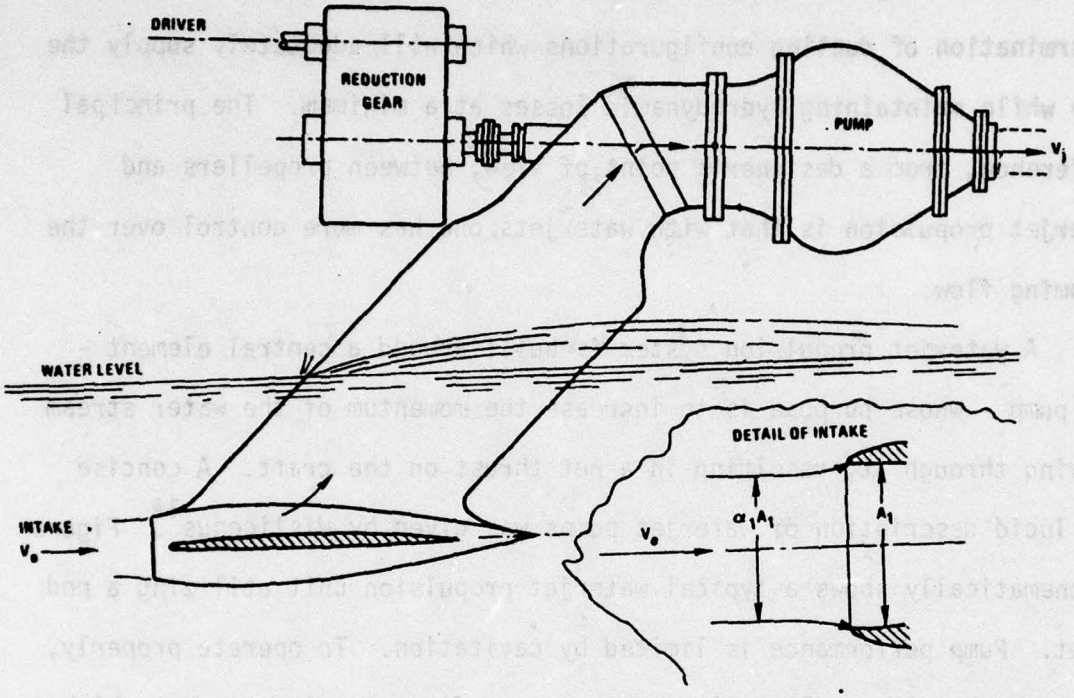

Figure 1 - Waterjet Propulsion Unit

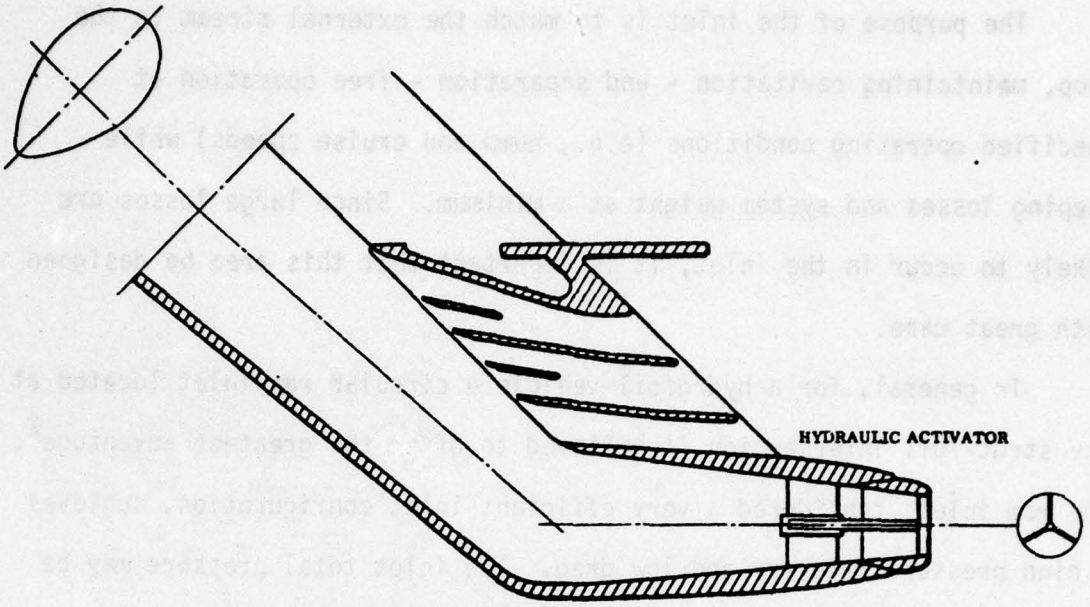

Pod With Slat and Auxiliary Doors (Expanded Duct Area)

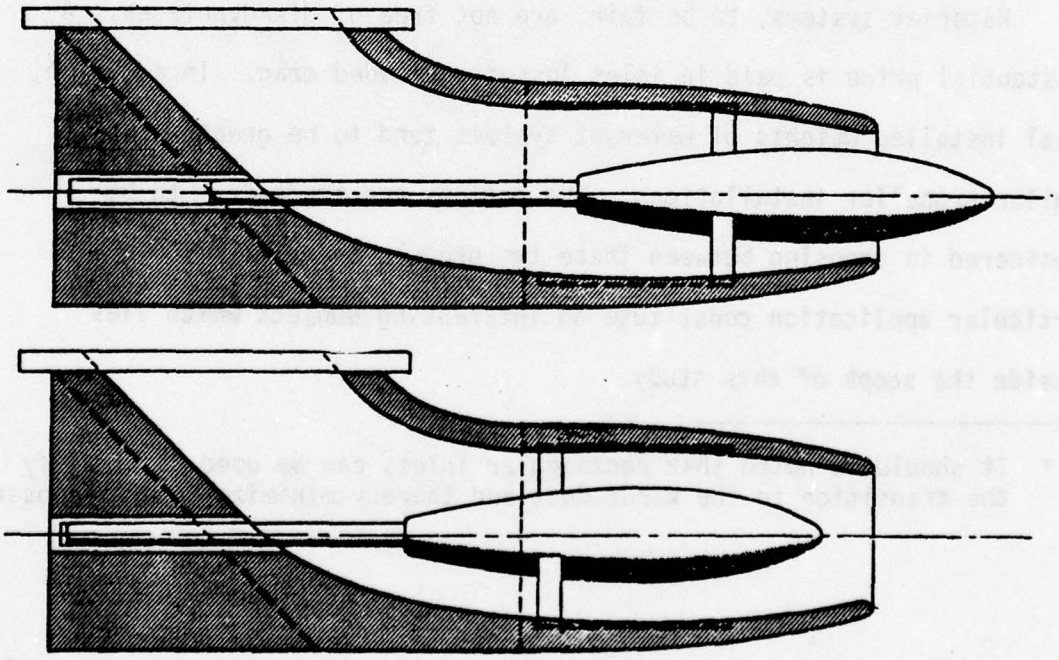

Figure 2 - Plug Inlet

The purpose of the inlet is to match the external stream to the pump, maintaining cavitation - and separation - free operation at specified operating conditions (e.g., hump and cruise speeds) while keeping losses and system weight at a minimum. Since large losses are likely to occur in the inlet, it is important that this area be designed with great care.

In general, for a hydrofoil vehicle a circular ram inlet located at the strut-foil intersection is believed to offer the greatest advantage[2]. The ram inlet, considered a very efficient inlet configuration, achieves a high pressure recovery and low drag. The inlet total pressure may be in the order of 98% of free stream total pressure. In addition, the circular inlet and nacelle offer a minimum circumference and therefore the least surface drag for a given inlet area. *

Waterjet systems, to be fair, are not free of disadvantages. A substantial price is paid in inlet losses and added drag. In addition, total installed weights of waterjet systems tend to be greater than similar propeller installations. The options and tradeoffs to be considered in choosing between these two propulsion systems for a particular application constitute an interesting subject which lies outside the scope of this study.

---

* It should be noted that rectangular inlets can be used to simplify the transition to the strut duct and thereby minimize internal losses

PRACTICAL DESIGN CONSIDERATIONS

The design of a waterjet inlet presents a formidable hydrodynamics problem touching upon several areas where fundamental understanding is still lacking. In response to the immediate need for practical designs, several approximations have been developed to simplify otherwise cumbersome procedures as well as to empirically compensate for a lack of understanding in certain areas. The art of inlet design has evolved around these approximations and the ways in which they are incorporated into various design programs.

In this section, we shall examine the various components of waterjet pod inlets and discuss the factors which must be considered in their design. This discussion will be maintained on a very general level, the details to be saved for the following section, where we discuss particular design procedures.

For waterjet inlets, and especially for inlets housed in a pod, we must distinguish between two separate flow regions. By internal flow, we shall denote the flow bounded by the centerline and the stagnation streamline ψ_s, as shown in Figure 3. The internal flow passes through the pump and is ejected as a high speed jet. The external flow is also bounded by ψ_s and passes over the external surface of the pod.

The basic criteria governing the design of external nacelle shape and strut are low drag and cavitation-free performance. This places limitations on total wetted surface area and on the maximum surface velocity. At very high craft speed (say 100 knots), it may become advantageous to ventilate parts of the strut-pod combination to reduce the wetted area.

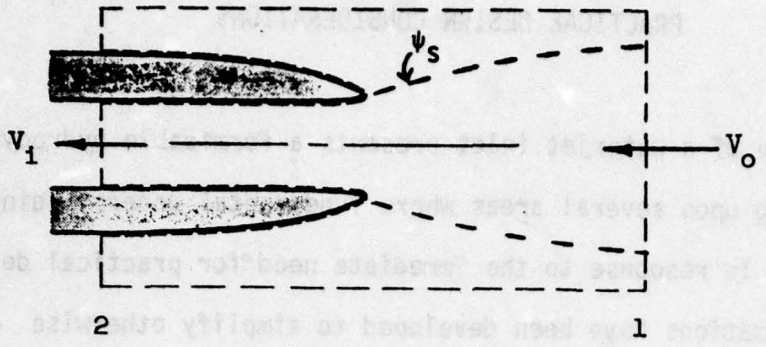

Figure 3 - Flow in the Vicinity of the Inlet

The inlet nacelle is assumed to be sufficiently removed from the hull that the latter's boundary layer has negligible effect on the former. The inlet's effect on hull pressure distribution can affect overall craft performance. Conversely, the hull, to a degree dependent upon strut length, influences the flow in the vicinity of the inlet. These effects are usually not considered in the design of strut-pod inlets.

The inlet lip is a very critical area of the inlet as it is extremely susceptible to cavitation and contributes significantly to drag. Figure 4 shows the flow in the vicinity of the lip for three values of the inlet velocity ratio. At low IVR's, the stagnation point is located on the interior side of the lip, forcing the external flow to turn around the lip, where it may experience large accelerations depending on the severity of the leading edge curvature. If sufficiently high flow speeds are reached, the pressure will drop to very low values

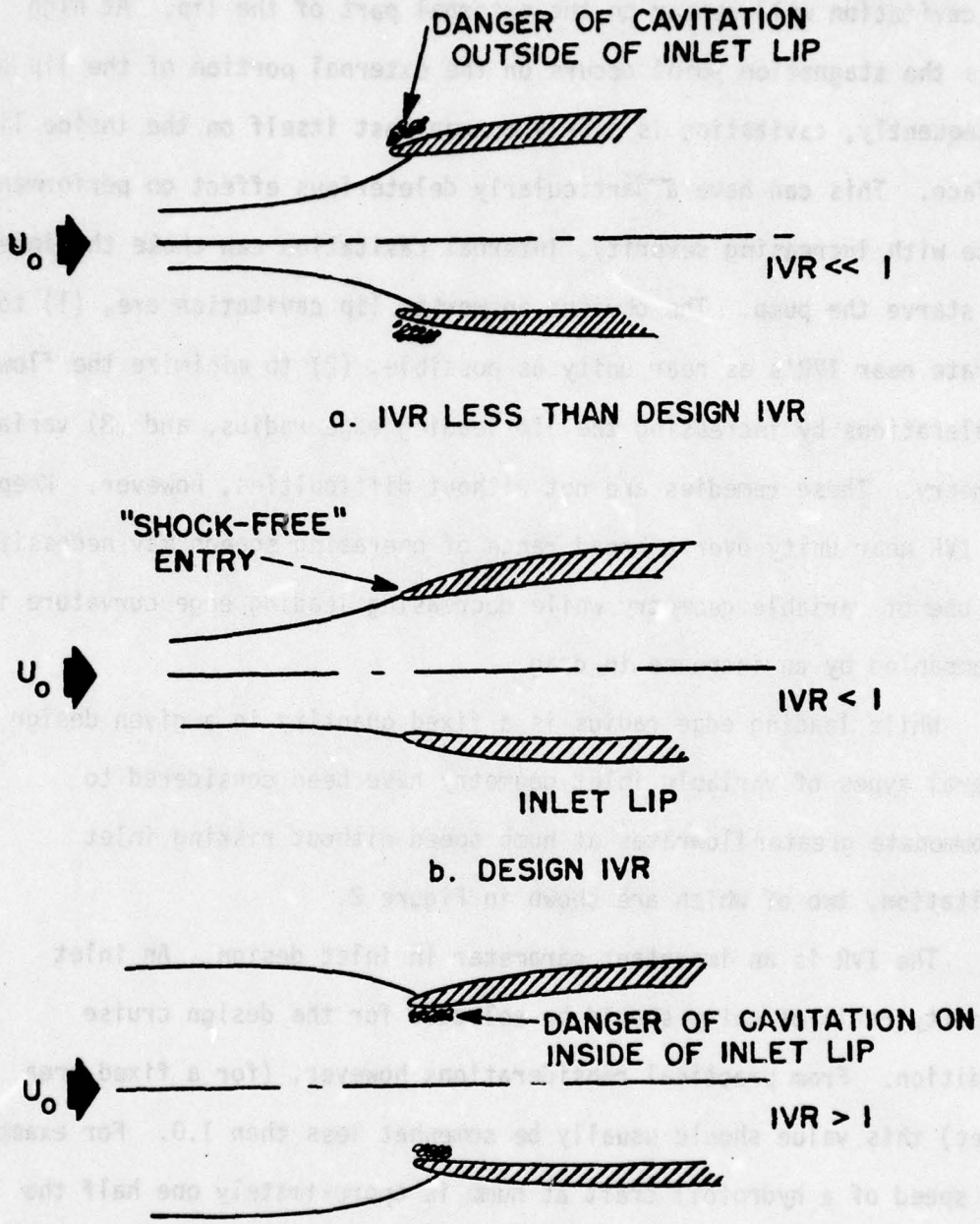

Figure 4 - Variation of Inflow Angle With Inlet Velocity Ratio (IVR) for a Typical Inlet

and cavitation will appear on the external part of the lip. At high IVR's the stagnation point occurs on the external portion of the lip and consequently, cavitation is likely to manifest itself on the inside lip surface. This can have a particularly deleterious effect on performance since with increasing severity, internal cavitation can choke the inlet and starve the pump. The obvious answers to lip cavitation are, (1) to operate near IVR's as near unity as possible, (2) to minimize the flow accelerations by increasing the lip leading edge radius, and (3) variable geometry. These remedies are not without difficulties, however. Keeping the IVR near unity over a broad range of operating speeds may necessitate the use of variable geometry while decreasing leading edge curvature is accompanied by an increase in drag.

While leading edge radius is a fixed quantity in a given design, several types of variable inlet geometry have been considered to accommodate greater flowrates at hump speed without risking inlet cavitation, two of which are shown in Figure 2.

The IVR is an important parameter in inlet design. An inlet velocity ratio of unity should be selected for the design cruise condition. From practical considerations however, (for a fixed area inlet) this value should usually be somewhat less than 1.0. For example, the speed of a hydrofoil craft at hump is approximately one half the cruise speed. For the same flowrate, unit IVR at cruise implies an IVR of 2 at hump, making cavitation on the internal lip very likely. Accordingly, the cruise IVR must be lowered as much as possible without incurring cavitation on the external lip. A viable solution to this

design problem is the use of auxiliary inlets or variable geometry to provide additional inlet area at hump with a reduction in inlet velocity.

Merging with the inlet lip and extending to the pump face is a duct section called the diffuser. For the purpose of analysis, the diffuser may be viewed as comprising three separate components, the inlet diffuser, the elbow, and the strut diffuser. The primary function of the diffuser is to supply the pump with the required flowrate while maintaining a minimum total pressure loss and flow distortion. Calculation of energy losses in such a complex system is well beyond present analytical capabilities and consequently, heavy use is made of empirical results. Diffuser performance is characteristically expressed in a "diffuser recovery factor" or pressure recovery, which is a measure of the recoverable ingested kinetic energy. The remaining energy fraction is irreversibly dissipated by such processes as skin friction or the generation of turbulent eddies following boundary layer separation, and contributes to inlet losses.

Diffuser contour shapes greatly affect performance and the bell shape contour has been shown to produce higher pressure recovery than equivalent straight wall or trumpet shaped diffusers.[3] The reason given for this is that the largest positive pressure gradient occurs where the boundary layer is still thin and able to overcome the retarding influence.

A study of prerotation of the flow just ahead of the pump to increase suction performance and ensure maximum takeoff thrust at low craft speeds has recently been experimentally investigated by Rockwell

International.[4] The purpose of this study was to investigate waterjet suction performance gains obtainable with a system of prerotator vanes.

A set of vanes, providing the requisite solid body prerotation, was designed, fabricated and tested with an existing scale-model Powerjet 20 inducer in a water tunnel. Analysis of test results indicate that introducing prerotation by means of an upstream vane system may likely create losses which will detract from gain in inducer suction performance obtained purely from flow prerotation. From pressure measurements, upstream pressure losses were found to be significant and possibly caused by vane blockage and flow separation. Further tests were recommended with a new vane geometry.

The problem of avoiding cavitation in the duct system is most critical at the hump and sub-hump speeds. From this point of view, the elbow between the inlet and the strut is the critical station in the system. The elbow between the inlet and the strut necessarily represents a radical change in both the flow direction and the shape of the passage. The flow is turned and the cross section of the duct changes from circular to a nearly two-dimensional form. No empirical information has been found on the performance of elbows that achieve both these functions simultaneously. A study[5] of available data on turning vane corners recommended thin, noncircular, arc vanes for turning the flow. A corner loss coefficient of 0.15 may be assumed and is believed to be attainable with a reasonably well designed elbow.

DESCRIPTION OF EXISTING DESIGN METHODS

To illustrate existing inlet design capability, this section reviews methods which have been used to generate waterjet inlet designs. This shall elucidate the use of material presented in the preceding sections and will hopefully show directions in which improvements can be made.

Sherman and Lincoln[3] presented a design method taking into account cavitation, internal and external losses. The authors state their intent to establish a guideline for the hydrodynamic design of ram inlets and to demonstrate a logical and consistent procedure for the accounting of external drag and internal system losses. Their paper does offer a very satisfying explanation of design philosophy, based on sound hydrodynamic principles. The occasional unfortunate abuses of syntax gives rise to unnecessary ambiguity.

Certain assumptions are made. First, it is assumed that an optimum pump flow rate has been established. Second, the external dimensions of the nacelle and strut are determined by cavitation criteria: the absence or presence of cavitation for the subcavitating and supercavitating cases, respectively. For a given craft, design speed, flowrate and IVR, the external nacelle and strut dimensions are selected according to cavitation requirements. This allows little latitude in designing the internal flow path. Therefore, the IVR is used as the independent variable to arrive at an optimum external and internal configuration. By

investigating a range of IVR's using a cavitation criterion, they are able to define a particular inlet system for each case, and to calculate internal and external performance for each design, thus determining the optimum IVR for the desired speed and flowrate.

The selection of the design IVR is shown to be very critical, making it necessary to adhere to the optimum value, or suffer high power losses. At 100 knot speeds, base vented inlets appear definitely superior with respect to drag over both subcavitating and supercavitating types.

The Douglas-Neumann program is used to compute the potential flow in and around the inlet. Considerable leakage is experienced, a common observation by users of that method. From these computations, the mass flowrate can be fixed and the surface pressure distribution determined.

For both high speed subcavitating and base vented inlets, the avoidance of cavitation is the prime design criterion. Cavitation will affect the contour of the nacelle and its thickness to chord ratio, and the shape of the inlet lip. Most important, cavitation will influence the selection of design IVR and the range of velocities through which the inlet is able to operate without geometry changes.

As a first step in the optimization process, values for the inlet drag coefficient and the inlet loss coefficient are assumed. A trade-off is made by varying the flowrate through the system at constant power and craft speed. The optimum system is selected by maximizing net thrust or payload capability (reducing system weight). These calculations are summarized in Figure 5.

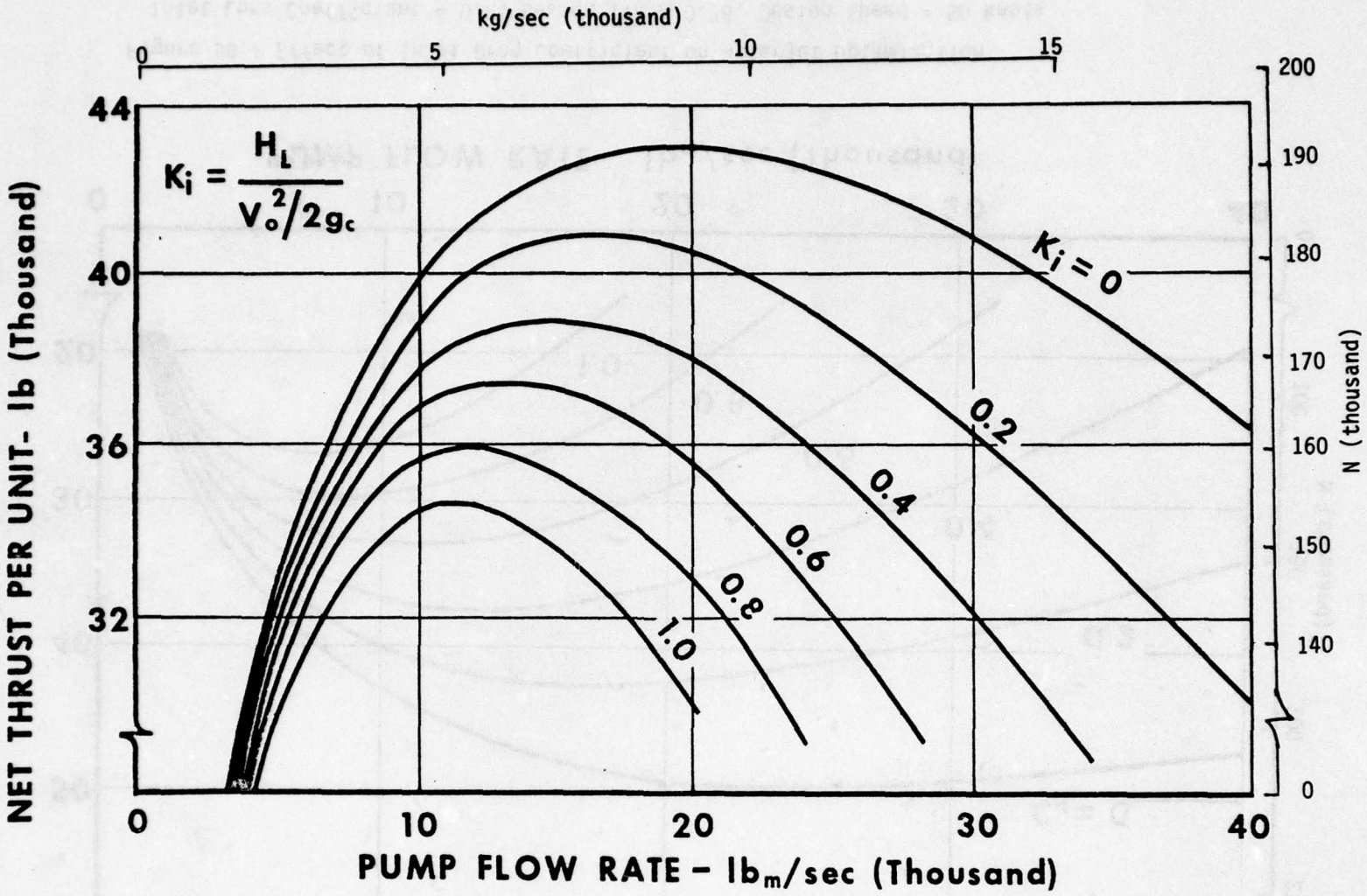

Figure 5A - Effect of Inlet Loss Coefficient on Waterjet Optimization
Inlet Drag Coefficient is 0.25, Design IVR = 0.75, Design Speed = 50 knots

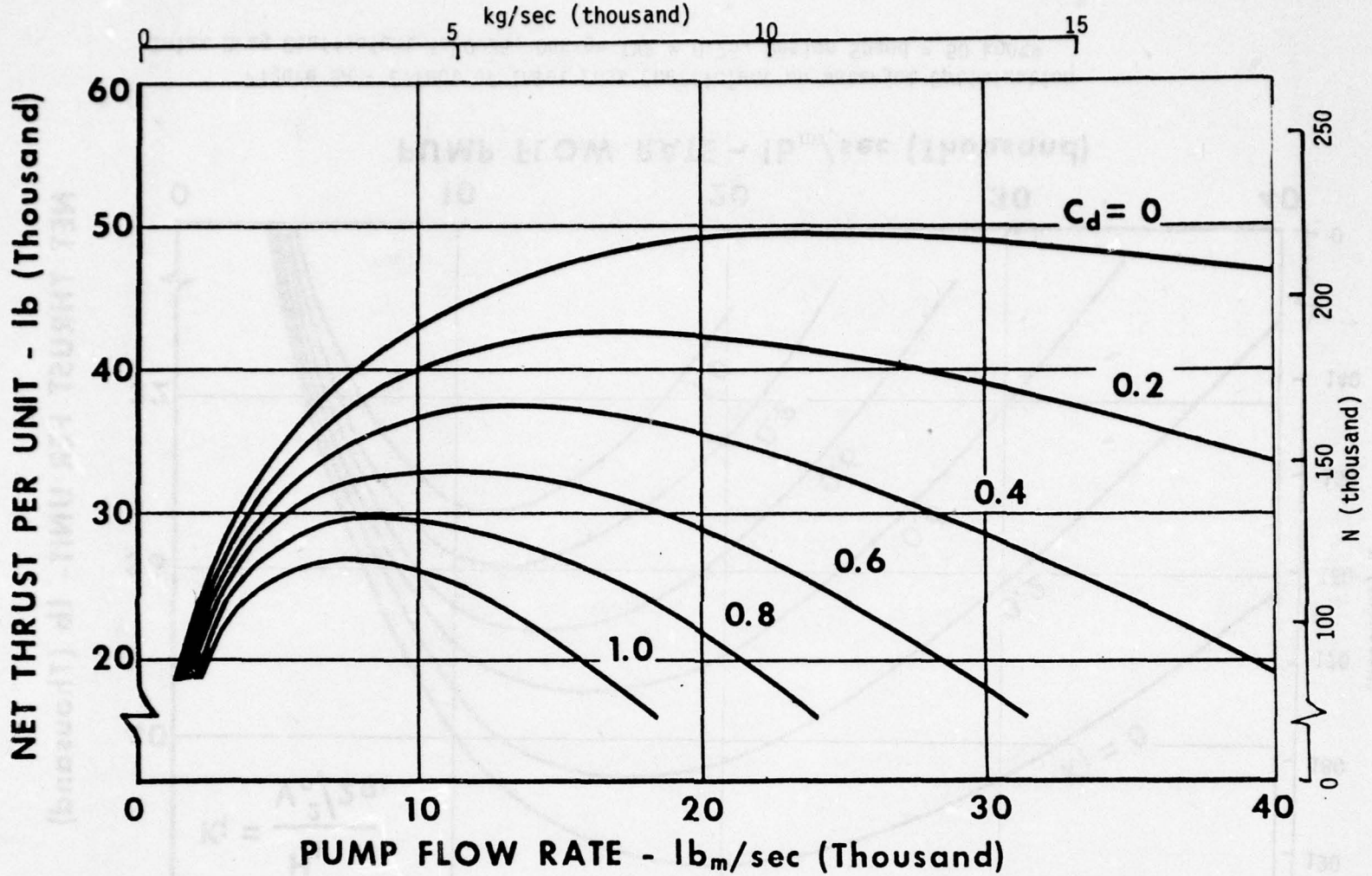

Figure 5B - Effect of Inlet Drag Coefficient on Waterjet Optimization
Inlet Loss Coefficient = 0.2, Design IVR ≈ 0.75, Design Speed = 50 knots

A computer program was developed which would take as its input the results of the Neumann program, and would calculate the inlet performance at each of the IVR's of interest.[3] This program gives total external drag coefficients, inlet lip cavitation characteristics, and internal system losses. The system was optimized by minimizing the combined sum of the external drag losses and the internal flow losses. From investigations with the Neumann program, it was ascertained that the most satisfactory inlet shape could be obtained with the NACA 16-series forebody thickness distribution generated on a camber line corresponding to a surface given by

$$\left(\frac{x}{x_o}\right)^2 + \left(\frac{y}{y_o}\right)^{2.4} = 1$$

where

$$\frac{x_o}{y_o} = \frac{1}{0.793\ \sigma_i^{5/8}}$$

The equation for the forebody of the NACA 16-series is

$$\frac{y}{t_m} = 0.9897\ \left(\frac{x}{c}\right)^{\frac{1}{2}} - 0.2392\ \left(\frac{x}{c}\right) - 0.0410\ \left(\frac{x}{c}\right)^2 - 0.5594\ \left(\frac{x}{c}\right)^3$$

Here, t_m and c can be used to scale the model.

The required thickness to chord ratio of a NACA 16-series section strut was calculated from the following formulas for a fully wetted strut:

$$\frac{t_m}{c_o} = \frac{-1 + \sqrt{1 + \sigma_i}}{1.15}$$

where σ_i is the incipient cavitation number,

and for a base vented strut:

$$\frac{t_m}{c} = \frac{-1 + \sqrt{1 + \sigma_i}}{1.10\ c/c_o}$$

The procedure for obtaining an "optimum inlet" from a given set of design conditions is, in the Sherman and Lincoln method, to run a matrix of cases, each case differing from the others in geometrical details. The cavitation characteristics of each case are then plotted. From these results, the proper forebody thickness distribution and lip thickness were selected.

Two specific ram inlet designs were initially contemplated, one for a 50 knot design speed and another for a 100 knot design speed. A range of design IVR's from 0.25 to 0.875 was considered. It was decided to concentrate on the 100 knot design because it was felt that more could be learned from this problem. This is because the 100 knot design requires more area for external diffusion (to keep the external maximum velocity within given limits), a larger variation in operational IVR's, and permitted less variation in local velocity above freestream. The operational IVR's for the two designs are given as a function of craft speed in Figure 6.

For the 100 knot design speed inlet, an optimum flowrate of 23,500 lb/sec (10660 kg/sec) was determined. Figure 7 shows the lip contours and Figure 8 shows the relationship between actual nacelle sizes. In the performance calculations, a 2 foot (0.61 m) strut was assumed.

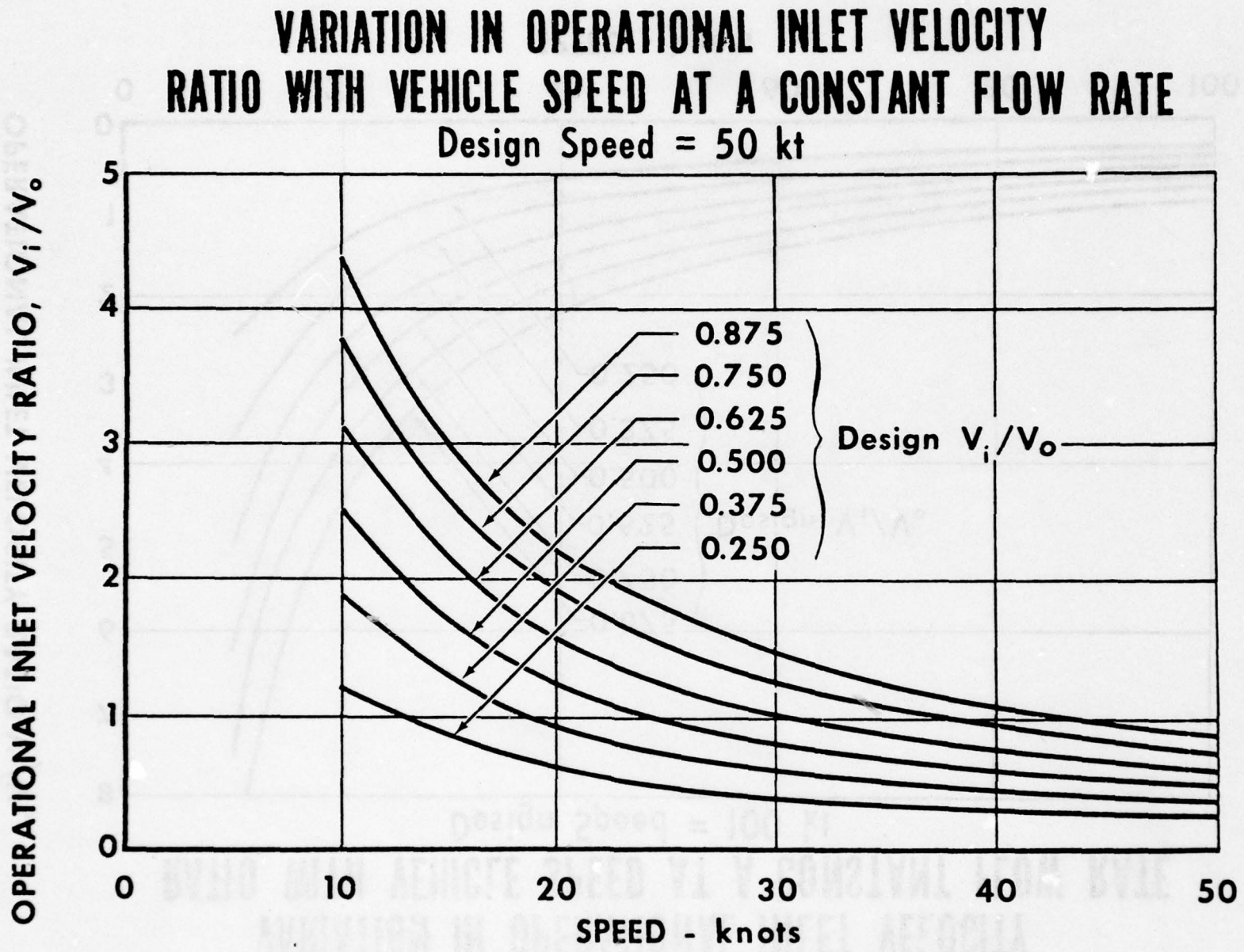
VARIATION IN OPERATIONAL INLET VELOCITY RATIO WITH VEHICLE SPEED AT A CONSTANT FLOW RATE
Design Speed = 50 kt
OPERATIONAL INLET VELOCITY RATIO, V_i/V_o
0
1
2
3
4
5
0
10
20
30
40
50
SPEED - knots
0.875
0.750
0.625
0.500
0.375
0.250
Design V_i/V_o

Figure 6A

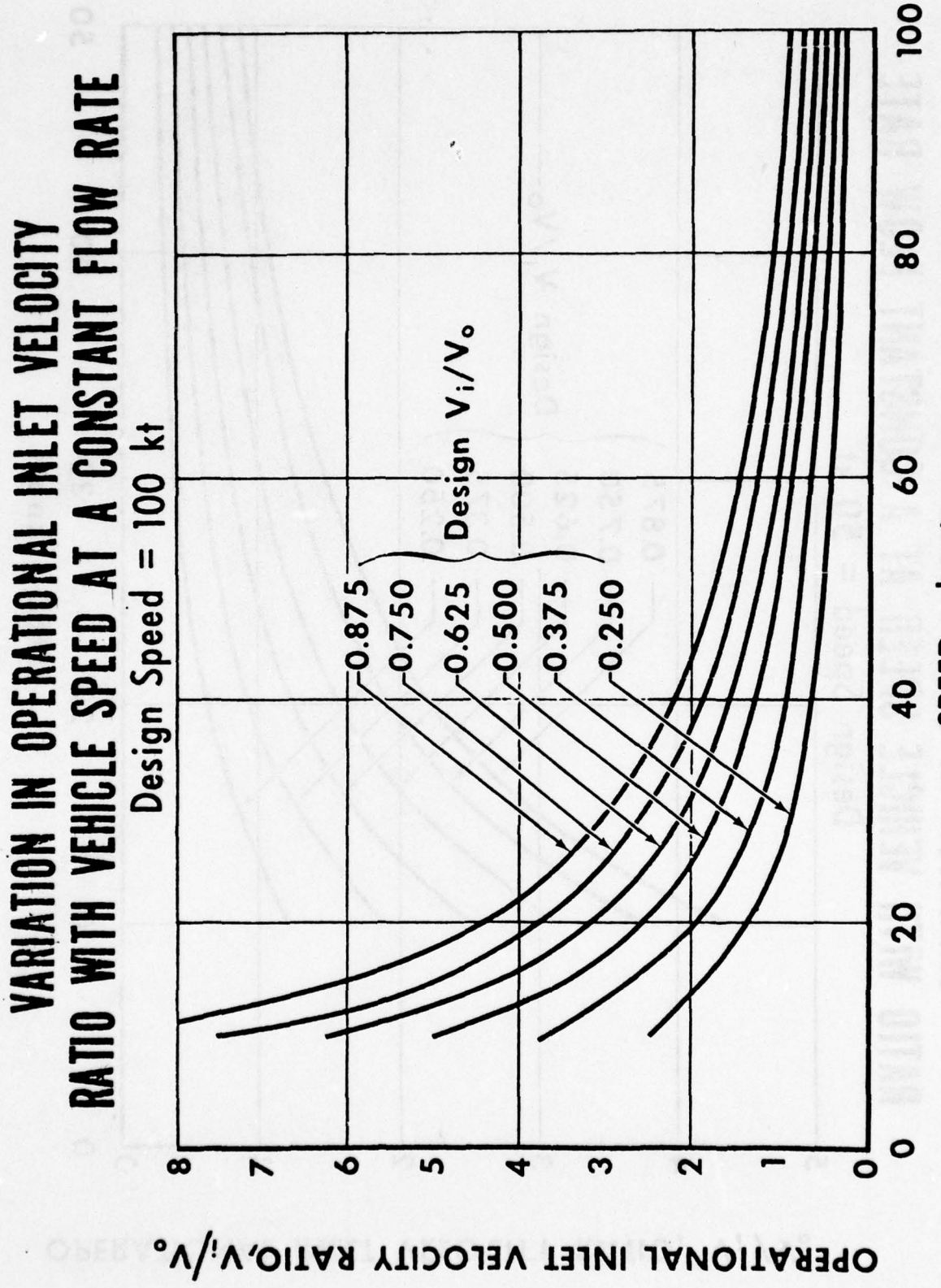
VARIATION IN OPERATIONAL INLET VELOCITY
RATIO WITH VEHICLE SPEED AT A CONSTANT FLOW RATE
Design Speed = 100 kt
OPERATIONAL INLET VELOCITY RATIO, V_i/V_o
SPEED - knots
Design V_i/V_o
0.875
0.750
0.625
0.500
0.375
0.250
0
1
2
3
4
5
6
7
8
0
20
40
60
80
100

Figure 6B

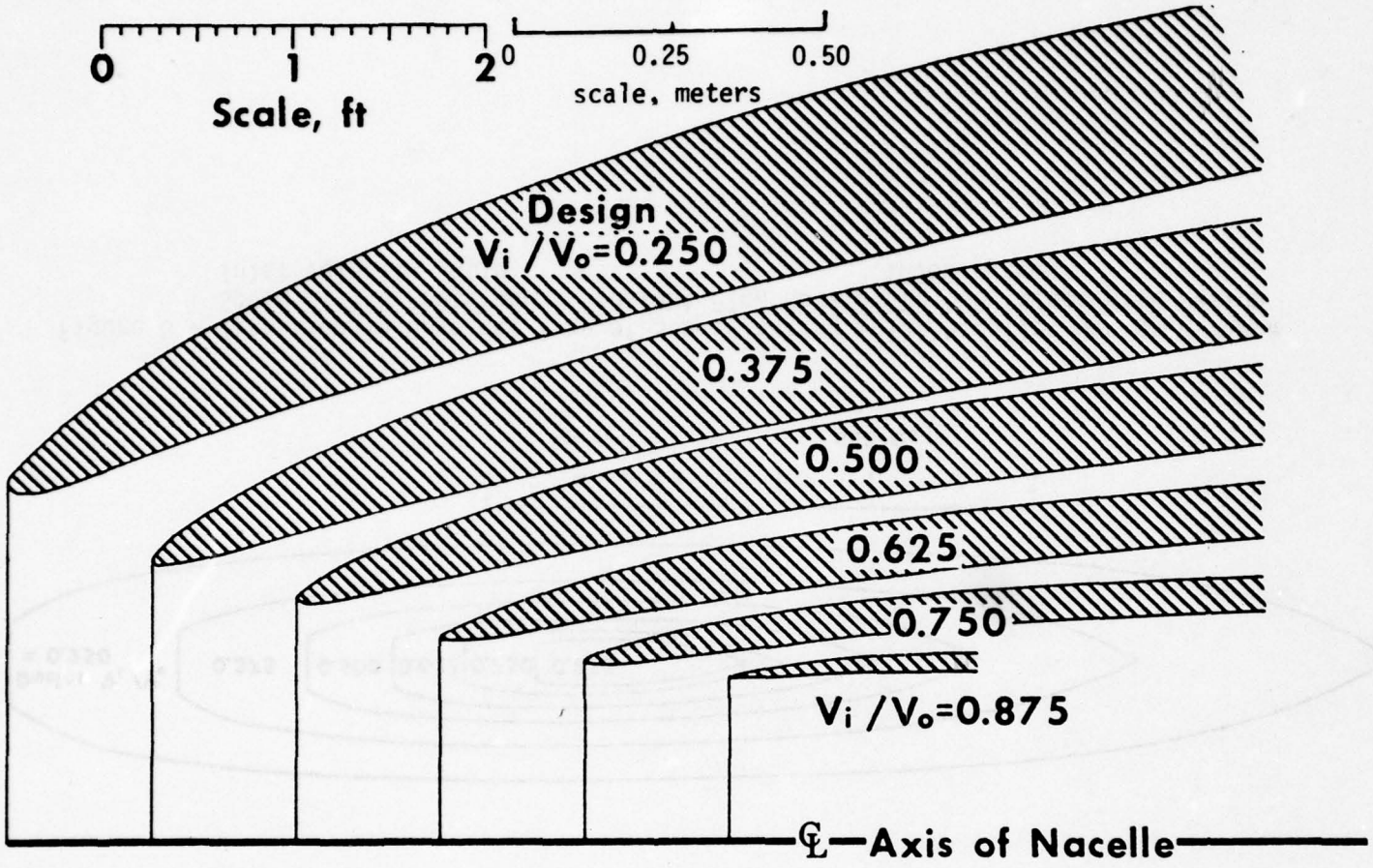

Figure 7 - Variation in Physical Size and Contour of Subcavitating Inlet Lips

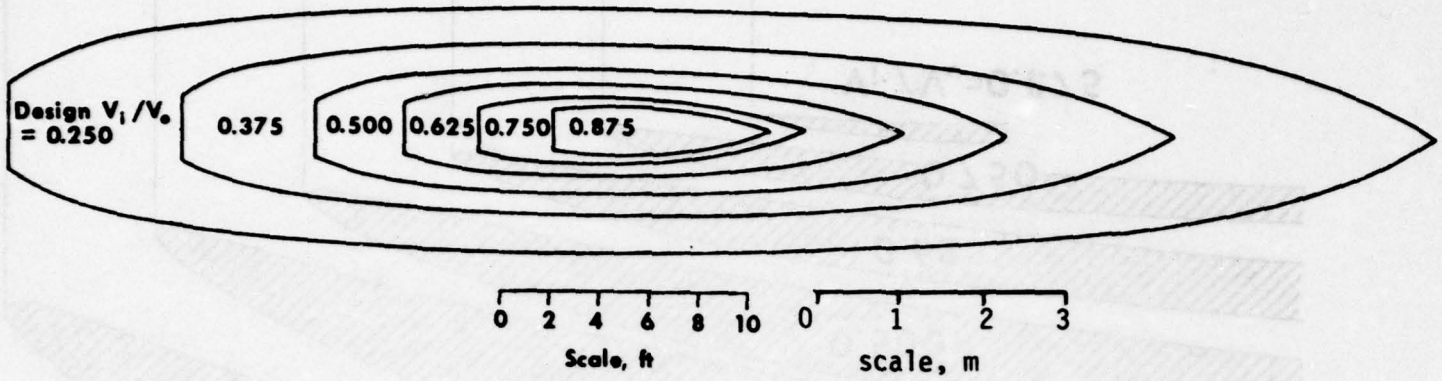

Figure 8 - Variation in Physical Size of Subcavitating Inlet Nacelles Designed for a Speed of 100 Knots and a Constant Flow Rate of 23,500 lb/sec with Design Inlet Velocity Ratio (10660 kg/sec)

The shapes of the cavitation buckets are shown in Figure 9 as a function of local velocity and IVR. This figure determines the operating conditions under which the inlet is free of cavitation.

Figure 10A shows the additive, system* and pressure drag coefficients, components of the external drag, as a function of the design IVR for a design speed of 100 knots. Figures 10B, C, and D are the corresponding plots for the base vented (at maximum thickness), base vented (forward of the maximum thickness) and supercavitating ram inlet systems, respectively. The total external drag coefficients for these inlets are compared in Figure 11, where one can see that the ventilated design is superior in terms of external drag at 100 knots.

The inlet loss coefficient $K_i = \frac{H_L}{V_o^2/2g}$, where H_L is the sum of all the internal losses, expressed as pressure heads, is used as a measure of internal performance. The total inlet loss coefficient is plotted as a funtion of the design IVR in Figure 12. A breakdown of internal losses by component is shown in Figure 13. The variation in component head losses with flowrate at an IVR of 0.75 are shown. The nacelle elbow losses are considerably higher than those of the other components, and all losses are seen to vary in almost direct proportion with the square of the flowrate. From Figures 10 and 11, we learn that the external drag decreases with design IVR, while Figures 12 and 13 show that the internal losses increase with increasing IVR. Remembering that design IVR's correspond to different inlet shapes (designs) which were chosen according to their cavitation properties, we are now in a position to effectuate a compromise between internal and external losses to determine

* The system drag evaluation is fully discussed in Reference 3

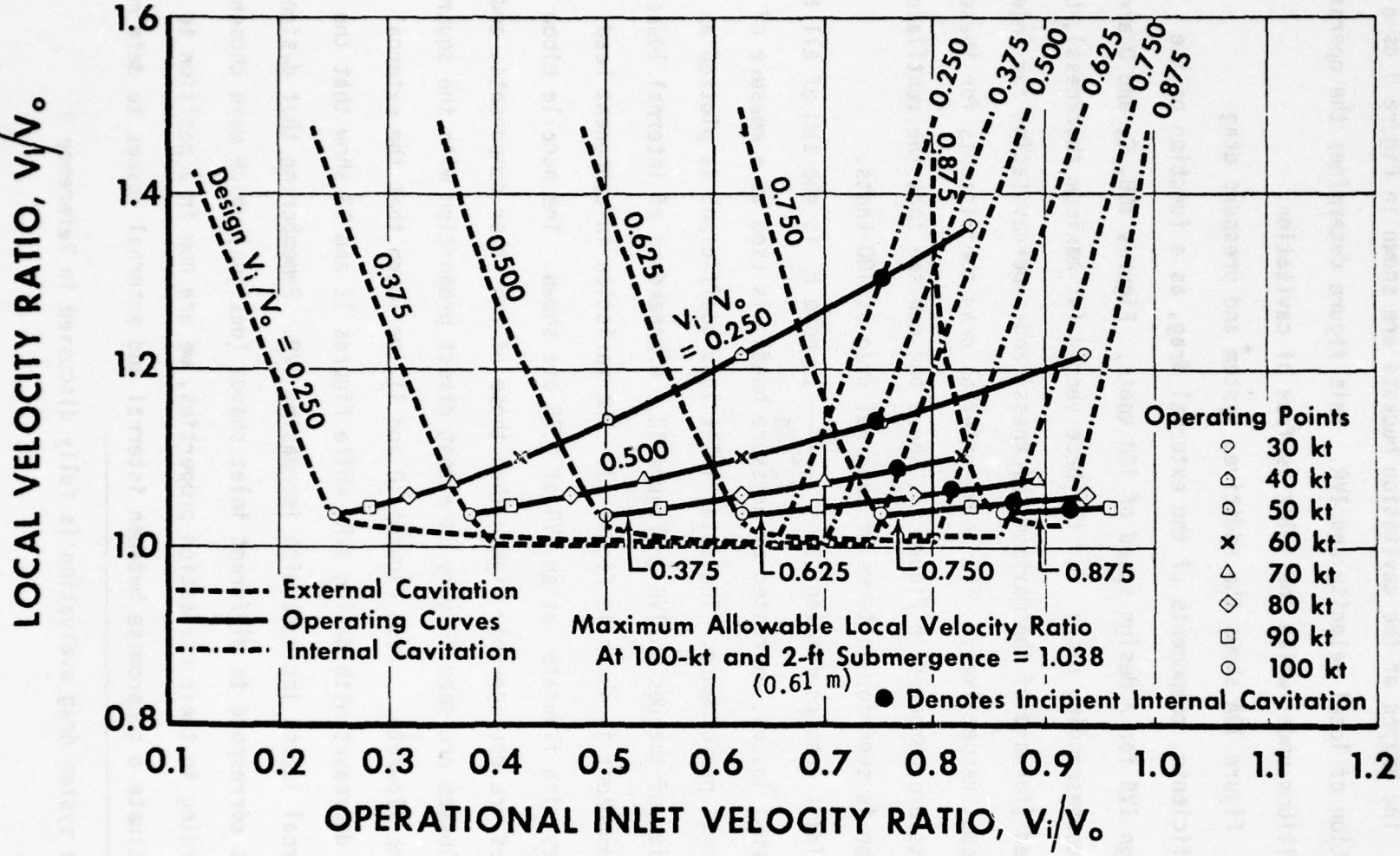

Figure 9 - Cavitation Characteristics of the Six Inlet Designs

VARIATION WITH DESIGN INLET VELOCITY RATIO OF THE COMPONENTS OF THE TOTAL EXTERNAL DRAG FOR THE SUBCAVITATING INLET SYSTEM

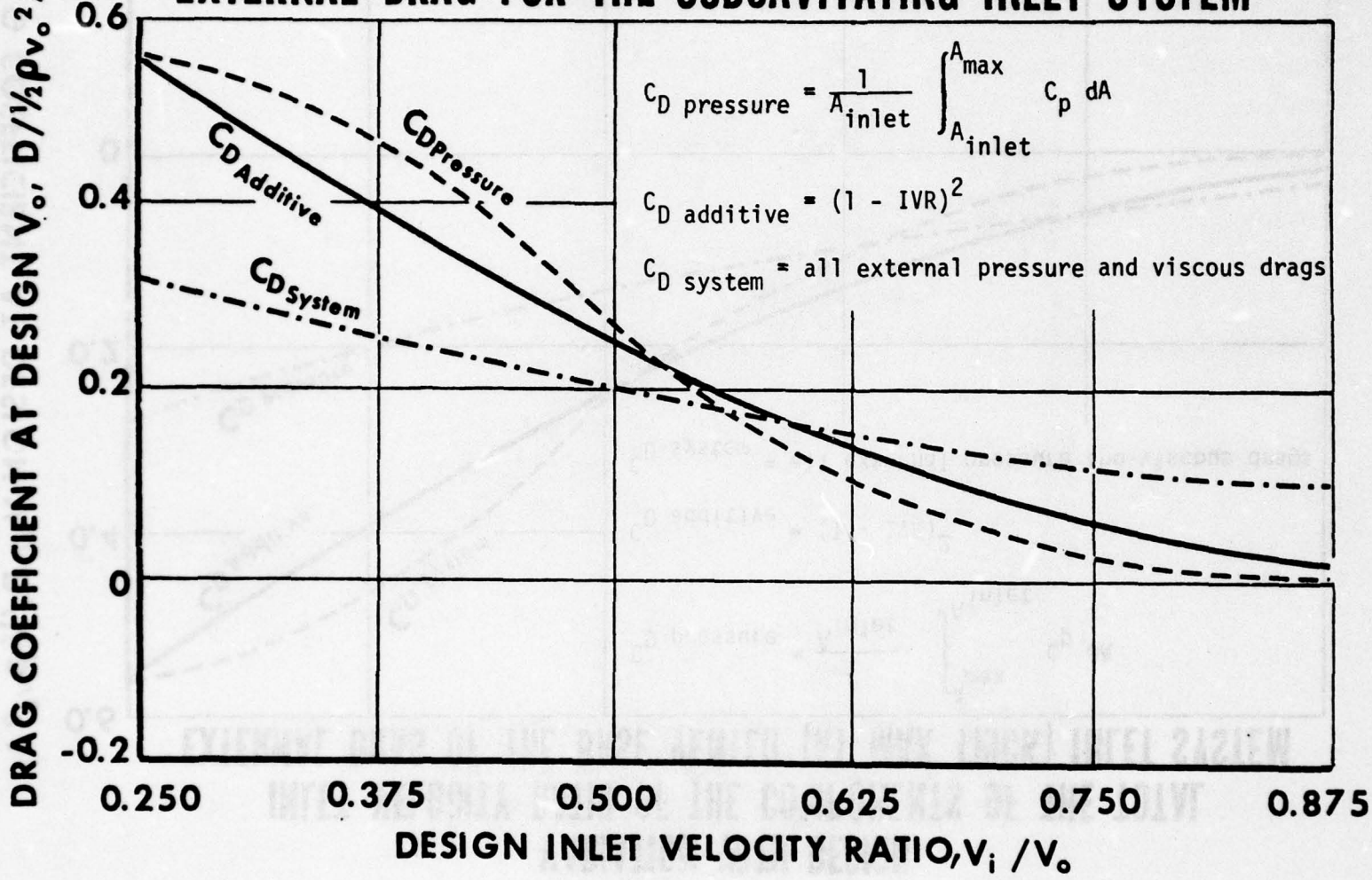

Design Speed = 100 kt

Figure 10A

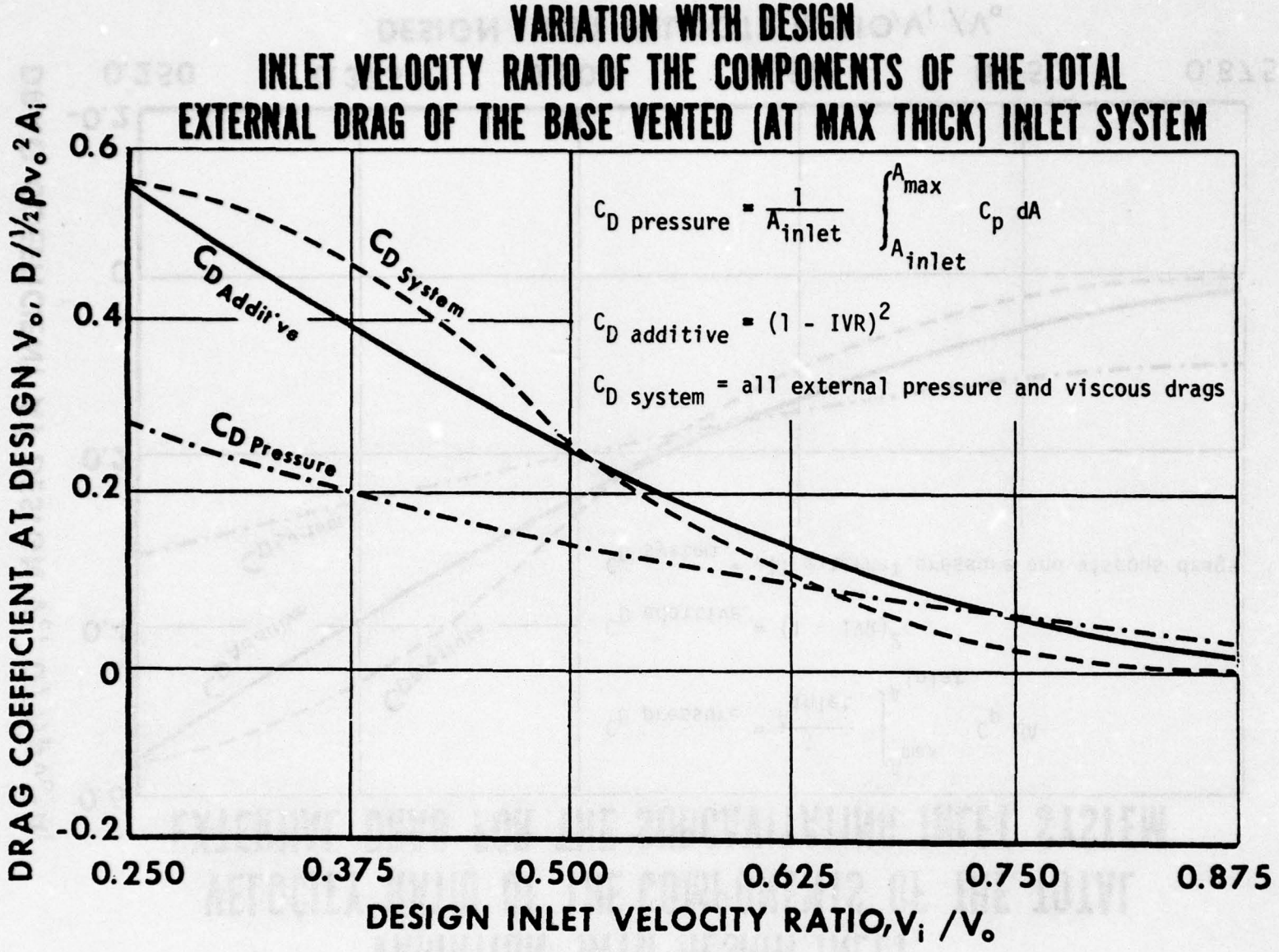
VARIATION WITH DESIGN
INLET VELOCITY RATIO OF THE COMPONENTS OF THE TOTAL
EXTERNAL DRAG OF THE BASE VENTED (AT MAX THICK) INLET SYSTEM
$C_{D\ pressure} = \frac{1}{A_{inlet}} \int_{A_{inlet}}^{A_{max}} C_p\ dA$
$C_{D\ additive} = (1 - IVR)^2$
$C_{D\ system}$ = all external pressure and viscous drags
$C_{D\ System}$
$C_{D\ Additive}$
$C_{D\ Pressure}$
DRAG COEFFICIENT AT DESIGN V_o, $D/\frac{1}{2}\rho v_o^2 A_i$
0.6
0.4
0.2
0
-0.2
0.250
0.375
0.500
0.625
0.750
0.875
DESIGN INLET VELOCITY RATIO, V_i / V_o
Design Speed = 100 kt

Figure 10B

VARIATION WITH DESIGN INLET VELOCITY RATIO OF THE COMPONENTS OF THE TOTAL EXTERNAL DRAG OF THE BASE VENTED (Fwd Max Thick) INLET SYSTEM

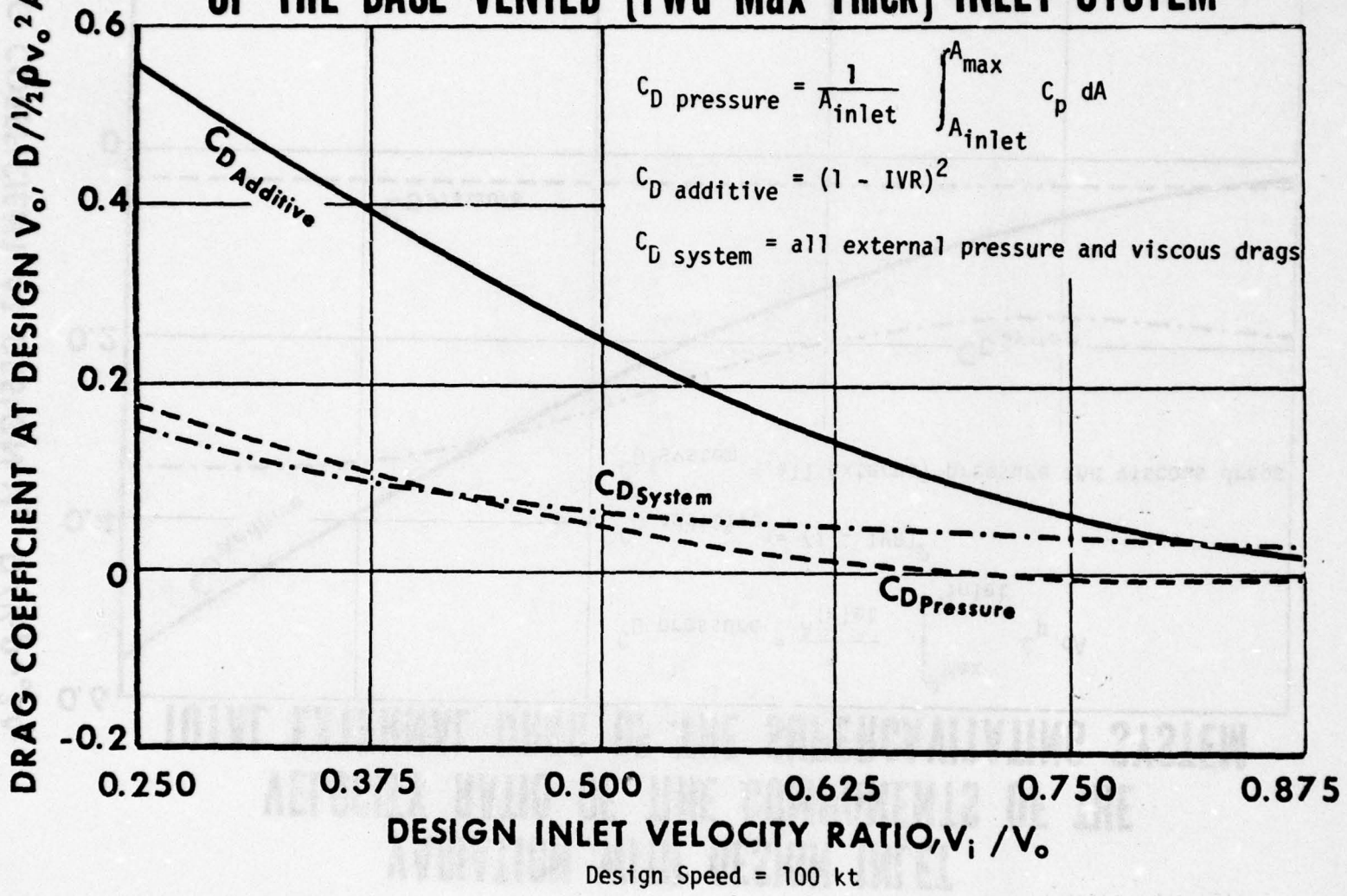

Figure 10C

VARIATION WITH DESIGN INLET VELOCITY RATIO OF THE COMPONENTS OF THE TOTAL EXTERNAL DRAG OF THE SUPERCAVITATING SYSTEM

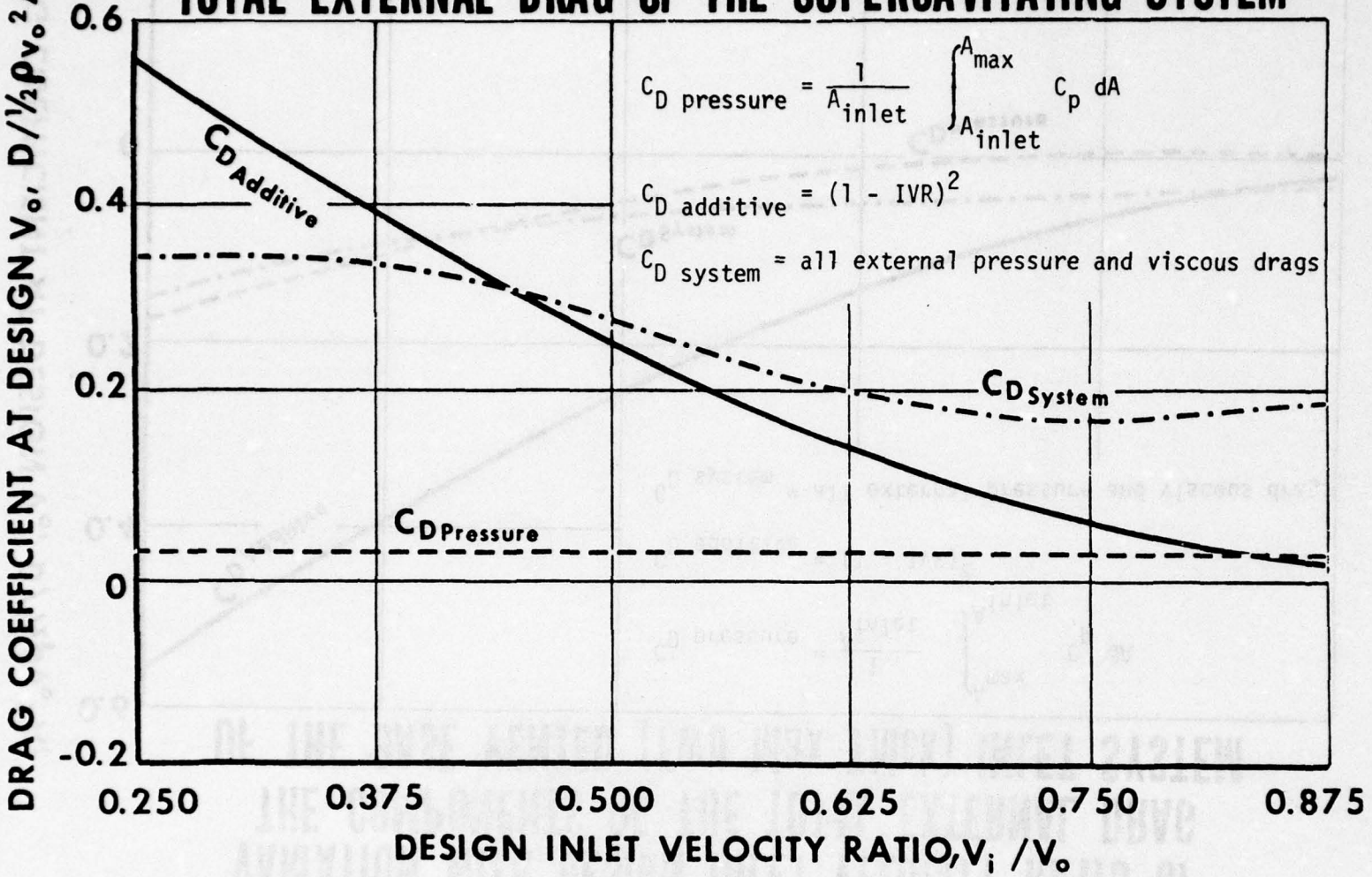

Design Speed = 100 kt

Figure 10D

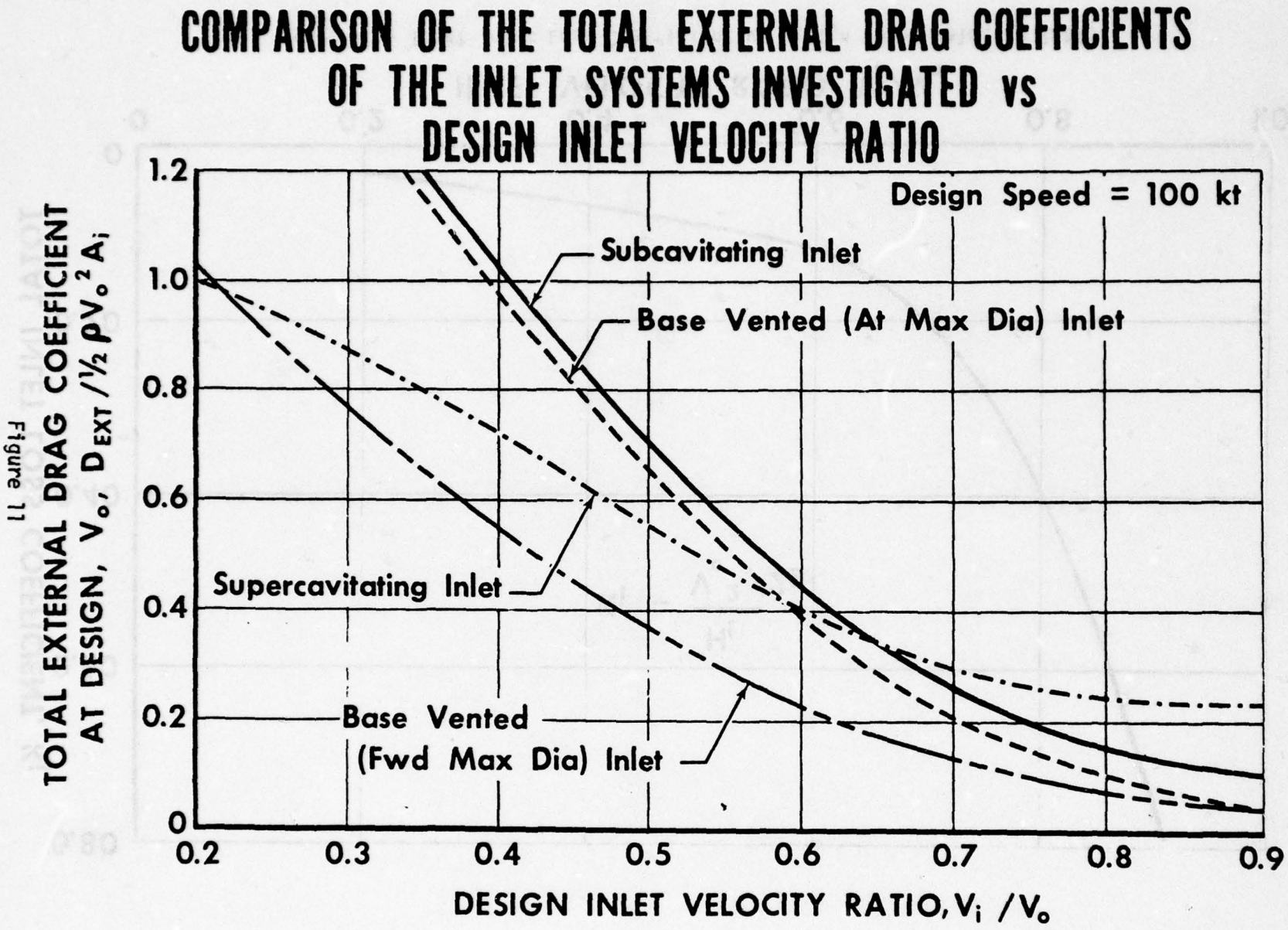
COMPARISON OF THE TOTAL EXTERNAL DRAG COEFFICIENTS OF THE INLET SYSTEMS INVESTIGATED vs DESIGN INLET VELOCITY RATIO
Design Speed = 100 kt
Subcavitating Inlet
Base Vented (At Max Dia) Inlet
Supercavitating Inlet
Base Vented (Fwd Max Dia) Inlet
TOTAL EXTERNAL DRAG COEFFICIENT AT DESIGN, V_o, $D_{EXT}/\frac{1}{2}\rho V_o^2 A_i$
DESIGN INLET VELOCITY RATIO, V_i/V_o
1.2
1.0
0.8
0.6
0.4
0.2
0
0.2
0.3
0.4
0.5
0.6
0.7
0.8
0.9

Figure 11

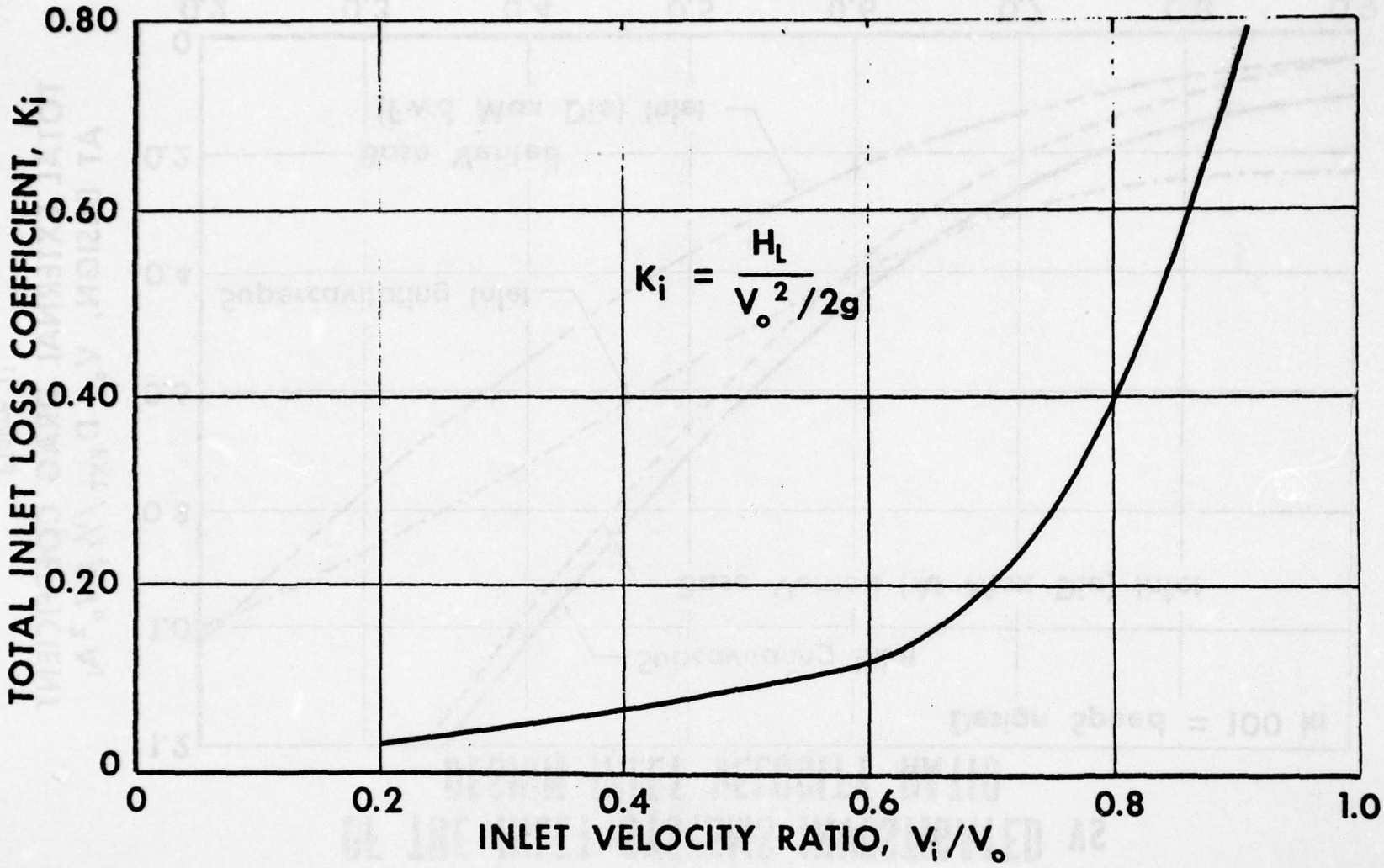

Figure 12 - Total Inlet Loss Coefficient vs Design Inlet Velocity Ratio

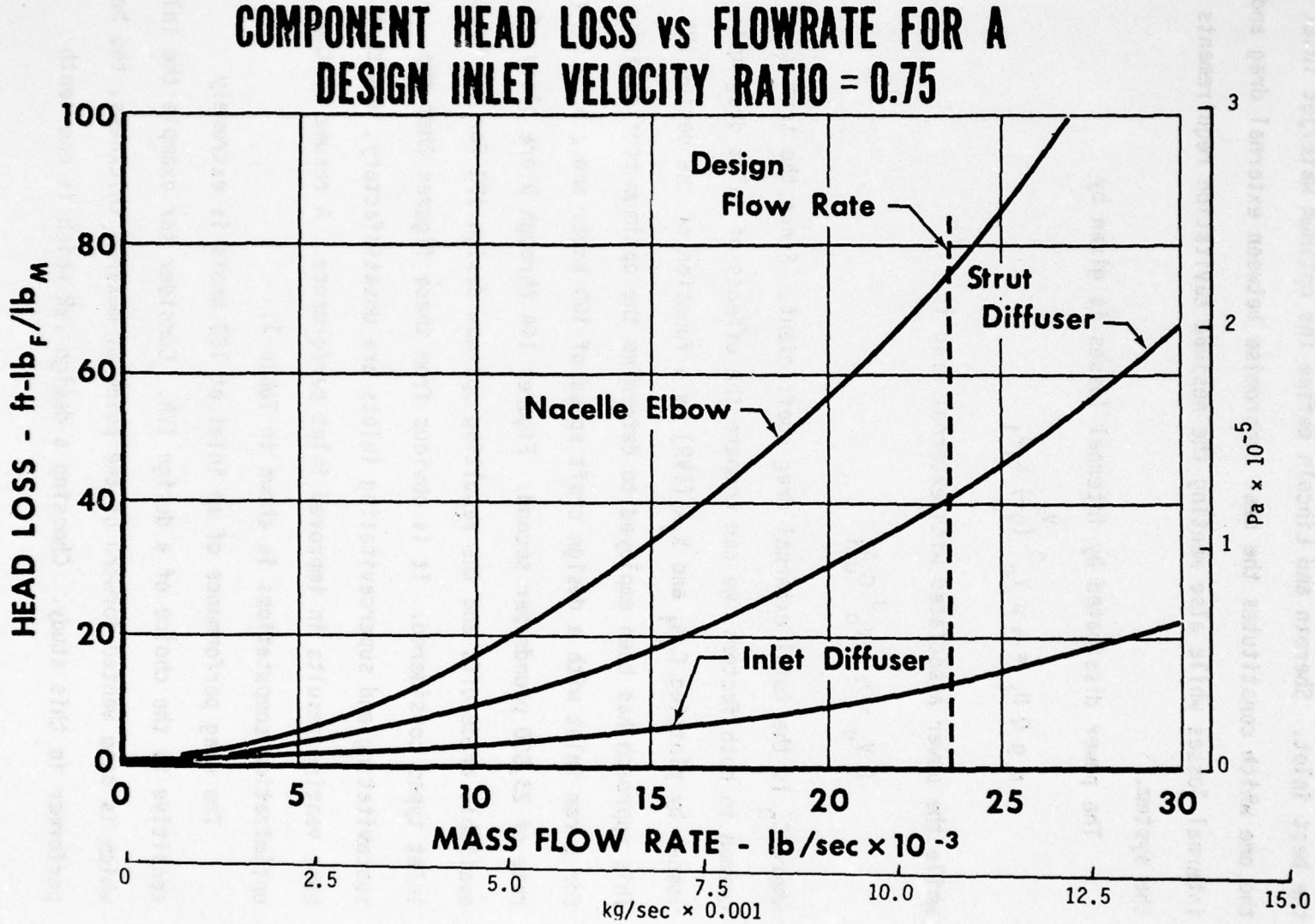
COMPONENT HEAD LOSS vs FLOWRATE FOR A
DESIGN INLET VELOCITY RATIO = 0.75
HEAD LOSS - ft-lb$_F$/lb$_M$
100
80
60
40
20
0
Design
Flow Rate
Strut
Diffuser
Nacelle Elbow
Inlet Diffuser
3
2
1
0
Pa x 10^{-5}
0
5
10
15
20
25
30
MASS FLOW RATE - lb/sec x 10^{-3}
0
2.5
5.0
7.5
10.0
12.5
15.0
kg/sec x 0.001

Figure 13

the best inlet. Sherman and Lincoln define the optimum waterjet inlet as the one which constitutes the best compromise between external drag and internal losses while also meeting the desired cavitation requirements of the system.

The power dissipated by internal losses is given by

$$\rho g Q H_L = \tfrac{1}{2} \rho V_o^3 \left(\frac{V_i}{V_o}\right) K_i A_i$$

while the power associated with external drag is

$$D V_o = \tfrac{1}{2} \rho V_o^3 C_D A_i$$

where C_D is the total external drag coefficient. Since the term $\frac{1}{2}\rho V_o^3$ is common to both factors, we can compare the effects of inlet drag and losses by plotting $C_D A_i$ and $K_i A_i$(IVR) as a function of the design IVR. This approach has been employed to determine the optimum configuration for a ram inlet with a design craft speed of 100 knots and a pump flow rate of 23,500 pounds per second. Figures 14A through D are plots of the available trade-offs and the resulting optimum design IVR for the basic inlet types considered. It is obvious from these figures that the subcavitating and supercavitating inlets are unsatisfactory, and that base venting results in improved inlet performance. A resume of the optimization computations is shown in Table 1.

The drag performance of an inlet at 100 knots is extremely sensitive to the choice of a design IVR. Consider for example the inlet which is base vented forward of the point of maximum thickness, the best performer in this study. Choosing a design IVR which is one tenth

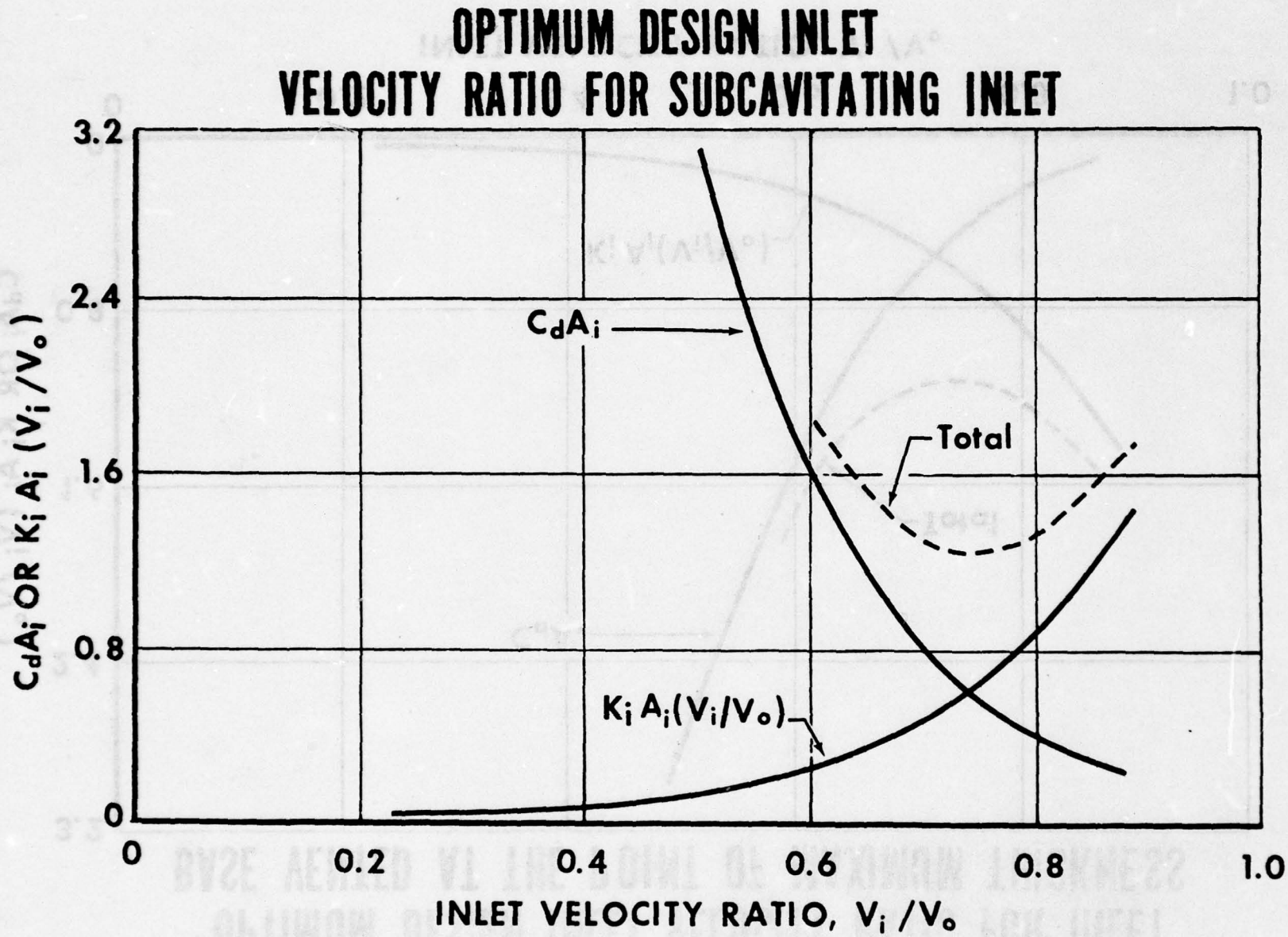
OPTIMUM DESIGN INLET
VELOCITY RATIO FOR SUBCAVITATING INLET
3.2
2.4
1.6
0.8
0
C_dA_i
Total
$K_i A_i(V_i/V_o)$
0
0.2
0.4
0.6
0.8
1.0
C_dA_i OR $K_i A_i (V_i/V_o)$
INLET VELOCITY RATIO, V_i/V_o

Figure 14A

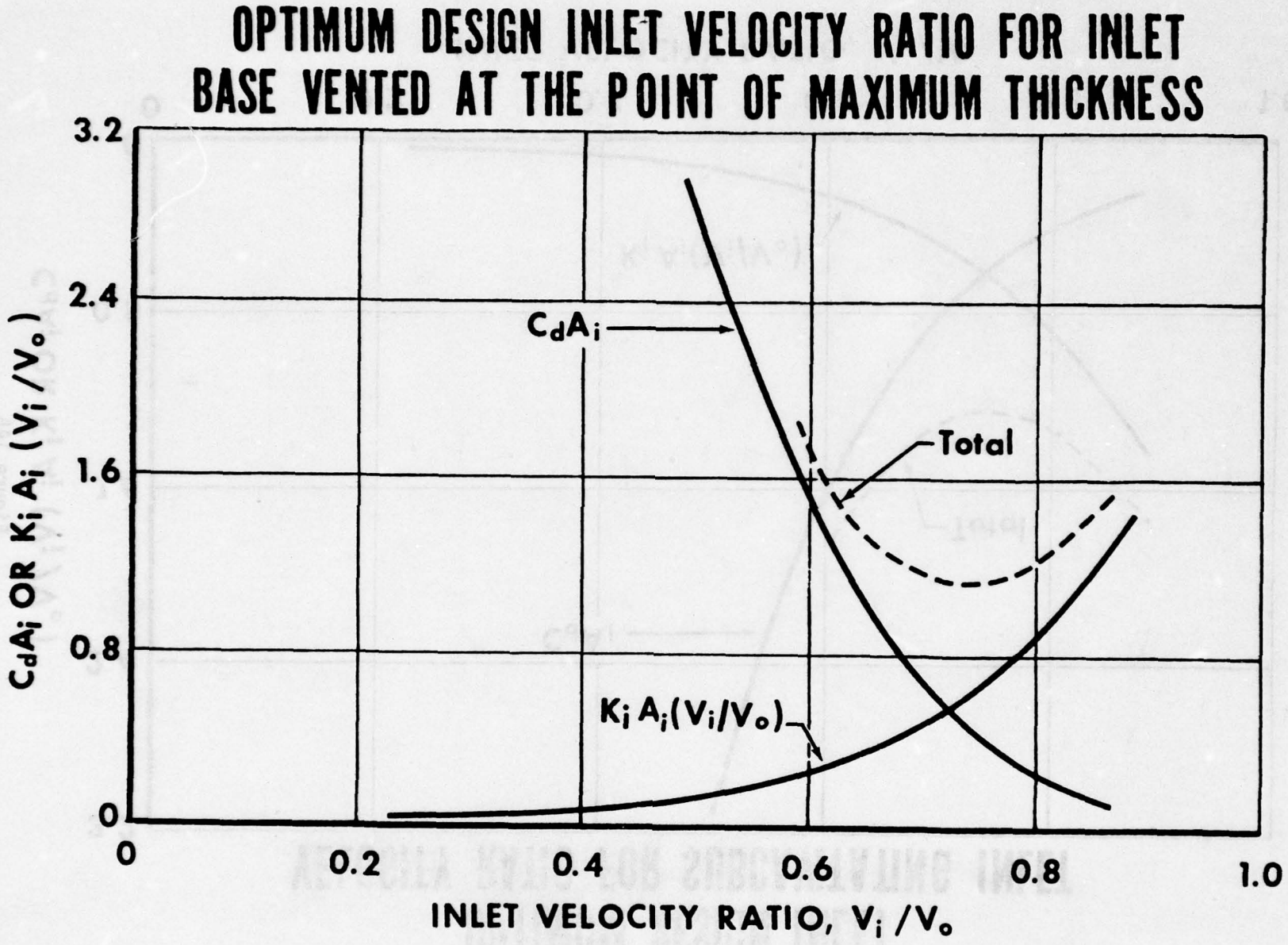
OPTIMUM DESIGN INLET VELOCITY RATIO FOR INLET BASE VENTED AT THE POINT OF MAXIMUM THICKNESS
3.2
2.4
1.6
0.8
0
0
0.2
0.4
0.6
0.8
1.0
C_dA_i
Total
$K_i A_i(V_i/V_o)$
C_dA_i OR $K_i A_i (V_i/V_o)$
INLET VELOCITY RATIO, V_i/V_o

Figure 14B

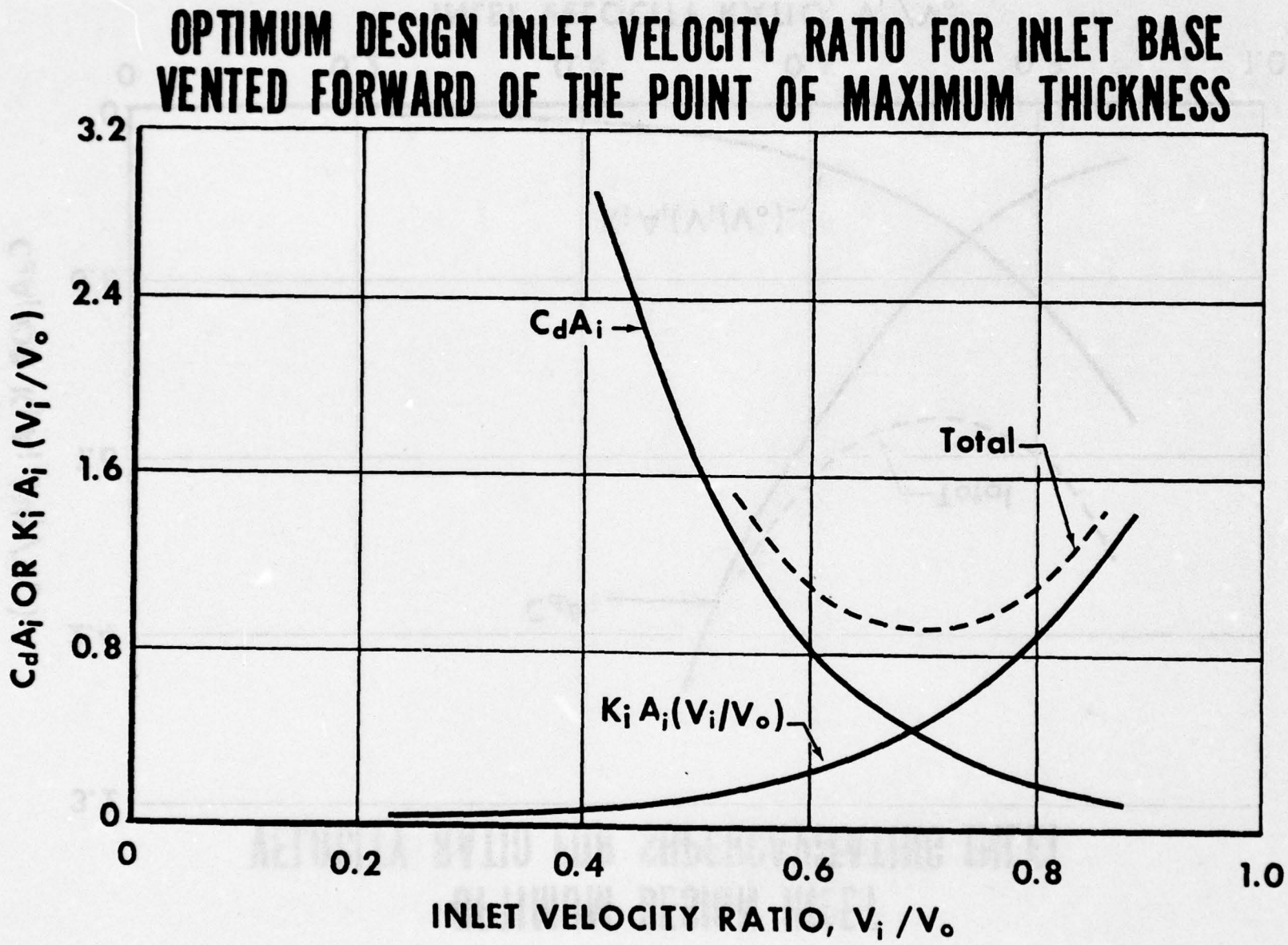
OPTIMUM DESIGN INLET VELOCITY RATIO FOR INLET BASE VENTED FORWARD OF THE POINT OF MAXIMUM THICKNESS
3.2
2.4
1.6
0.8
0
C_dA_i
Total
$K_i A_i(V_i/V_o)$
C_dA_i OR $K_i A_i (V_i/V_o)$
0
0.2
0.4
0.6
0.8
1.0
INLET VELOCITY RATIO, V_i/V_o

Figure 14C

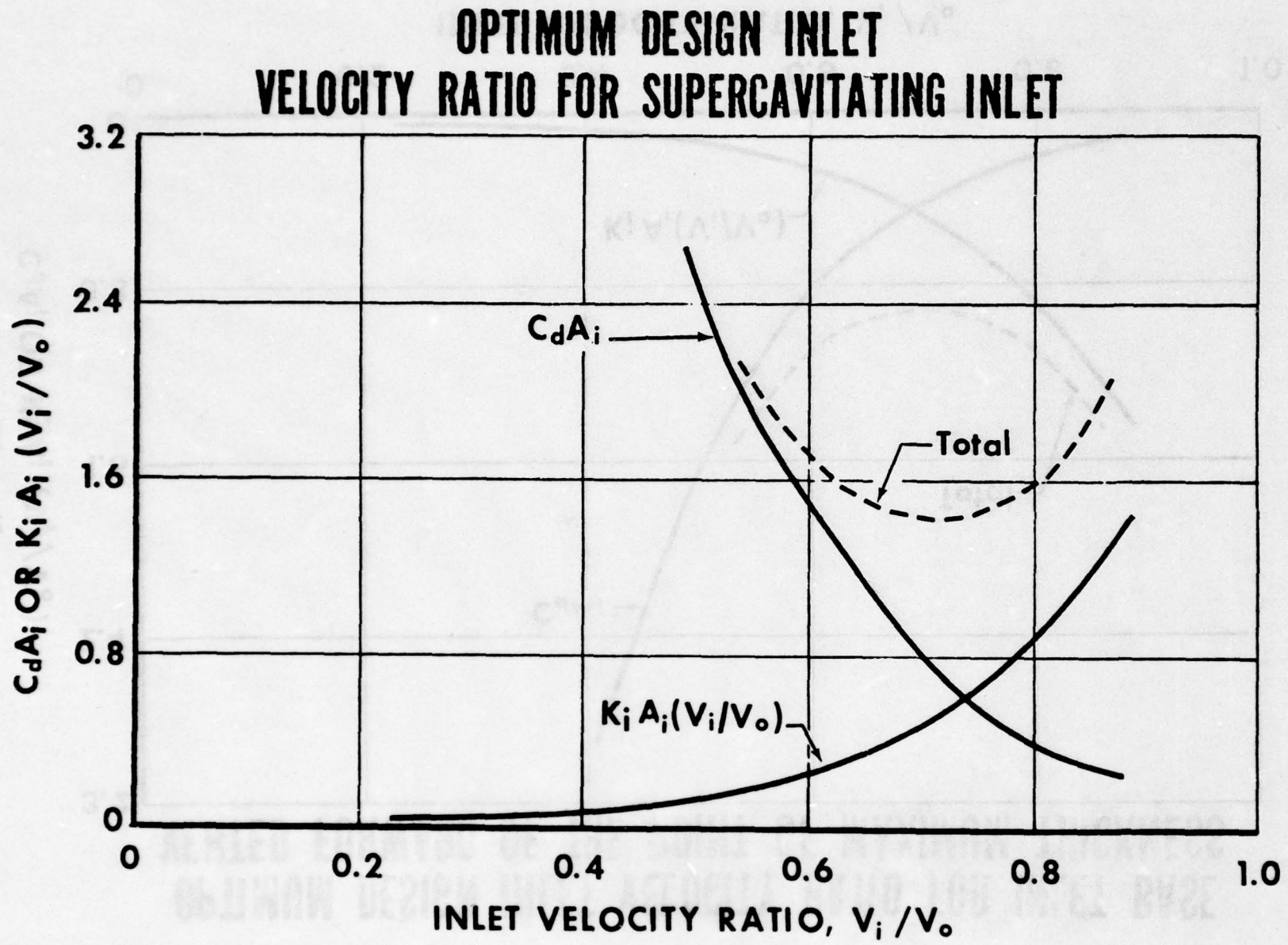
OPTIMUM DESIGN INLET
VELOCITY RATIO FOR SUPERCAVITATING INLET
3.2
2.4
1.6
0.8
0
C_dA_i
Total
$K_i A_i(V_i/V_o)$
0
0.2
0.4
0.6
0.8
1.0
C_dA_i OR $K_i A_i (V_i/V_o)$
INLET VELOCITY RATIO, V_i/V_o

Figure 14D

Inlet Type	Optimum Inlet Velocity Ratio	Inlet Loss Coefficient	Inlet Drag Coefficient	Power Loss	
				Horsepower	Kilowatts
Subcavitating	0.735	0.268	0.220	10,750	8,016
Base Vented at Max Thickness	0.745	0.285	0.153	9,520	7,099
Base Vented Forward of Max Thickness	0.700	0.215	0.138	7,825	5,835
Supercavitating	0.720	0.245	0.285	12,400	9,247

TABLE 1 - RESULTS OF DESIGN INLET VELOCITY OPTIMIZATION

greater than optimum results in a 23.4% increase in power loss. A design IVR which is ten percent smaller than optimum increases the power losses by 19%. There appears to be a very definite optimum design inlet velocity ratio for a 100 knot ram inlet system and designing even slightly off this optimum results in large power losses. If the optimum base vented inlet and its corresponding design IVR are selected, very little latitude in craft speed is allowed and in particular, the inlet will choke due to cavitation with a 20 knot drop in craft speed. The important conclusion to be drawn from this is that this inlet could never accelerate from rest to its design speed because of choking. Hence, a variable geometry inlet is an absolute necessity in this case.

Developmental Sciences, Inc. (DSI) has reported on the analysis and design of pod inlet.[6,7] Their reports are not very descriptive and do little to explain their inlet design method.

From the given thrust requirements of the propulsion system and preliminary pump characteristic, the (minimum) pressure recovery factor

is estimated, using Bernoulli's law. As viscous losses are not included in this calculation, the figure is likely to be low. Then the design cruise IVR is selected and cruise and hump inlet areas are determined. Then, cavitation choking of the flow in the 96 degree turn into the strut is examined. For this consideration, the hump (but foil-borne) operating condition is the most critical. The criterion which is used is that there be enough diffusion to balance any cavitation inducing pressure drop across the turning vanes.

The pod and plug geometries are determined primarily by the duct area and the inlet area at hump and cruise conditions. Where the plug is fully retracted, the inlet and duct exit areas are required to be identical. It is further specified that the open area distribution along the pod between these two points be constant. This implies that, (1) once the internal area distribution of the pod is specified, the plug shape is determined, (2) the shaped portion of the plug must have the same length as the diffuser part of the pod.

Therefore, the internal shape of the pod surface is determined by the external pod shape which is in turn, designed on the basis of cavitation-free external flow at 100 knots. The diffuser length is ideally determined by the requirement that the flow be diffused without separation. This is considered impractical since in order to achieve fully attached flow, the pod (and hence the extended centerbody) become unacceptably long, resulting in high drag and structural difficulties. Furthermore, a longer diffuser means a longer plug which results in greater boundary layer development, which requires an even longer

diffuser to avoid separation. Whether these statements were investigated or were simply speculations, is not mentioned.

A balance must be struck between short and long diffusers so that at the cruise deployment, the separation point is located such that the required total recovery is achieved.

A number of inlet shapes having different diffuser lengths, contours, etc. were generated for preliminary screening analysis. By trial and error, the one best satisfying the requirements was selected and analyzed in detail. The geometric construction of the final selected inlet is shown in Figure 15. A circular arc is used to describe the external pod surface. The equation

$$\left(\frac{y}{1.13026}\right)^2 = \frac{144}{\pi}\left[0.852 + 0.748\left(1 + \frac{k_x}{1.13026\ \ell_d}\right)^{0.21}\right]$$

where $k = 47.21637$ and $\ell_d = 20$

represents the internal pod surface. Ellipses are used to fair the inlet nose into the diffuser and external pod surfaces.

A one-fifth scale model of the DSI-designed inlet was built and tested at the 36 inch VPWT at DTNSRDC.[8] The pressure recovery performance of the inlet-diffuser is presented as a loss coefficient in Figure 16. At the design IVR of 0.85, the pressure loss coefficient is approximately 0.25, which compares with the predicted value of 0.242 for the cruise condition. For the low speed condition corresponding to simulated speed of 35 knots and a fully retracted centerbody, the pressure loss coefficient is shown in Figure 17. Rather high losses are indicated. At the hump speed design IVR of .89, the value of the model

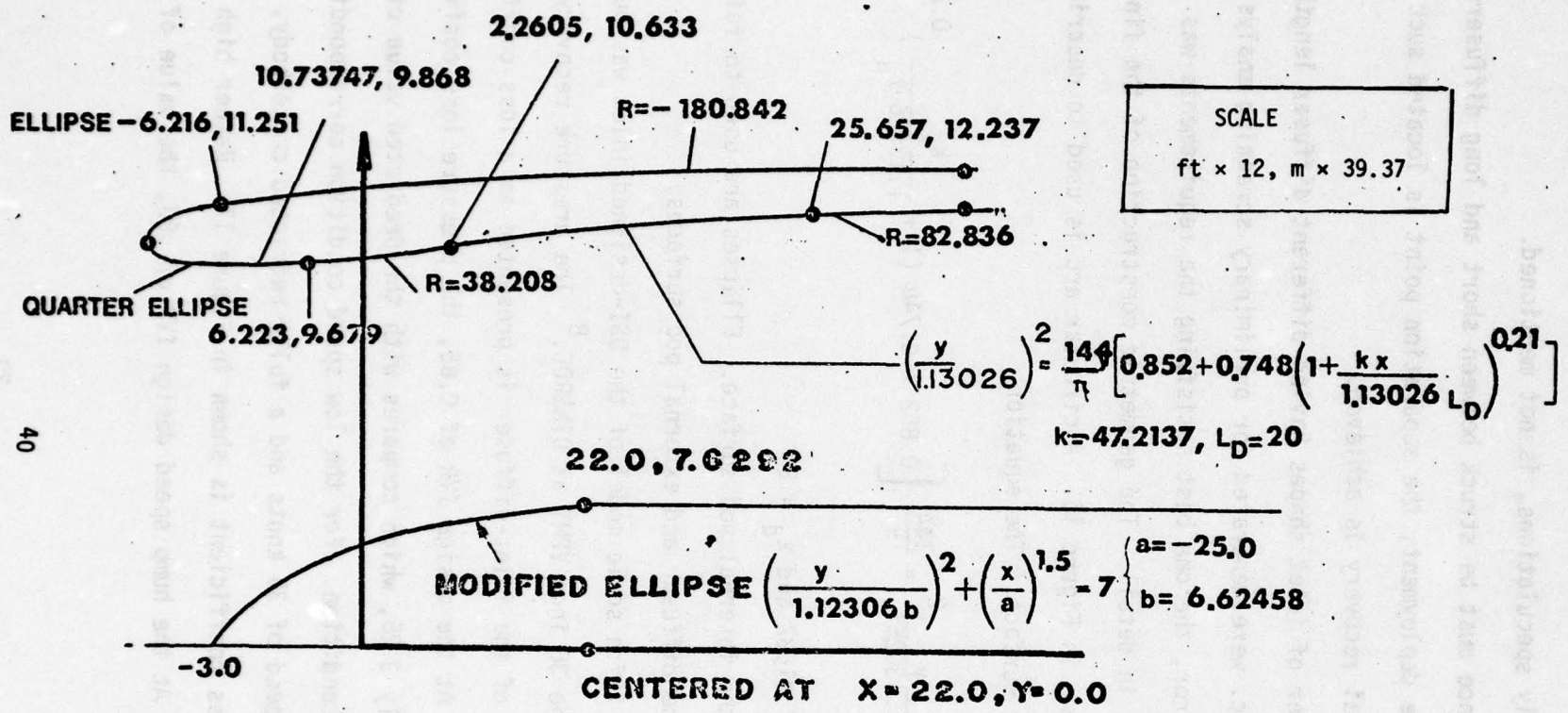

FIGURE 15 - CONFIGURATION IN THE RETRACTED POSITION OF CENTER BODY

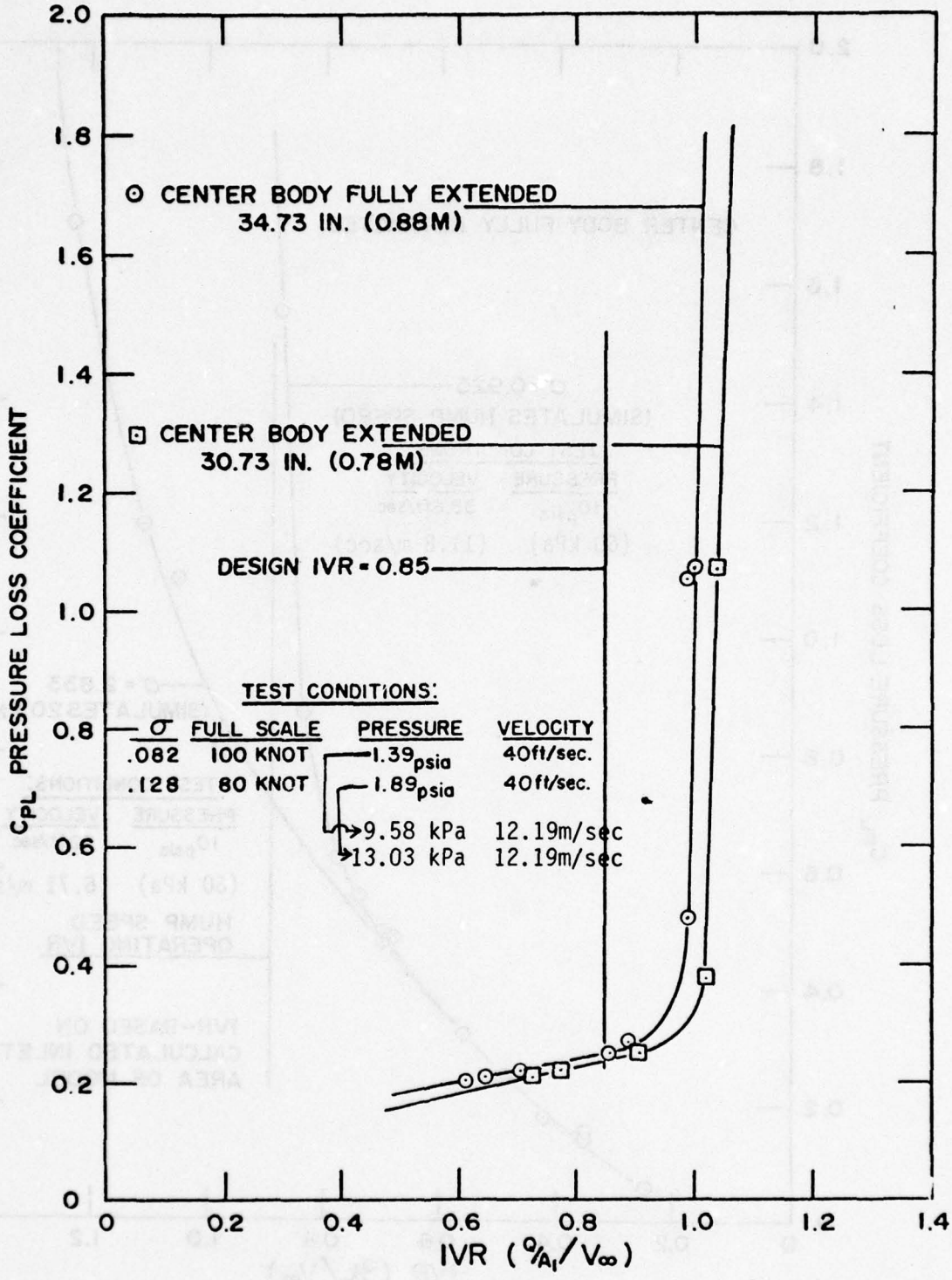

Figure 16- Internal Pressure Loss Performance - High Speed Conditions

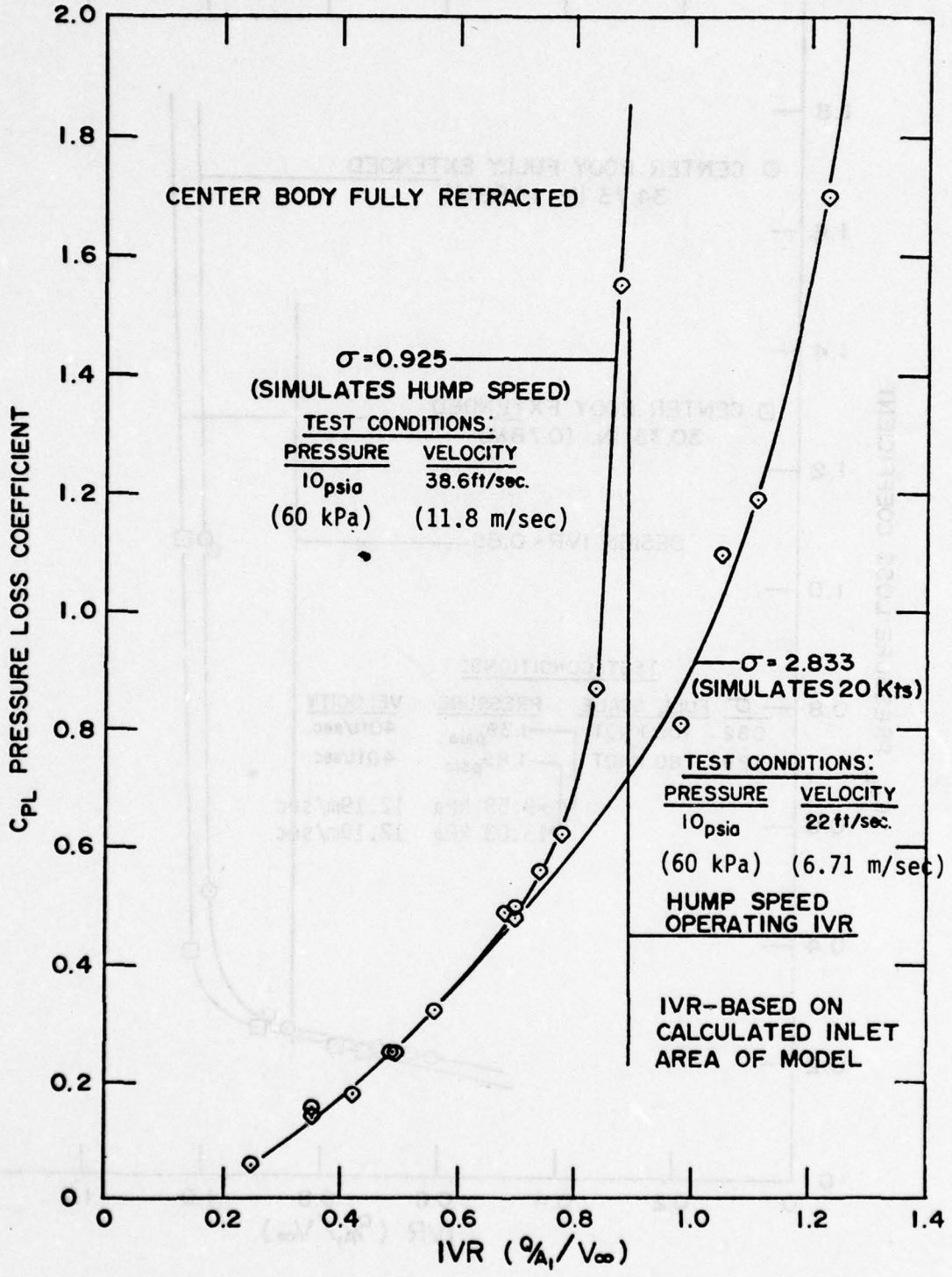

Figure 17 - Internal Pressure Loss Performance - Low Speed Conditions

pressure loss coefficient is 1.60. The test report attributes this to internal cavitating conditions. This value greatly exceeds the predicted value of 0.282. From this data, it is concluded that the inlet design will not provide the required performance at the hump speed.

The inlet cavitation inception boundaries for the cruise configuration (centerbody fully extended) are shown in Figure 18. Cavitation was found to occur on the inner and outer surfaces of the inlet lip near the leading edge. No cavitation was observed on the centerbody. Therefore, the design does meet its requirements at 100 knots. Furthermore, the experimental data and prediction for external cavitation are in good agreement. The data for internal cavitation indicate a higher attainable IVR than predicted. At simulated high speeds, 80 knots or better, cavitation was observed at the strut-pod intersection, indicating that further refinements of the fairing are required in this region. The inlet cavitation inception boundaries for the centerbody fully retracted are presented in Figure 19. Internal and external cavitation did occur on the inlet lip leading edge. At conditions simulating 35 knots - 18 feet (5.49 m) submersion, cavitation was observed with an IVR of 2.32 and maximum choked flow at an IVR of 2.42 (based on cruise inlet as area). At simulated 35 knots - 4 feet (1.22 m), submergence, internal cavitation inception occurred at an IVR of 2.15 and choked flow at an IVR of 2.20, indicating that the IVR of 2.35 required to accelerate the craft through the hump would probably not be achievable as the craft rises.

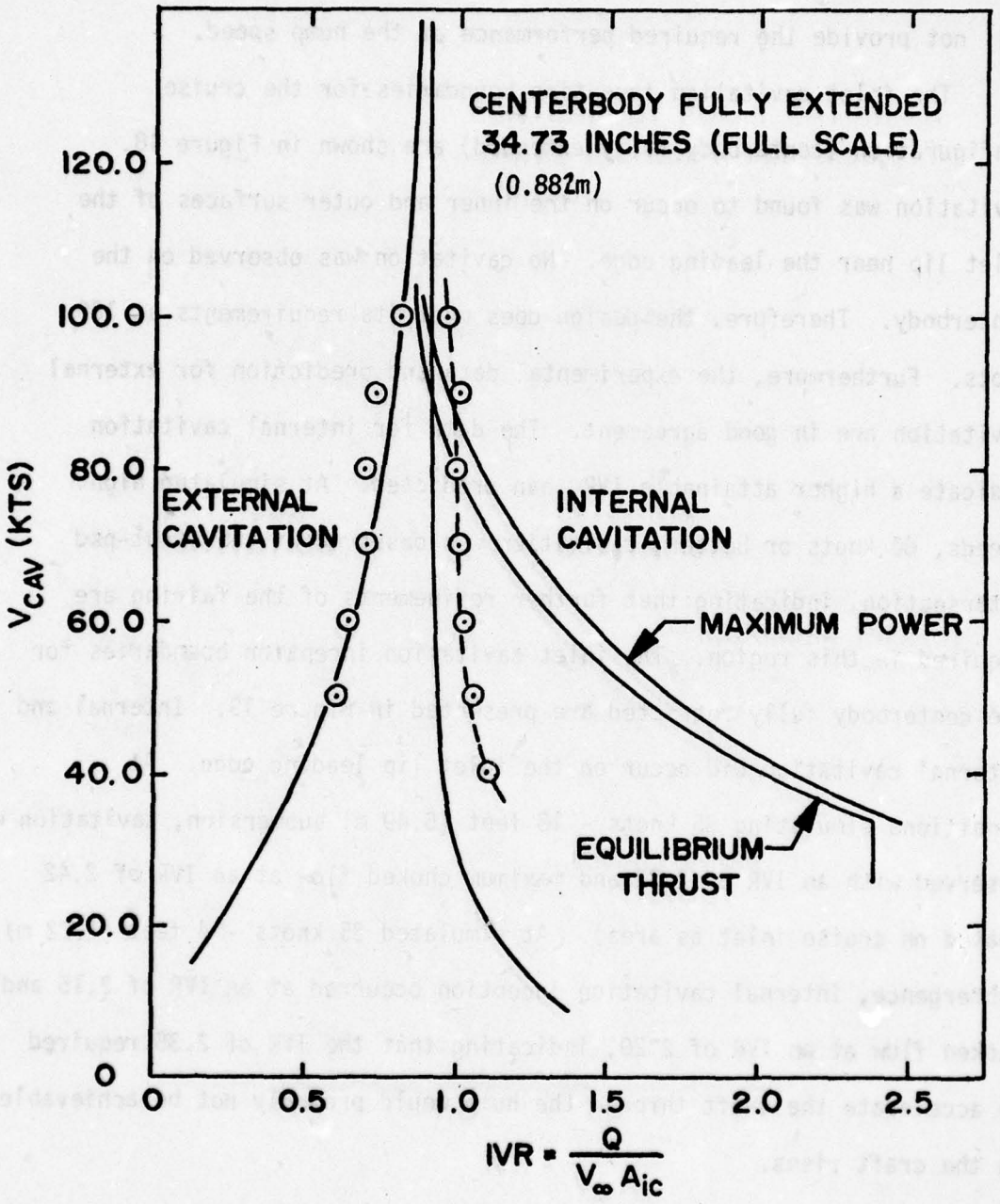

Figure 18 - Inlet Cavitation Boundaries Measured and Predicted, for the 34.73 Inch (0.882 m) Centerbody Extension (Fully Extended)

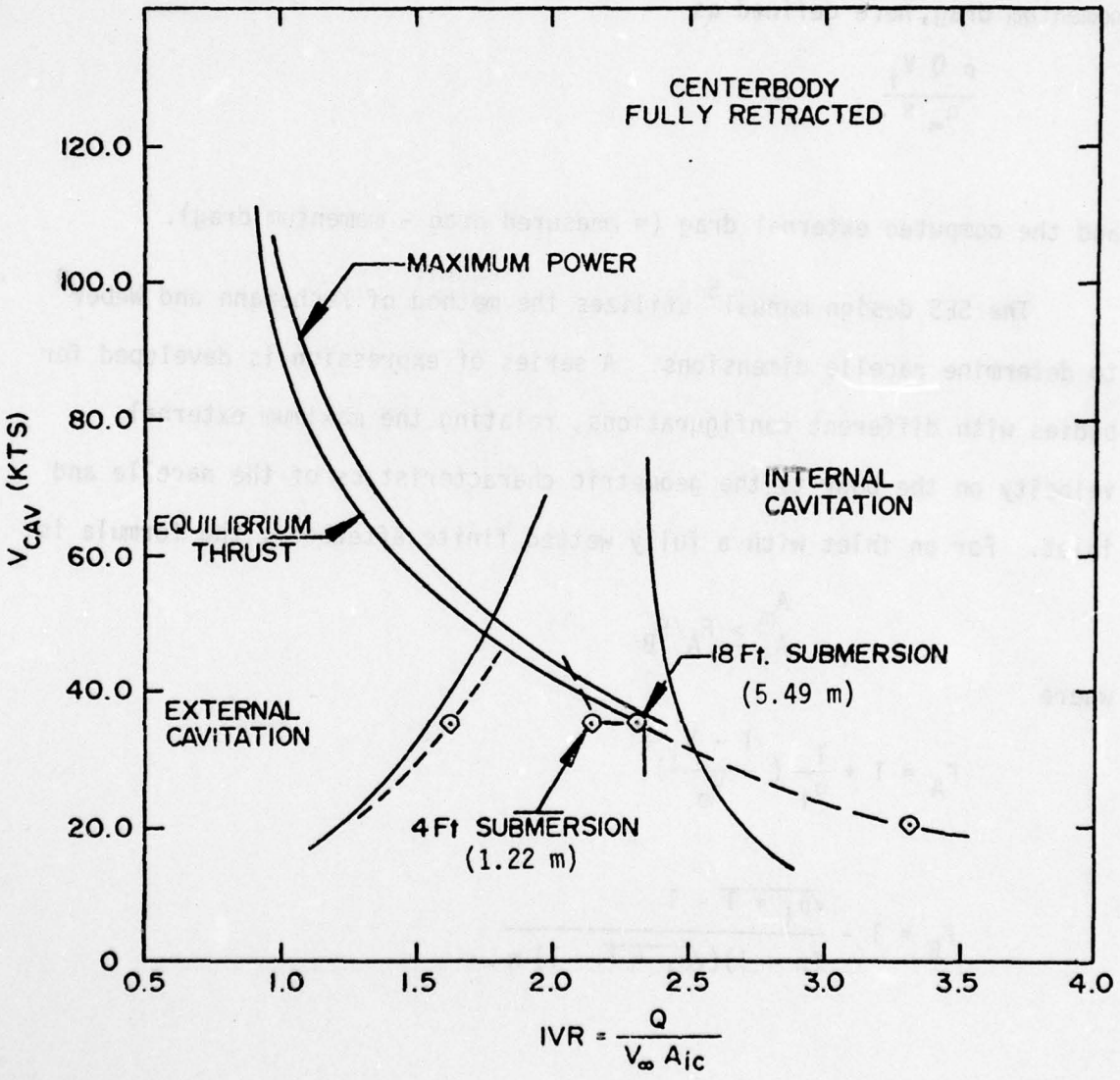

Figure 19 - Inlet Cavitation Boundaries, Measured and Predicted, for the 0.0 Inch Centerbody Extension (Fully Retracted)

Figure 20 shows typical inlet drag performance for the inlet with fully retracted centerbody at a cavitation number of 2.83 simulating 20 knots full scale. Figure 21 shows similar data for the fully extended centerbody at a cavitation number of 0.082, simulating 100 knots full scale. The quantities shown are the total measured drag, the inlet momentum drag, here defined as

$$\frac{\rho\, Q\, V_i}{q_\infty\, S},$$

and the computed external drag (= measured drag - momentum drag).

The SES design manual[5] utilizes the method of Küchemann and Weber[9] to determine nacelle dimensions. A series of expression is developed for bodies with different configurations, relating the maximum external velocity on the body to the geometric characteristics of the nacelle and inlet. For an inlet with a fully wetted finite afterbody, the formula is

$$\frac{A_m}{A_i} \geq F_A/F_B$$

where

$$F_A = 1 + \frac{1}{\sigma_i}\left(\frac{1 - V_i}{V_o}\right)^2$$

$$F_B = 1 - \frac{\sqrt{\sigma_i + 1} - 1}{(n - 1)(\sqrt{\sigma_i + 1} - 1)\, n}$$

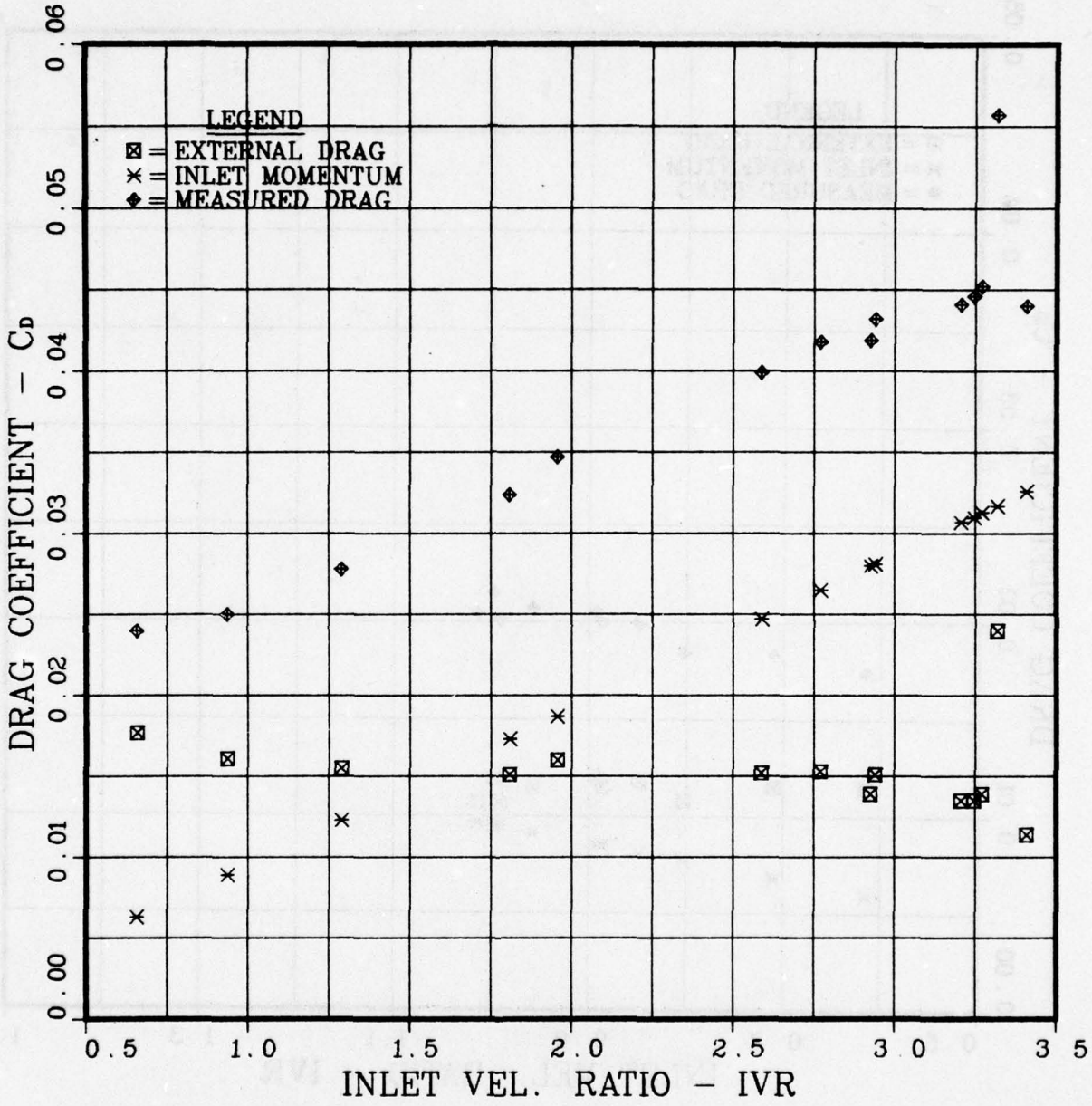

Figure 20 - Typical Inlet Drag Performance for a Range of IVR, Centerbody Retracted, Simulated 20 Knots

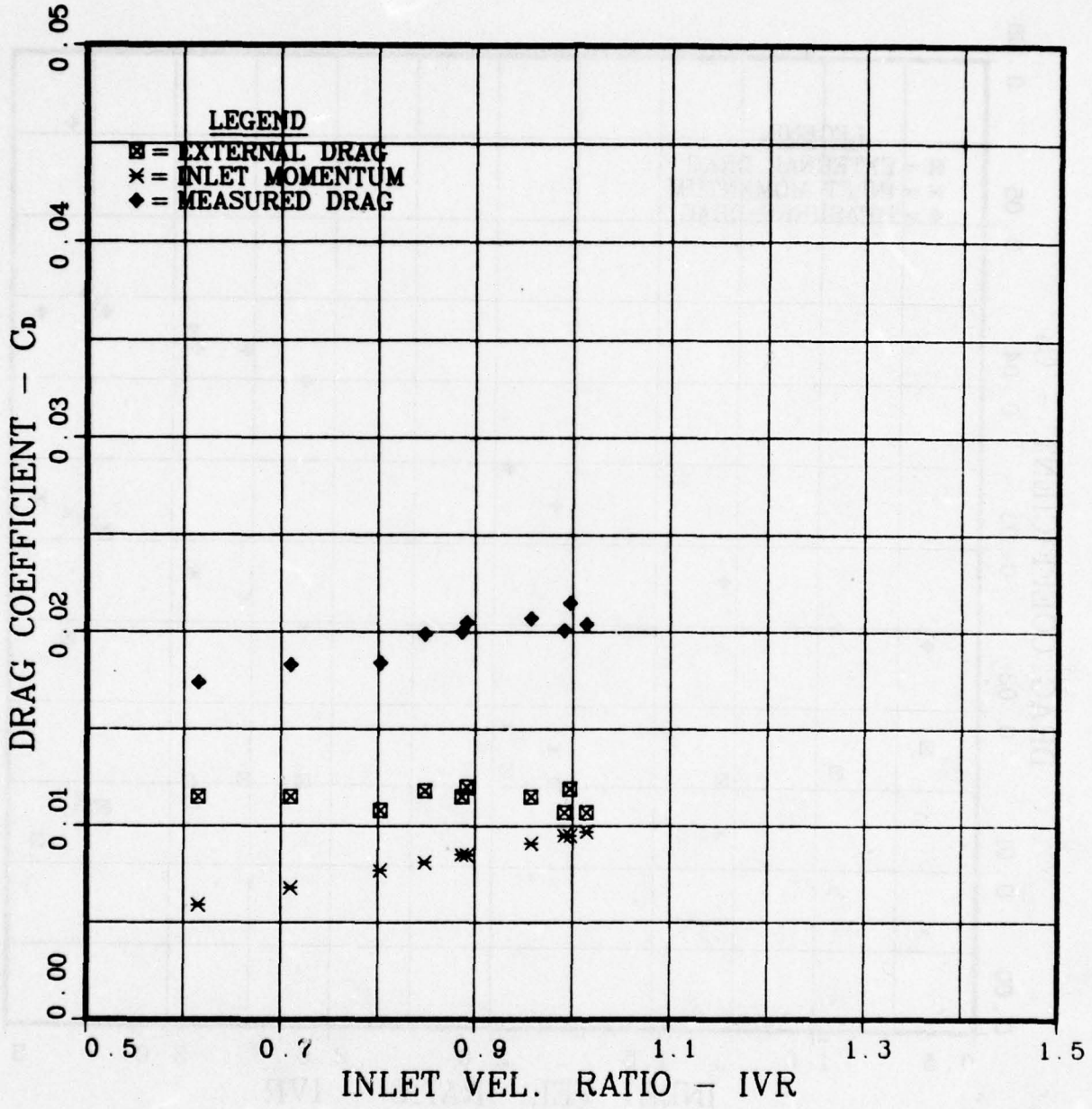

Figure 21 - Typical Inlet Drag Performance for a Range of IVR, Centerbody Extended, Simulated 100 Knots

where σ_i is the incipient cavitation number, A_m = the maximum cross-section area, A_i is the inlet area, and n is between 2 (for long bodies) and 3 (short bodies). Nothing is said about specific inlet shapes, and drag computations are not mentioned.

The basic premise in the Lockheed[2] inlet design method is that there exists an optimum relationship between internal system losses, external drag, and system weight such that the propulsive power required to produce a given thrust is a minimum.

The ideal jet propulsive efficiency is[10]

$$\eta = \frac{\text{work per unit time by thrust}}{\text{work per unit time by ideal pump}}$$

Assuming an IVR of unity, we obtain

$$\eta = \frac{\rho Q V_o (V_j - V_o)}{\frac{1}{2} \rho Q (V_j^2 - V_o^2)}$$

where ρ is the fluid density, Q is the volume flowrate, V_o is the inlet speed (= craft speed at unit IVR) and V_j is the jet speed. This expression reduces to

$$\eta = \frac{2}{1 + V_j/V_o}$$

This equation indicates that the propulsive efficiency is increased with lower values of jet velocity, which corresponds to higher values of flowrates for a given thrust. However, high flowrates require a ducting system with large cross-section areas to minimize the flow velocity. This large duct result in prohibitive values of both external drag and

system weight. Therefore, it is necessary to balance the internal flow losses of a given system configuration against the associated external hydrodynamic drag, while taking into account the resulting propulsive efficiency. Two optimization procedures are considered. One produces a ship with the minimum shaft horsepower for the displacement, speed and drag prescribed. In the other, the system is optimized for the maximum payload with a given maximum displacement.

The Lockheed optimization procedure relies heavily on drag estimates. For preliminary design purposes, total vehicle drag estimates are obtained first. These are used to determine power requirements, engine selection, etc., and to obtain rough layouts for all system components. These initial drag estimates are made without regard to the optimized propulsion system. To optimize the system, subsequent external drag calculations must be made to obtain the proper trade-offs between internal and external flows. The resulting shapes and drag coefficients can then be used to size the configuration, consistent with the system optimization requirements. Additional external drag calculations may be necessary to optimize a particular component, such as a diffuser, again independent of the system optimization.

The relative performance of selected inlet lip profiles can be evaluated on the basis of pressure distributions for a range of inlet IVR's. The minimum allowable cavitation number is determined from the operational conditions and requirements of the craft and the internal flow requirements to provide the necessary thrust over the entire speed range. Waterjet inlets should be designed for minimum external drag

within the limitations of internal flow and cavitation requirements. Minimum drag dictates a small external diameter, a minimum lip thickness, and minimum external length. Inlet lips are relatively short, and their length is normally not important for drag considerations.

A combination of internal and external lip shapes has been developed numerically to satisfy the requirements of hydrofoil vehicles. The basic precedure used is the numerical solution of the Neumann problem for potential flow. Once the basic profiles are determined by trial and error, the internal and external shapes are geometrically expanded to provide data on a family of inlets with varying diameter, length and thickness. Final designs for actual craft may require further considerations and possibly a final computation for the selected inlet. The Lockheed design method, therefore, relies heavily on interaction with the designer.

One of the most important factors to be considered in the design of high speed subcavitating inlets for waterjet propulsion is cavitation of the nacelle. The proper IVR must be selected such that no cavitation exists for the desired design conditions and preferably over the entire operating range. The occurrence of cavitation on an inlet can be controlled by the proper nacelle contour and IVR. For increasingly greater forward speeds, the critical pressure at which cavitation occurs decreased, with the associated requirement for more streamlined shapes. These shapes, however, result in longer nacelles and consequently greater drag.

The series A inlet (see Reference 9) was selected as the basic profile for the parametric computer calculations. Several members of this series were analyzed with the Neumann program to determine the pressure coefficient distribution. The selection of a particular design begins with the determination of the allowed pressure coefficient from cavitation requirements and the known operating conditions. From the propulsion requirements, an IVR can be estimated. With this IVR and the help of external pressure distribution curves, the designer selects an inlet size which will avoid cavitation, i.e., he/she chooses a particular member of the series A on the basis of external cavitation performance. Once this shape is selected, the pressures on the internal lip at other operating conditions can be checked. If these conditions are not satisfied, it may be necessary to select another shape and re-check. When the final selection is made, the nacelle size is determined. The drag must then be calculated and checked with the preliminary design assumptions to determine if the total vehicle drag will change significantly. If so, another iteration may be necessary.

Internal and external flow tests were made on a one tenth scale model of the Lockheed ram inlet design for a 550 ton, 80 knot supercavitating hydrofoil, and for a typical 50 knot subcavitating hydrofoil. The models represented the nacelle-inlet foil-strut configuration to scale, both externally and internally, up to the pump.

Subcavitating model:

The internal ducting for this model consists of a straight wall conical diffuser having a total included angle of 12 degrees and an

(area) diffusion ratio of 1.40 which reduces the flow velocity approximately 40% prior to entering the elbow. The area in the elbow is then reduced by 20% to minimize pressure losses and match the available area in the strut. The strut flow is then diffused with a total angle of 3.5 degrees and an area ratio of 1.90. The strut flow is divided into three channels by two splitters, the location of which is such that the diffusion rate is the same for each channel. The splitters also help provide structural rigidity.

Towing basin tests were run. At the scaled cruise velocity of 50 knots, the model was found to be free of cavitation at IVR's of .52 and .70. Similarly, no cavitation was found at 30 knots, the take-off speed. The overall pressure loss coefficient, excluding elevation losses, is shown is Figure 22, plotted against the Reynolds number based on inlet diameter and velocity. Total inlet drag is presented in Figure 23 as a function of IVR for two values of the submergence. Interestingly, the foil accounts for about 40% of the total drag.

Supercavitating model:

Provisions were made to allow the testing of various configurations of the system by interchanging the following duct components:

(a) two inlet lip contours,

(b) three elbows with varying rake angles,

(c) a variety of turning vanes, and

(d) two strut diffusion ratios.

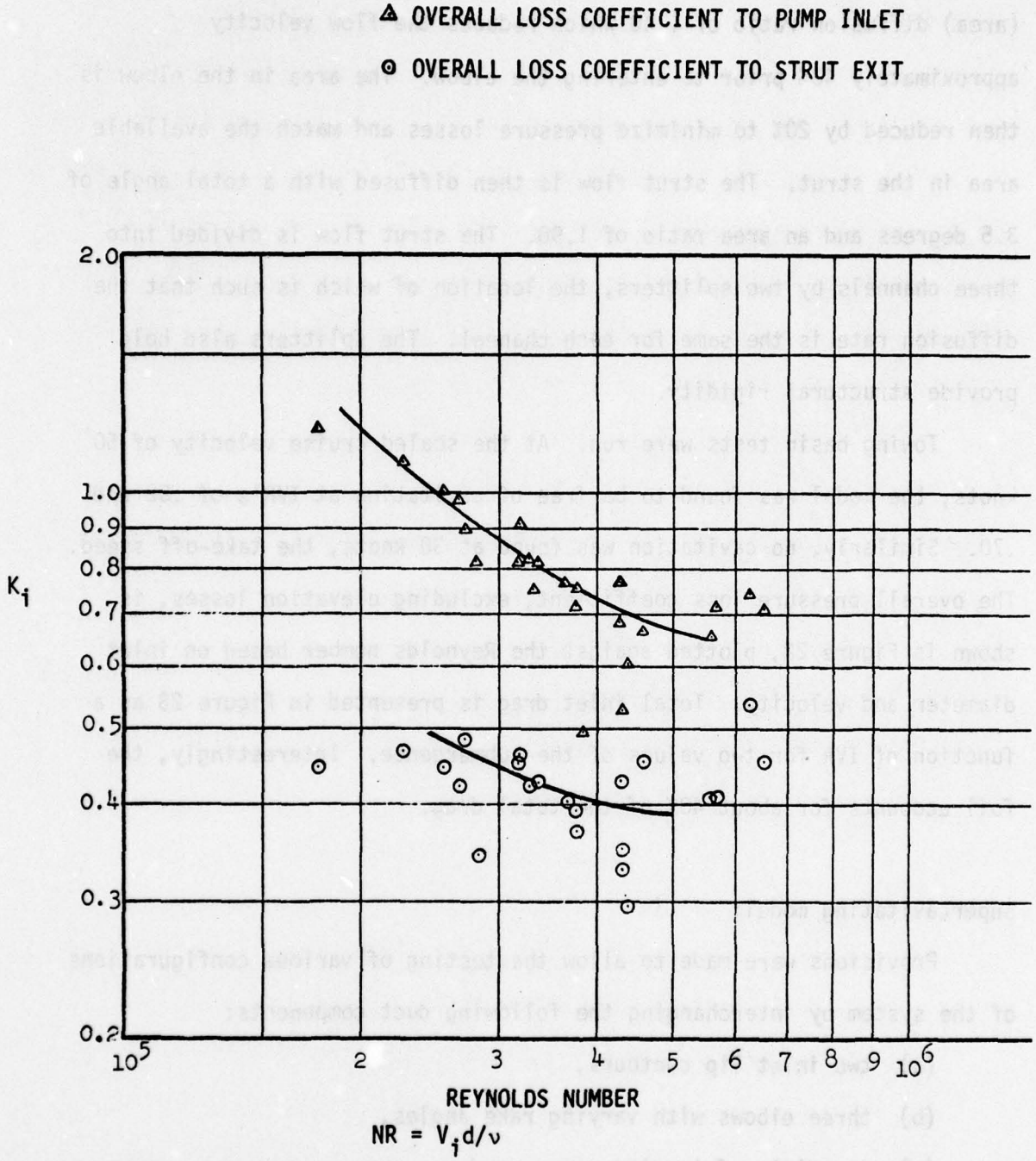

Figure 22 - Subcavitating Model - Overall Pressure Loss

$$K_i = \frac{p_{freestream} - p_{strut\ exit}}{q_{inlet}}$$

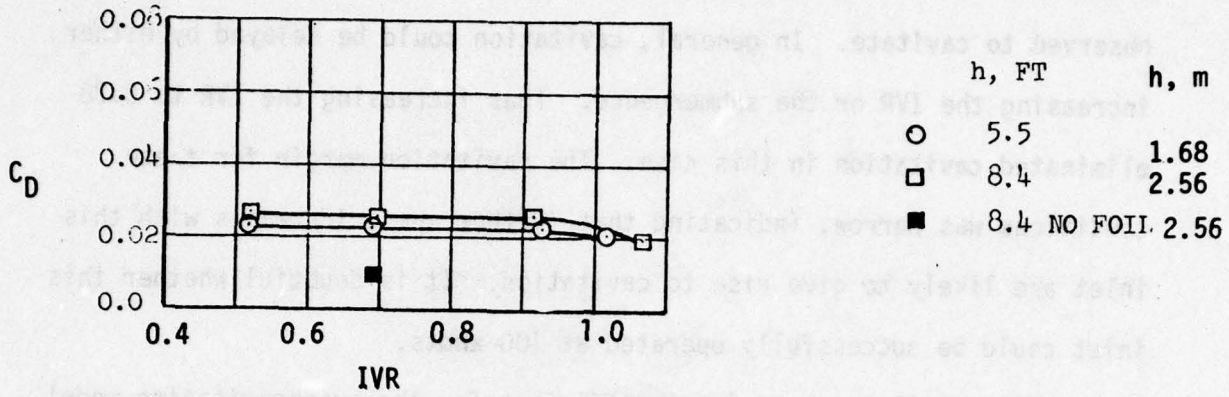

CRUISE 50 KT

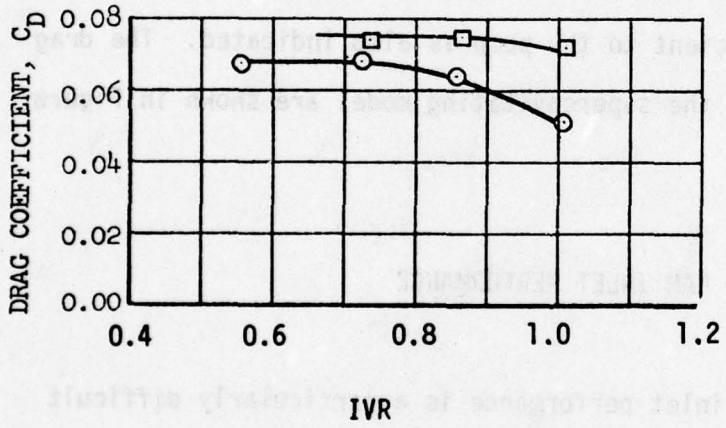

TAKE OFF 30 KT

Figure 23 - Drag Coefficient for Subcavitating Lockheed Model

This model was equipped with supercavitating foils. The nacelle itself was not meant to be operated under cavitating conditions. At 76 knots with an IVR of 0.52 and a submergence of 8.4 feet (2.56 m), the nacelle was observed to cavitate. In general, cavitation could be delayed by either increasing the IVR or the submergence. Thus increasing the IVR to 0.78 eliminated cavitation in this case. The cavitation margin for these conditions was narrow, indicating that further speed increases with this inlet are likely to give rise to cavitation. It is doubtful whether this inlet could be successfully operated at 100 knots.

The overall pressure loss coefficient for the supercavitating model includes all losses, with the exception of cavitation, from free stream to strut exit, and are plotted in Figure 24 against Reynolds number. In addition, the loss coefficient to the pump is also indicated. The drag coefficients obtained for the supercavitating model are shown in Figure 25.

RAM INLET PERFORMANCE

The subject of ram inlet performance is a particularly difficult one to address at this time in view of the (surprising) paucity of experimental data. The performance data presented in this section are derived exclusively from experimental results. This, it was felt, could provide the most reliable way of comparing various concepts for the purpose of singling out a particular concept on which to concentrate further research and developmental efforts. Three inlets are compared in

△ OVERALL LOSS COEFFICIENT TO CARRIAGE PUMP INLET

⊙ OVERALL LOSS COEFFICIENT TO MODEL STRUT EXIT

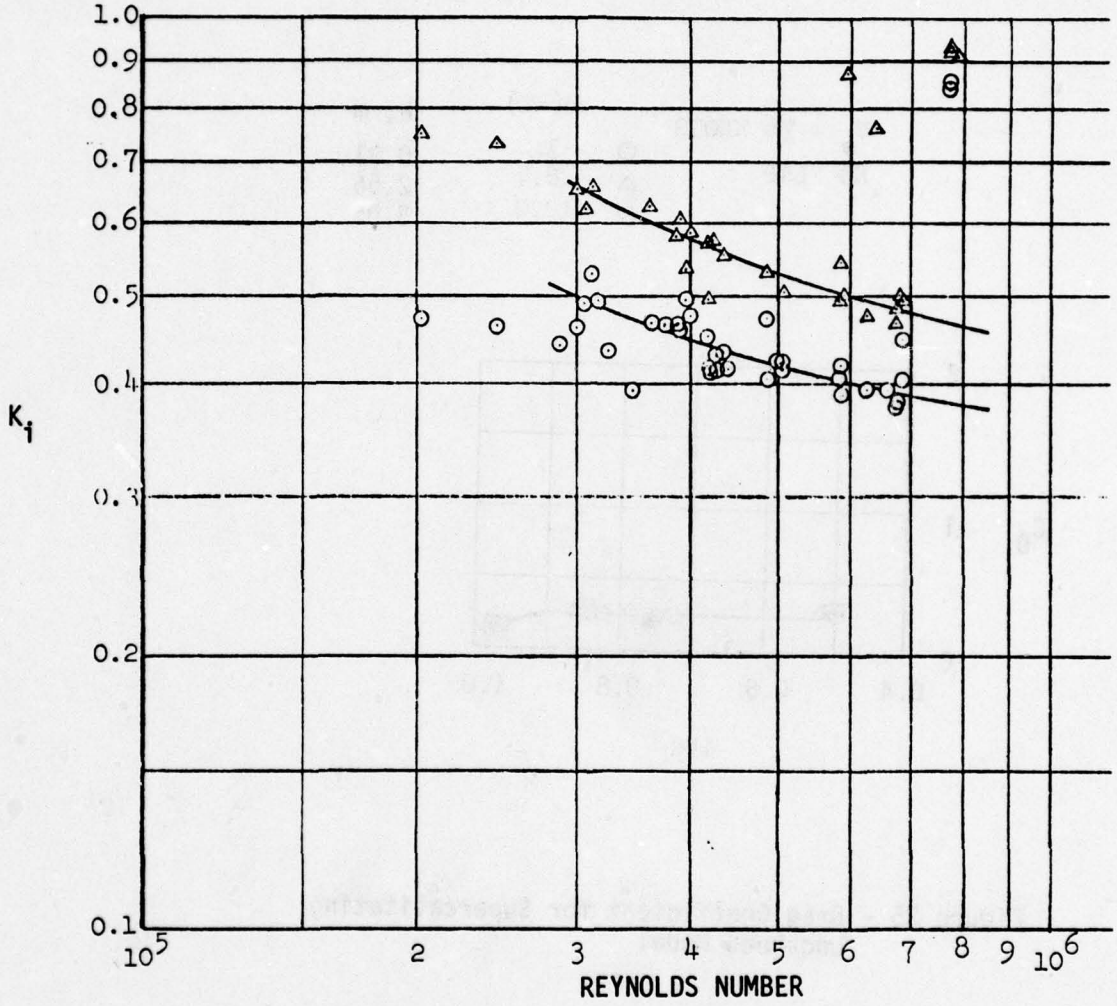

$$NR = V_i d/\nu$$

Figure 24 - Supercavitating Model - Overall Pressure Loss

$$K_i = \frac{p_{freestream} - p_{strut\ exit}}{q_{inlet}}$$

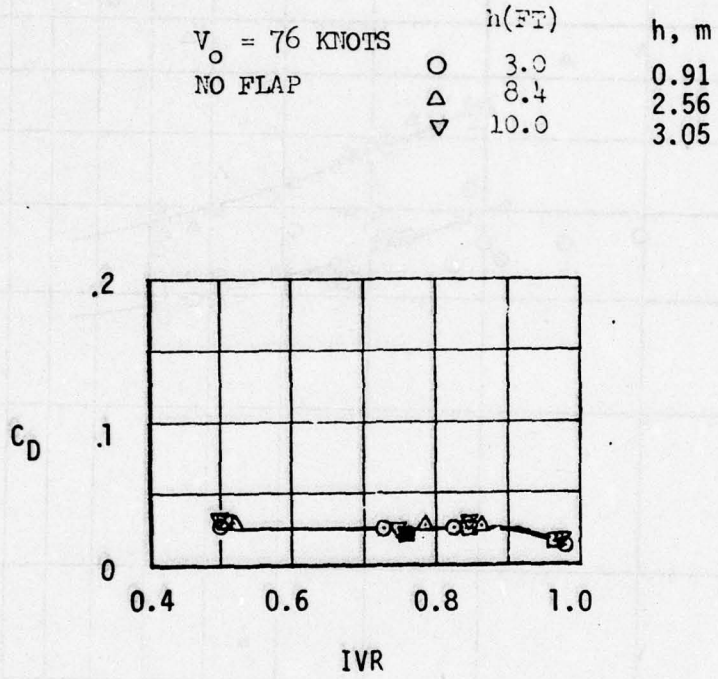

Figure 25 - Drag Coefficient for Supercavitating Lockheed Model

this section: the DSI pod with moveable centerbody, the Lockheed inlet, and the Aerojet inlet used on the SES 100A. The data for these inlets were taken primarily from References 2, 7, 8, 11, and 12.

The successful operation of strut-pod-propelled craft such as the Aerojet SES 100A and the PGH-2 Tucumcari has demonstrated the practicality of such inlets. The design technology for ram inlets is, in view of all the available experimental evidence obtained thus far, approximately as advanced as that for flush inlets. The Aerojet SES 100A has achieved a maximum speed approaching the design maximum speed with waterjet propulsion and a base-vented strut-pod inlet. The strut and pod are base-ventilated to achieve cavitation-free performance at the high maximum speed and to reduce inlet system drag. An auxiliary inlet located in the strut leading edge provides variable inlet area.

The SES 100A model test data, while limited, are useful in setting an upper bound on inlet drag for very high speed, variable area inlets. These data indicate a high speed inlet drag coefficient (based on high speed inlet area and ship speed) of about 0.45. The energy recovery data are complicated by the complex internal ducting. The data of Reference 13, for a simplified geometry, indicate a loss coefficient of 0.10 to 0.15 at a typical design IVR of 0.7-0.8 for the initial portion of the inlet. From these data, overall loss coefficients of 0.20 to 0.25 seem probable at typical design IVR's.[11]

Three inlet lips were tested with inlet-to-pod diameter ratios of 0.4, 0.45 and 0.50. For each of these, the internal and external cavitation boundaries were determined. Figure 26 indicates the

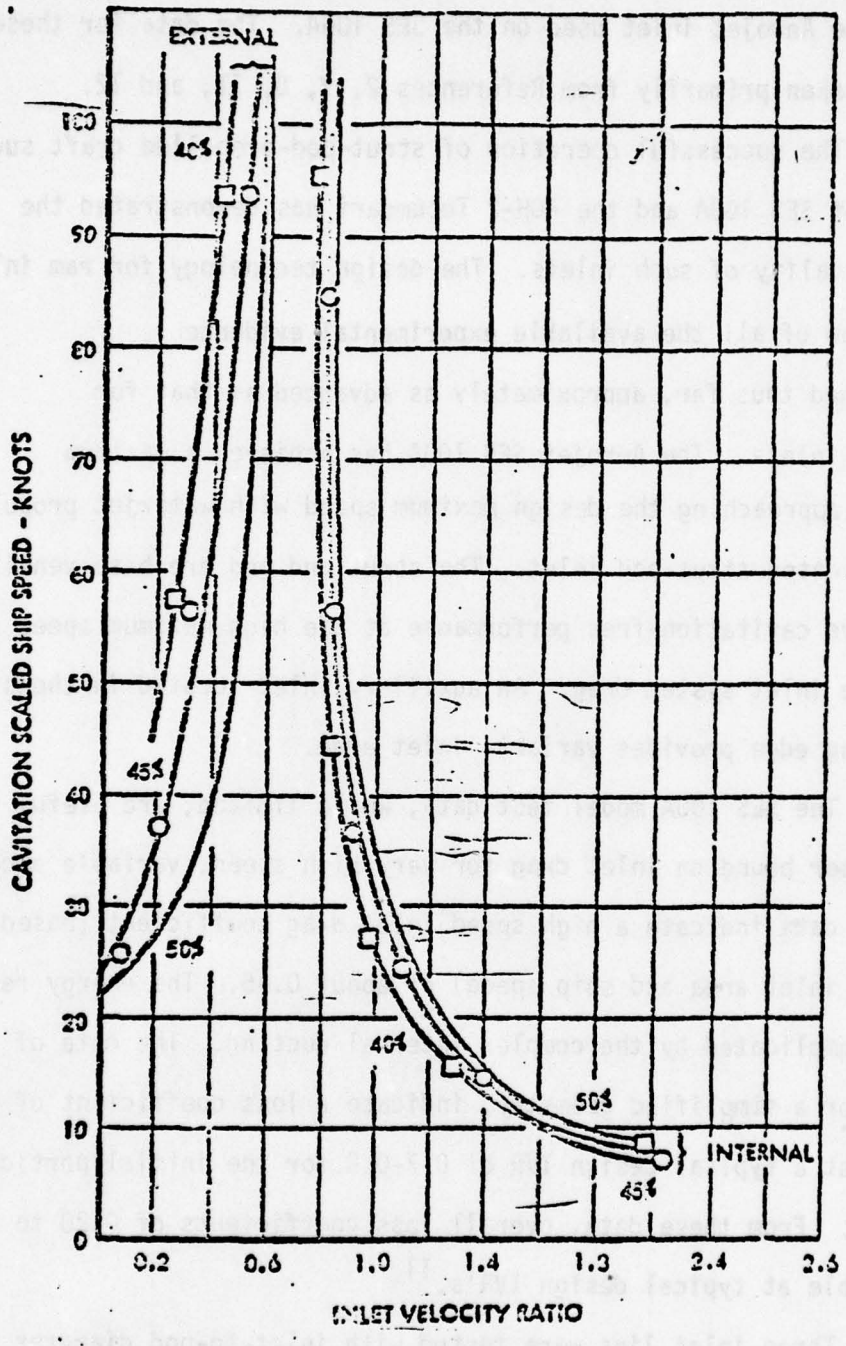

Figure 26 - Comparison of Cavitation Characteristics for Primary Inlet to Pod Diameter Ratios of 40%, 45% and 50%

cavitation performance of each diameter ratio inlet. Based on its high cavitation-free internal flow capability, the 0.50 diameter ratio inlet was selected for complete performance evaluation. The auxiliary inlet was tested at the full open (8.5 inches, .216 m) position in conjunction with the 0.45 diameter ratio primary inlet. Within the speed and IVR ranges investigated, the primary inlet would cavitate internally before inception took place on the auxiliary inlet, see Figure 27.

The cavitation performance of the DSI pod was found to be satisfactory at scaled cruise speed, but the inlet choked at scaled hump speed. From this, it was concluded that the inlet could not accelerate the craft beyond the hump condition. Although it has been speculated that a redesign of the centerbody could solve this problem, no steps, theoretical or experimental, have been taken in this direction.

The drag figures reported for various inlet concepts are not easy to interpret. For example, the drag coefficients which are presented for the DSI pod[8] are based on <u>estimated</u> total wetted surface area. Drag figures obtained from different tests cannot be compared since typically, different inlet components are included. For example, Sobolewski[8] reports on measurements performed on the pod plus a nearly vertical strut, while the test performed on the Aerojet inlet[13] included the pump and nozzle. While shaft and nozzle thrust were "measured out," pump, ducting and exit nozzle drag were not included in the final drag figures. The effects of interactions near the impeller can only be guessed at. For these reasons, it is not possible to meaningfully compare drags from various tested inlet concepts. Similarly, the lack of uniformity in

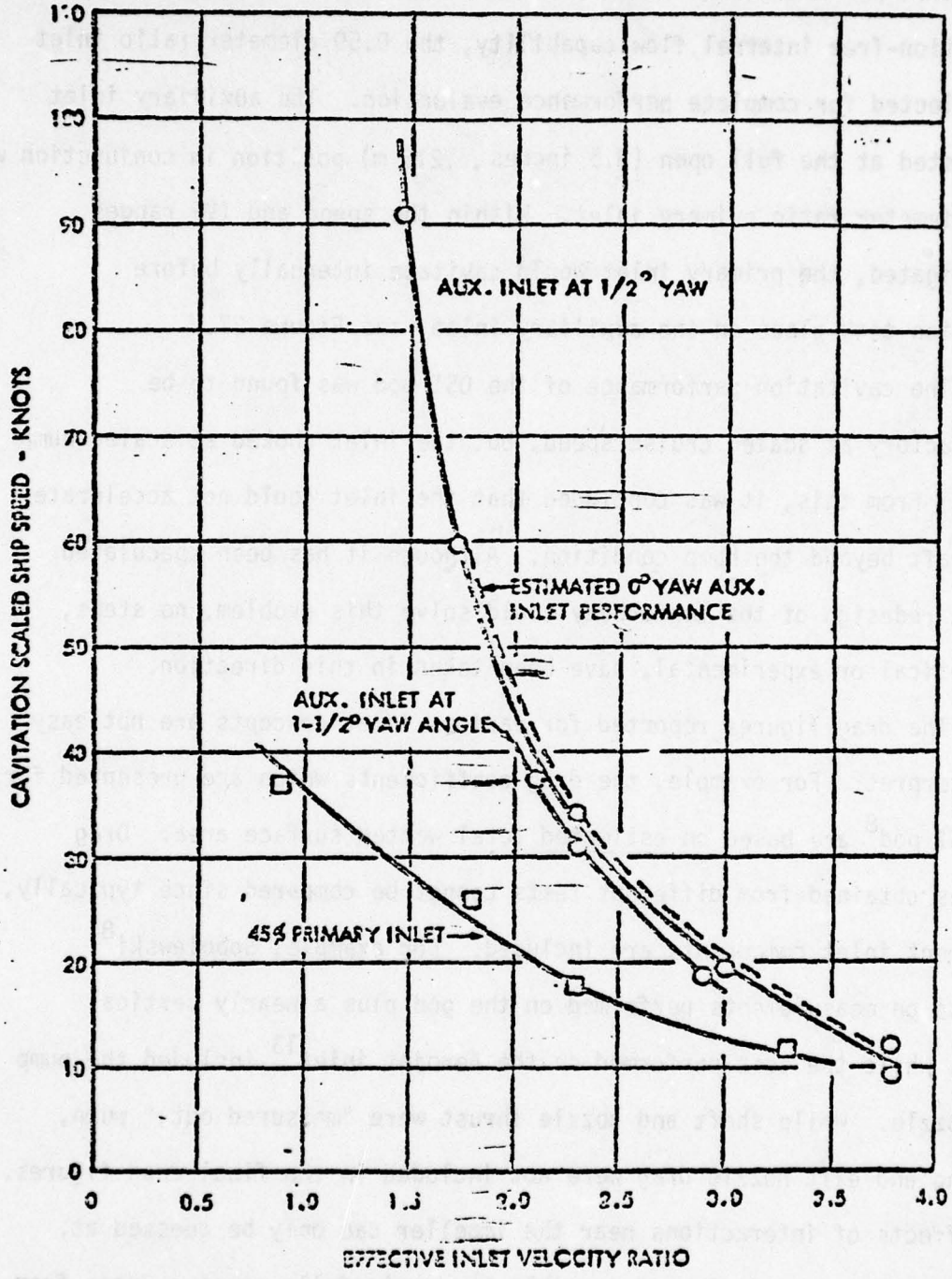

Figure 27 - Internal Cavitation Inception Speed vs Effective Inlet Velocity Ratio for 45% Inlet Cowl; Constant Auxiliary Inlet Opening of 8½ in. (0.22 m).

reporting pressure losses makes it difficult to establish comparisons. Cavitation, on the other hand, is less ambiguously reported, simply because of the qualitative nature of the data. A performance chart, Table 2, comparing the three tested inlet systems summarized the relevant experimental data. On the basis of cavitation alone, the Aerojet inlet is the only one which performed satisfactorily; presumably, the DSI and Lockheed inlets could be redesigned to avoid cavitation, but the Aerojet inlet is already full-scale proven concept.

The most important performance criterion for waterjet inlets is that they operate without choking at hump condition and without extensive cavitation at cruise speed. An inlet's first requirement is that it operates without unwanted cavitation. Secondary requirements include efficient performance (low drag, good pressure recovery). From this point of view the Aerojet inlet is superior to its candidates, with a respectable cavitation margin $\Delta IVR = 0.2$ at 100 kt with an IVR of 0.70. The Lockheed inlet system, which barely avoids cavitation at 76 kt with an IVR of 0.75, and the DSI inlet with its hump cavitation choking, are poorer performers. It would appear that Aerojet's strut auxiliary openings constitute an effective and proven method of increasing the flowrate at hump condition.

Inlet Description and Reference	Type	Design Speeds (knots) Cruise/Hump	Measured Energy Recovery Ratio	Drag Coefficient based on		Cavitation	Comments
				Total Wetted Area	Inlet Area		
DSI (7,8)	ventilated base variable area movable centerbody	100/35	0.75/0.60 at 75% of strut height	.02/.04*	1.67*	lip cavitation at cruise speed, but meets flowrate	chokes at hump, * drag figures include strut drag
Lockheed (2)	subcavitating fixed area	50/30	0.68*	.025/.07 **		cavitation free	*form and friction losses to strut exit included **foil drag included
	supercavitating fixed area	80/40	0.65*	.03/.13 **		nacelle cavitates	
Aerojet (12)	auxiliary inlet on strut SES 100A	100	0.90*		0.45	ΔIVR = 0.2 at 100 kt	* to inlet discharge flange proven in full scale tests

TABLE 2 - SUMMARY OF INLET PERFORMANCE

DISCUSSION AND RECOMMENDATIONS FOR INLET DESIGN

Three ram inlet design methods were reviewed. The DSI method designs an inlet according to cavitation requirements and then calculates the resulting drag. Should the inlet be too draggy, modifications are made on the basic design. The Lockheed method is similarly not suited for computer implementation as it relies heavily on humans flipping through graphs and charts. The Sherman and Lincoln method, however, can be adapted for numerical optimization. Here, the various drag formulas can be entered as separate program elements and the optimization can effectively be made by computing the trade-offs between internal losses and external drag.

Certain incertitudes remain, especially with regard to the relation between pressure and additive drag. Clarifications should be made in this area. In addition, the drag computation method could be updated to include recent developments in this field. With these improvements, the Sherman and Lincoln method could be adapted as the Navy's in-house design method for ram inlets.

According to Etter,[14] for speeds less than 50 knots, fixed geometry waterjet inlets are acceptable. In the case of high performance craft, especially those with low speed humps, the inlet design may be governed by the need for variable geometry in order to accommodate a cavitation-free passage through the hump speed. For SES and hydrofoil ships, which have

nearly equal flow requirements at hump and cruise speeds, the inlet must either have a variable area capability or be able to operate over a wide range of IVR's. Etter maintains that the most practical variable area scheme for pod-strut inlets is the use of an auxiliary strut inlet which can be opened or closed with a sliding gate. The only other variable area concept which appears feasible for high speed pod-strut inlets is the "sliding centerbody" concept.

Barr and Stark[11] reviewed the performance of existing waterjet-propelled high speed craft. The SES 100A utilizes base-vented strut-pod inlet. Variable geometry is achieved by means of an auxiliary inlet located in the strut leading edge, allowing a 135% area increase over that of the pod alone.

For high speed craft such as hydrofoils and SES, which have large thrust requirements at low speed, the use of variable area inlets is essential. As the flowrate requirements at hump and cruise speeds are approximately equal in the applications, a wide variation in operating IVR's is needed to accommodate the flow. A fixed area inlet operating over a wide range of IVR's would necessarily have a large inlet radius, which in turn significantly adds to the inlet drag. A completely variable inlet, on the other hand, can accommodate a constant flowrate over the entire speed range without any change in IVR, and requires no leading edge radius. Such an inlet has a lower drag coefficient. A realistic design is a compromise between these two extremes, with a finite leading edge radius allowing operation over a limited range of IVR's.

In a review of waterjet propulsion,[14] Etter remarks that the strut cross section must provide adequate structural strength and internal duct

area and must permit cavitation-free operation at all operating speeds and yaw angles. Below 60 knots, fully wetted sections have the lowest drag. At high speeds, fully wetted sections have poor strength and inadequate resistance to cavitation at yawed conditions due to their small thickness, making base-vented sections preferable.

The comparison of various design concepts is a difficult task for several reasons. Inlet design is still in its infancy and the current state-of-the-art leaves plenty of room for improvements, particularly in the area of drag and cavitation predictions with flow over complex boundaries. The comparison of experimental data is not so clearly defined either. For example, Boeing designed an inlet system for the PGH-2. These fixed area, rectangular-shaped inlets were designed for a cruise speed of 50 knots and tested at the St. Anthony Falls Hydraulic Laboratory.[15] The pressure loss coefficient was measured over IVR's ranging from 1.20 to 2.5. The lack of data below unit IVR makes comparisons difficult with other data. Furthermore, the PGH-2 inlet has several strut elbows, a lossy duct geometry. On the other hand, the craft operated satisfactorily for several years. No serious cavitation damage occurred.

It is recommended that the Sherman-Lincoln design philosophy be utilized in developing a computer code for the generation of axisymmetric strut pod inlet systems. The program should have a modular struture to facilitate improvements (see for example Reference 16). The nacelle shape families and the drag estimation methods should be reviewed in the light of recent developments.

Based on admitedly limited test data on auxiliary inlets and variable geometry, it appears that the high speed aerojet concept is superior.

It is therefore recommended that the high-speed Aerojet concept be adopted for further development. This system utilizes an auxiliary opening situated on the strut leading edge and operated by a sliding gate. Unlike the movable centerbody concept, no increase in nacelle size is needed to accommodate the increased flowrate mechanism. This concept was successful in the SES 100A and therefore has proven potential as a parent form for similar strut pod inlet systems. The preliminary developmental design work performed by Code 1532 can be applied to the design of such inlets.

When high speed (≃ 100 kt) applications are considered, Sherman and Lincoln[3] have convincingly demonstrated the need for a variable inlet for cavitation-free operation. For relatively low speed applications (< 50 kt) where a significant hump drag does not exist, fixed area waterjet inlets may be acceptable, according to Etter.[14] In any case, caution should be exercised when designing inlets for the upper end of this speed range, where additional inlet area may prove beneficial at off-design conditions. This makes the Aerojet auxiliary strut apertures even more attractive since they represent an easier design problem than the fitting of a moveable centerbody. In designing for this speed range, a fixed area inlet should first be considered. If adequate flowrate is not provided at off-design conditions, then auxiliary inlets can be added to the design without altering the nacelle itself. Thus, for the intermediate speed range, it is recommended that the benefits of having additional intake area be investigated on a case-by-case basis.

ANALYTICAL DRAG PREDICTIONS

The success of any inlet design method to a large extent depends on its ability to estimate drag accurately. This section reviews drag calculations within the context of waterjet inlet design. We first present a brief discussion of the various forms of drag (e.g., skin friction drag, form drag, etc.), emphasizing fundamental hydrodynamic principles. A brief review of current theoretical predictive techniques follows. Design programs usually utilize drag prediction methods which are based on empirical knowledge, an attempt to fill in, by careful usage of experimental data, the large gaps in the formal theories. Various design programs will be reviewed and their drag prediction methods outlined.

Skin Friction Drag

Viscosity, through the action of shear force, couples the body surface to the fluid, allowing the body's momentum to diffuse throughout, resulting in fluid acceleration. The body therefore experiences a force, called skin friction or viscous drag, contrary to the direction of flow in the vicinity of its surface. Where the flow is laminar, viscous diffusion of momentum is the only source of skin friction drag, and a reliable theory has been developed. With turbulent flow, eddies contribute to momentum transfer by a convective process for which no rigorous theory exists at present. However, many useable empirical results exist (e.g. the Schoenherr line).

Form Drag

Whereas skin friction drag is (locally) a tangential force, a normal force of viscous origin can also arise when flow occurs past a surface which is not everywhere parallel to the main stream. This force is known as the pressure drag or, since it depends on the shape of the boundary, the "form" drag. Another name often used is "viscous pressure drag," which necessarily excludes the induced drag due to lift.

An important cause of form drag is flow separation. A boundary layer in an adverse (positive) pressure gradient will experience a retarding effect which will be particularly strongly felt near solid boundaries, where the fluid possesses little momentum. In fact, the layer of fluid immediately adjacent to the solid boundary may lose all of its streamwise momentum, and reverse its direction under the influence of the adverse pressure gradient . The recirculation (separation) regions thus created are typically at lower pressures than we would expect from purely potential flow pressure recovery. Thus, pressure differences can be induced across a body by flow separation, resulting in a net drag.

At the base of projectiles, there originates a pressure drag which is consequently termed "base drag." This is a result of the boundary layer separation at the base edge. A good discussion of this phenomenon is given by Hoerner.[17]

Cavity Drag

The drag of bodies that are exposed to cavitation or ventilation, is not the same as that for the fully wetted case. Generally, cavitation is

a condition to be avoided in the design of strut-pod inlets. There are situations however when ventilation cannot be avoided, or when cavitation (or ventilation) are deliberately introduced to reduce the wetted area even at the expense of increased cavitation drag. It is with the last situations in mind that we now consider the subject of drag at low cavitation numbers.

The cavity drag of a body corresponds to an average positive pressure on its wetted side and to the uniform negative pressure within the cavity.[17] The drag coefficient of sharp-edged bodies (e.g., discs and cones) can be reliably predicted with the relation

$$C_D = C_{D_o} (1 + \sigma)$$

where $\sigma = (p_o - p_{vapor})/q_\infty$ is the cavitation index, and C_{D_o} is the drag coefficient for the $\sigma = 0$ condition. This formula is also valid for supercavitating wedge-shaped struts.[18]

The precise effect of cavitation number on the drag of even simple bodies of revolution with fixed detachment is not entirely understood. The drag coefficient is known to increase asymptotically ($\sigma \to 0$) according to the above-given formula. However, the magnitude of the σ range over which this law is applicable depends on the fullness of the body.

Interference Drag

This is an inherently "engineering" term, a powerful reminder of the complexities and apparent vagaries of fluid dynamics, and a testimony to the engineer's determination. Interference drag, unlike skin friction,

form drag or cavity drag, is not related to any specific physical phenomenon. Rather, it arises when complex flows are regarded as being formed of a superposition of simple (and calculable) flows, plus an ad hoc "interference" or interaction term to account for any difference between this simplistic and asynergistic model and reality.

A good review of hydrodynamic interactions on high performance craft propulsion systems is given in Reference 19.

Wave drag, the resistance associated with energy being radiated away in the form of surface gravity waves, is usually considered negligible for strut-pod inlets, since wave drag decreases markedly with increasing submergence. Furthermore, at the high Froude numbers encountered wave drag is expected to be small.

PREDICTIVE STATE-OF-THE-ART

In this section, we describe analytical methods representative of our current state of knowledge in the area of hydrodynamic drag prediction. Rather than being fully understood, the major contributing factors to drag are subjects of active research. Few are the instance where we stand on firm theoretical ground and consequently, empiricism is often used.

Excluding cavity and lift effects, hydrodynamic drag is a consequence of fluid viscosity. The relationship between viscosity and drag may be a direct one, as in the case of skin friction drag, or indirect, as where flow separation or turbulence occur. The concept of

the boundary layer, either laminar or turbulent, is almost always used so that potential flow calculation methods do find their place in hydrodynamic drag predictions, as a first step in the evaluation of boundary layer effects. Potential flow has been extensively studied and a mathematically rigorous theory has been firmly established. Unfortunately, the small number of practical cases for which analytic solutions can be obtained precludes a general analytical approach to design problems. With the advent of digital computers and efficient numerical techniques, potential flow problems with complicated boundaries became tractable. Two general approaches can be taken. In one, the equations of Laplace (or Poisson, where sources are present) are directly solved by finite difference schemes within boundaries on which the flow is prescribed. The solution must be found at every mesh point even though one may only be interested in the flow over a certain limited subdomain, over a body surface for example. This method will not be considered here. An alternative and more economical approach consists in replacing bodies with appropriate source distributions giving the same normal flow at the boundaries. The total number of nodal points is therefore reduced to that necessary to describe body surfaces, and the problem reduces to a computation of the source strength, from which the flow at any point external to the body may also be found. This approach has been refined by J.C. Hess and A.M.O. Smith.[20] Axial symmetry can be exploited to further reduce the number of surface elements and allowances can be made to introduce in the computation those flow components which can be described analytically, resulting in an increased computational flexibility. Thus, potential flow calculations are well in hand.

A distinction must be made between theoretical calculations used as research tools and design computational methods. Rather than offering an exhaustive review of recent advances in the fundamental research of boundary layers, flow stability and other topics of significant relevance to drag prediction, we choose rather to concentrate on calculational methods actually used by designers, and the drag models used to motivate these techniques; we pay only cursory lip service to research calculations.

Reliable methods for the numerical computation of boundary layers have been developed.[21-24] These solve the boundary layer equations in their differential form and therefore provide information about details of the flow. These methods can, and indeed have been used in drag calculations, but require numerous computational steps resulting in much information, little of which is directly relevant to viscous drag. The reason is that drag is an integral property of the flow and can be computed without a detailed knowledge of the boundary layer structure. More economical approaches in drag predictions have evolved from so called integral methods in which the boundary layer equations are first integrated in the cross-stream direction to provide relationships between various gross features of the flow.

The viscous friction experienced by a body in motion in a real fluid can be obtained from the body's influence on the surrounding fluid. Through the action of viscosity, momentum is imparted to the fluid, evident at first as large velocity gradient in the boundary layer. The effect is cummulative as one proceeds from the leading edge stagnation

point to downstream stations. Increments in body surface result in increased viscous drag and additional shed momentum, which diffuses and contributes to the thickening of the boundary layer. Clearly then, an evaluation of the accummulated momentum deficit at the trailing edge or in the wake can be utilized in calculating the viscous drag. Such methods have been developed by integral calculations and have produced various "approximate formulae" relating drag to body shape, potential flow and kinematic viscosity. As a rule, models ignore separation and are regime-dependent. That is, a uniformly valid formula for laminar and turbulent flow cannot be found. Although these formulas are relatively accurate, their applicability to practical cases depends upon reliable methods to determine the point separating the laminar and turbulent flow regions. Often, laminar separation trigger turbulence so that its onset must also be considered.

In the drag prediction methods whose descriptions follow, a pattern is seen to emerge. The flow is divided into various regions: potential away from the body, a laminar boundary layer grows from the stagnation point up to a transition point whose location is determined by one of several semi-empirical techniques. Thereafter, the flow is assumed to be fully turbulent.

Laminar separation presents additional problems which have been conveniently dismissed with the assumption that the elimination of separation form drag represents the first step in finding optimal body shapes. Consequently, most design methods are concerned with reducing drag on nonseparating bodies.

To be sure, laminar separation can be predicted numerically, and shows up as a singularity beyond which boundary layer computations cannot be continued. The singularity, however is a consequence of the mathematical formulation used, and not a feature of the flow to be studied. Nevertheless, it does serve as an indicator of separation. The parabolic nature of the boundary layer equation precludes a continuation of the solution within the separated region in the absence of upstream boundary conditions. These and other topics related to our current state of knowledge on boundary layer are lucidly treated in two excellent review papers.[25, 26]

J.L. Hess presented a method[27] to design by analytic means a class of axisymmetric bodies having low drag in incompressible flow for the case where the boundary layer is fully turbulent over the entire body. He compared various drag calculation methods to find that the Truckenbrodt formula,[28] which expresses drag as an integral of a power of the potential surface velocity, is sufficiently accurate, and this formula is adopted as his chief analytical tool:

$$C_D = \frac{2\pi L^{1/7}}{A} C_f \left[\int_{body} \left(\frac{u_s}{u_\infty}\right)^{10/3} r_o^{7/6} \, ds \right]^{6/7}$$

where the integral is over the entire body profile. L is the body length, u_s the potential surface velocity, s the arc length and C_f is the skin friction coefficient, which for smooth bodies is taken to be

$$C_f = \frac{0.455}{(\log N_R)^{2.58}}$$

where N_R is the Reynolds number based on body length. This expression differs little from the friction coefficient obtained from the Schoenherr line as expressed by the formula

$$\log (N_R C_f) = \frac{0.242}{\sqrt{C_f}}$$

A comparison of the two appears on Table 3.

$\log R_e$	Schoenherr $\times 10^3$	$\frac{455}{(\log N_R)^{2.58}}$
5	7.18	7.16
6	4.40	4.47
7	2.93	3.00
8	2.07	2.13
9	1.53	1.57
10	1.17	1.20

TABLE 3 - SKIN FRICTION COEFFICIENTS

In this paper, three drag prediction methods were compared with experimental data to determine the relative accuracy of these methods. The Truckenbrodt formula was compared with the result of using the finite difference boundary layer method in Young's formula. The outcome of this comparison was that the simplified integral formula of Truckenbrodt is definitely more accurate. Next, the momentum integral boundary layer

method, Patel[29], was used in conjunction with Granville's drag formula[30]

$$C_D = \frac{4 \pi r_o \theta}{A} \left(\frac{u}{u_\infty}\right)^{(7H + 17)/8}$$

This was compared with Truckenbrodt's formula, and with the finite difference-augmented Young formula. The calculation based on the momentum integral (Patel-Granville) was found to be the most accurate of the three methods studied. Despite this, Truckenbrodt's formula was preferred over the other two methods due in large part to its simplicity. It seemed unlikely to the author that any overall conclusions drawn on the basis of this formula would be drastically overturned by use of the momentum integral method. The experimental data were obtained, Gertler[31], for a series of eight bodies of revolution in a towing tank. Results of the comparison are shown in Table 4. The comparison is shown in terms of the r.m.s. fluctuations between theory and experiment. No results are reported for the momentum integral approach at a Reynolds number of ten million.

	$N_R = 10^7$	$N_R = 2 \times 10^7$
Truckenbrodt	3%	5%
finite difference	6%	8%
momentum integral	—	3%

TABLE 4 - RMS % ERROR IN HESS' DRAG COMPUTATIONS (See Ref. 27)

The small number of bodies used by Hess to justify the use of the Tuckenbrodt formula was deemed insufficient by White[32] to establish the method's validity. An extensive comparison of the Truckenbrodt formula with experimental drag data obtained from seven series of model forms comprising nearly fifty bodies was undertaken. The computed drags show very little sensitivity to such parameters as the prismatic coefficient, the position of maximum section, and the nose and tail radii. The author concludes that the Truckenbrodt formula cannot be recommended for preliminary design or drag evaluation purposes, and that while the formula does in certain cases predict drag trends which agree with experimental data, it is by no means capable of defining optimums and is very likely to be in error for many cases. A summary of White's comparisons appears in Figure 28.

Kerney and White[33] recently introduced a method for the calculation of viscous drag on streamlined (i.e., non separating) bodies of revolution. Their approach was to use an integral method based on Granville's, supplemented by recently improved methods for predicting the transition point and for calculating the turbulent boundary layer. The Douglas-Neumann program is used to compute the inviscid pressure distribution over the body. This is used as an input to the boundary layer calculations which, in the laminar case, are identical to those of Granville.[30] The transition point is found from a new correlation of transition data for bodies of revolution in terms of the difference between the momentum-thickness Reynolds number at the transition and neutral stability points, and the rate of change of body shape. This method was proposed by Granville[34] and applied to curved bodies. Their predictions

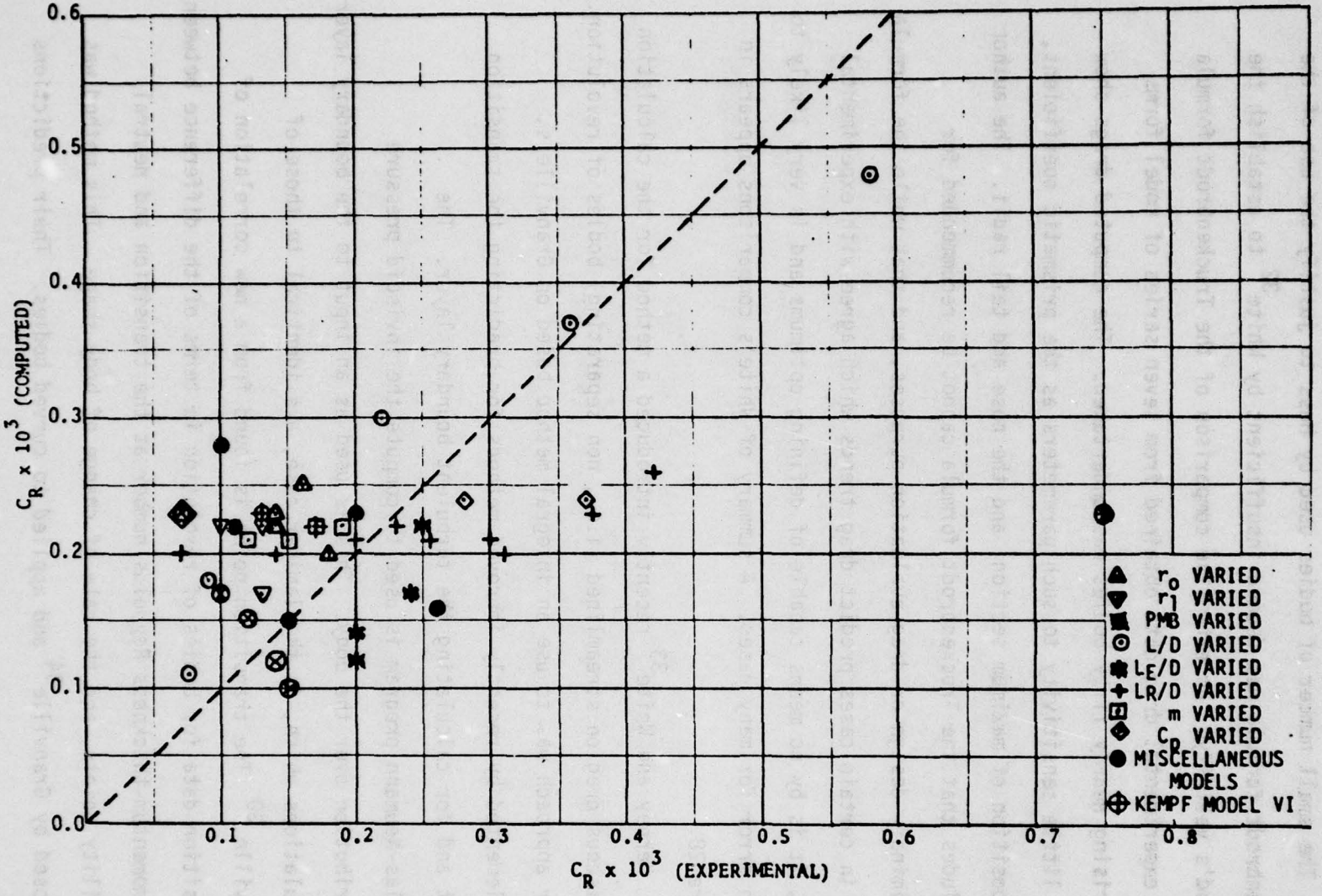

Figure 28 - Summary Comparison for Computed and Experimental Residuary Drag Coefficients ($C_R = C_D - C_f$) for all Cases

were compared with data on bodies of revolution with and without parallel middlebodies from recent experiments. Bodies without straight middle sections were represented by the DOLPHIN, from drop tests in the Pacific Ocean,[35, 36] whereas data on three bodies of revolution with parallel middlebodies came from recent DTNSRDC towing tank tests of models 4620-2, 4620-3 and 4620-4. Predicted and observed drag coefficients and transition points for DOLPHIN exhibited considerable scatter, which was attributed to variations in the ocean ambient turbulence level between tests, but Granville's 1953 method was deemed a better predictor of transition. Consequently, drag was also predicted more accurately with this method. Models 4620-2, 4620-3, and 4620-4 have streamlined forebodies and afterbodies separated by parallel middlebodies (see Figure 29). Drag predictions in the 3% to 7% accuracy range were typical, with better accuracies obtained above Reynolds numbers greater than ten million. The authors conclude that the updated turbulent boundary layer of Granville [37] is capable of giving reasonable predictions of the viscous drag on streamlined bodies of revolution as long as the transition point is accurately located. Their program, however, does not take into account displacement effects (which would increase the form drag). For Reynolds numbers less than ten million, they suggest that a better method of prediction for the transition point is needed.

A.M.O. Smith and T. Cebeci[38] presented the results of an attempt to improve presently available methods for predicting viscous drag. Two approaches were taken. In the first, they attempted to directly compute the drag from the shear and pressure stresses with the Douglas-Neumann

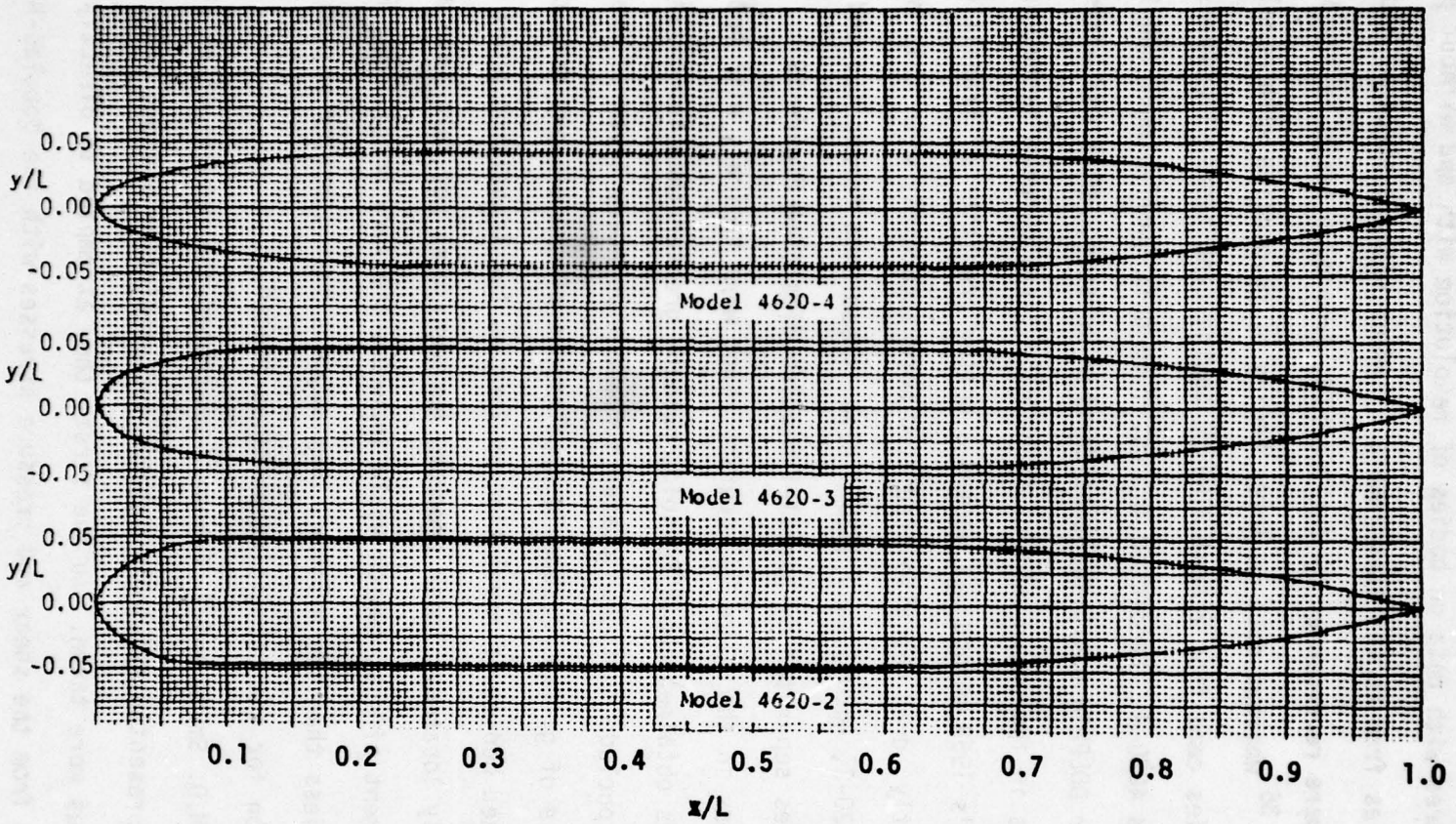

Figure 29 - Nondimensional Plot (x/L, y/L) of Series 4620- 2, 3, 4, Models

potential flow program, and the Cebeci-Smith turbulent boundary layer program, which in principle are ideally suited for this type of study. This approach was found to produce reasonable shear stresses, but the pressure drag calculations were all wrong, being negative in some instances. The exact reason for this strange result is not known, but the authors suspected difficulties arising partly from improper boundary conditions near the body's trailing edge.

The second approach was to stick to the basic momentum defect method, and to try to improve the calculations in the wake, resulting in a possible improvement over the Squire-Young formula. Direct numerical calculations (finite difference) were coupled to the Squire-Young formula. The Squire-Young formula was used, but the boundary layer parameters were obtained from finite difference calculations using the Cebeci-Smith method. The turbulent calculations on the body were done using the eddy viscosity concept, and the calculations were extended into the wake by using the mixing length approach. This enabled the computation to proceed through the problematic region of large changes near the trailing edge. The results were found to be closer to experimental data than the unmodified Squire-Young approach, leading the authors to conclude that their method is promising. They noted, however, large differences in their results depending on how far downstream the wake calculation was carried. Much more work, therefore, needs to be done in this area before a design technique can take advantage of the modified Squire-Young technique.

Parsons et al.[39] presented a method for the synthesis of minimum drag hulls for axisymmetric vehicles of specified enclosed volume and constant speed submerged in incompressible viscous fluid at zero incidence. The

flow was assumed to be nonseparating and noncavitating. Drag reduction was accomplished solely through variation of vehicle hull shape. They claimed their drag model to be representative of the state-of-the-art in drag prediction methods.

The boundary layer was assumed laminar from the stagnation point (leading edge) up to a transition point after which it was assumed to be fully turbulent. Turbulent separation was not allowed. The mainstream inviscid velocity distribution along the body surface was computed with the help of the Douglas-Neumann[20] program; viscous displacement effects were not considered. The incompressible axisymmetric boundary layer equations were solved iteratively using an implicit finite difference method developed by Cebeci and Smith.[21] A two-layer eddy viscosity model is used in the turbulent boundary layer computation. Boundary layer transition to turbulence is predicted by the Smith-Gamberoni method, or by laminar separation/assumed turbulent reattachment, whichever occurs first. The Smith-Gamberoni method calculates from the Orr-Sommerfeld equation the amplification rate of Tollmien-Schlichting waves in the laminar boundary layer. Transition is assumed to occur where the amplification factor exceeds a certain empirically determined value, in this case, e^9.

The drag coefficient is calculated using Young's formula[40]

$$C_D = \frac{4\pi}{V^{2/3}} r_o \theta \left(\frac{u_e}{u_o}\right)^{(H+5)/2} \Bigg|_{T.E.}$$

evaluated at the trailing edge, where V is the body volume, and u_e is the velocity at the edge of the boundary layer.

No direct comparison with experimental data is presented, however, a design is arrived at which has a lower drag coefficient (0.0051) than the DOLPHIN (0.0076) at Re = 10^7.

In 1970, W.L. Moore[41] reported a computer program bringing together the best techniques then available for calculating the forces on the components of a hydrofoil boat. All flows were considered turbulent, with the Schoenherr mean line used throughout the calculations to define the friction coefficient, since a compromise had to be effected between accuracy and required computing time. The techniques used to calculate strut drag are those suggested by Hoerner.[17] The foil profile drag is calculated by using the formula

$$C_D = 2\, C_f \left[1 + 2\left(\frac{t}{c}\right) + 60\left(\frac{t}{c}\right)^2\right]$$

where C_f is the Schoenherr friction coefficient, and t/c is the maximum thickness-to-chord ratio on the foil. This formula includes the effects of skin friction and form drag on the foil. This formula is used incrementally and then integrated numerically to account for any variations of strut thickness ratio and strut chord along the strut length. In the case of surface-piercing struts, an empirical term is added to account for spray drag, with the spray drag coefficient equal to 0.24. For totally submerged struts, a term is included to account for the interference drag between strut and hull

$$C_D = 0.75\left(\frac{t}{c}\right) - 0.0003\left(\frac{t}{c}\right)^2$$

where the reference area is taken to be the square of the strut thickness.

Pod drag is calculated using empirical equations fitted to certain unpublished TMB-series 58 body of revolution drag measured at various angles of attack. No further details are given on pod drag.

Strut-pod interference drag is calculated using Hoerner's method,[17] which is to calculate twice the drag of that portion of the strut covered by the pod. This is added to the calculated drag of the uncovered part of the strut.

The method was primarily developed for strut-foil and strut-pod-foil combinations, as reflected in the awkward presentation of the drag data: the lift coefficient is plotted against the drag coefficient. Drag predictions are good at low values of the lift coefficient but rapidly drop below the 10% accuracy level at lift coefficients corresponding to angles of attack exceeding 6 degrees.

Nakayama and Patel[42] calculated the viscous resistance of bodies of revolution in the absence of separation. Their method consists in separately calculating laminar and turbulent components of the resistance, with the transition point to be determined empirically. Although their paper emphasizes difficulties associated with the thickening of the boundary layer near the tail of the body, their drag calculations are relevant to our study. They find that the resistance of bodies of revolution can be predicted with considerable accuracy provided the exact location of the transition point is known or can be found. This gives confidence in the various integral methods which are used to calculate the viscous resistance in various flow regimes (laminar, turbulent), and emphasizes the importance of being able to predict the transition from one flow regime to another.

AD-A052 710 DAVID W TAYLOR NAVAL SHIP RESEARCH AND DEVELOPMENT CE--ETC F/G 20/4
A REVIEW OF RESISTANCE PREDICTION AND DESIGN METHODS FOR STRUT---ETC(U)
MAR 78 P LAFRANCE

UNCLASSIFIED SPD-789-01 NL

2 OF 2
AD
A052710

END
DATE
FILMED
5-78
DDC

From a potential flow calculation, Nakayama and Patel proceed to compute the boundary layer momentum thickness with a simple quadrature formula of the form

$$\delta_\theta^2 = \frac{0.47\nu}{r_o^2 u_e^6} \int_o^x r_o^2 u_e^5 \, dx$$

which is essentially the method of Thwaites.[43] Here, δ_θ is the momentum thickness, ν the kinematic viscosity, x the distance measured along the surface from the stagnation point, $r_o(x)$ the radius distribution of the body, and $u_e(x)$ is the freestream (potential) velocity outside the boundary layer. The momentum thickness was used in the prediction of the transition to turbulence. Other boundary layer parameters required in the transition prediction were obtained from Pohlhausen-type velocity profiles.

Transition to turbulence was determined from four empirical or semi-empirical criteria, namely those of Michel,[44], Granville,[30] Crabtree,[45] and van Driest and Blumer.[46] The turbulent boundary layer calculations were carried out according to a method developed by Patel.[29] The drag was evaluated by a computation of the momentum deficit at the tail of the body, by using Young's formula.

Comparisons with experimental data revealed that no one transition prediction method is to be preferred over the other. In view of this, experimentally obtained transition point locations were used in boundary layer calculations. In other words, rather than using empirically derived transition information, the authors sought guidance from experiments for this part of the computations. It was subsequently found that the

development of the laminar and turbulent boundary layers is predicted satisfactorily, provided the transition point is accurately specified. Resulting drag predictions were found to be quite good, many within one percent of the experimental value.

Cebeci et al.[47] presented calculations of viscous drag for two dimensional and axisymmetric bodies. Drag was calculated from Granville's formula

$$C_D = \frac{2\theta}{A} \left(\frac{u_e}{u_\infty}\right)^B , \quad B = \frac{(H + 2)\, n + 3}{n + 1}$$

evaluated at the trailing edge of the body. The above formula reduces to the Squire-Young formula for two dimensional bodies by setting $n = 1$ in which case θ is the momentum thickness and A is the chord. For axisymmetric bodies, $n = 7$, θ is the momentum area, and A is a suitable area characteristic of the body. Cebeci et al. obtained their boundary layer parameters not from an integral approach, but from a more exact finite difference solution developed by Cebeci and Smith.[22] Boundary layer separation was not considered. To predict transition to turbulence, the empirical method of Michel[44] was utilized. This method is based on a correlation of transition-momentum-thickness Reynolds number $N_{R,\theta}$ with transition x-Reynolds number, $N_{R,x}$ approximated by the formula

$$N_{R,\theta} = 1.174 \left(1 + \frac{22400}{N_{R,x}}\right) N_{R,x}^{0.46} , \quad 10^5 \leq N_{R,x} \leq 6 \times 10^7$$

Theoretical predictions of the drag coefficients were compared to experimental data for airfoils. The r.m.s. error based on 57 drag values was found to be 2.9%. The error in calculated drag increased with the angle of attack. Displacement thickness corrections were found necessary for bodies with fineness ratios (length/maximum diameter) less than 4, while for slenderer axisymmetric shapes, skin friction accounted for the experimental drag.

DRAG PREDICTION METHODS ACTUALLY USED IN DESIGN PROGRAMS

In this section we discuss drag prediction methods which have been implemented in strut pod design programs.

Developmental Sciences, Inc. (DSI) designed a pod inlet[7] for a 200 ton, 100 kt hydrofoil craft. The external pod shape was determined by the requirement that there be no external cavitation at cruise speed. Details about their calculation methods are sparse, making an evaluation of their design difficult. The external drag was determined by computing the turbulent boundary layer over the exterior surface and integrating the skin friction up to the point of separation. the calculations were then continued beyond the separation point by using an unexplained empirical relationship. Four options were analyzed: i) fully wetted pod with short boattail, ii) a linear extension of the boattail which eliminated separation, iii) a ventilated base and iv) extended base ventilation. The relative magnitudes of skin friction and form drag are not discussed, nor is any account made of the strut drag, or strut-pod interference effects.

A very understandable account of the problems associated with strut-pod inlet design was presented by Sherman and Lincoln.[3] The stagnation streamline divides internal and external flows and the total drag is the sum of internal and external drags.

$$F_{NET} = F_{INT} + F_{EXT}.$$

The external drag coefficient is given by

$$C_{D_{ext}} = \frac{1}{A_i} \int_{A_i}^{A_{max}} C_p \, d A + \left(1 - \frac{V_i}{V_\infty}\right)^2 + C_{DS}$$

where A_i is the inlet area, V_i/V_∞ the IVR, and C_{DS} is the "system drag" which is the summation of all the external viscous drag forces plus any external pressure and interference drags not previously accounted for. The second term in the above expression, dubbed "pre-entry drag," has its origin in the acceleration of the flow in the region ahead of the inlet.

For fully settled turbulent flow, the system drag coefficient of the ram inlet nacelle based on its external wetted area is estimated from the following formula allegedly obtained from Hoerner:[17]

$$C_D = C_{fn}\left[1 + 1.5\left(\frac{d_m}{\ell_o}\right)^{1.5} + 7\left(\frac{d_m}{\ell_o}\right)^3\right]$$

where d_m is the maximum external nacelle diameter, ℓ_o the nacelle length and C_{fn} is not defined by the authors. Similarly, the fully wetted external turbulent viscous drag coefficient for the supporting strut is obtained from the same source:

$$C_D = 2\, C_{fs}\left[1 + 2\left(\frac{t_m}{c_o}\right) + 60\left(\frac{t_m}{c_o}\right)^4\right]$$

where t_m/c_o is the thickness to chord ratio. Any interference drag between the nacelle and strut is considered negligible for small values of strut thickness to chord ratio. The spray drag based on strut planform area is given by

$$C_D = 0.03 \frac{t_m}{c_o}$$

for Froude numbers (based on the chord) greater than 3.

The external viscous drag of the system is reduced if a base vented strut and nacelle are used. In this case spray drag may be anywhere from 1/6 to 1/2 of the total strut drag. Using Hoerner's method for determining the total drag of a base vented strut (including spray drag), the following formula is obtained

$$C_D = 2\, C_{fs} \left[1 + 2 \left(\frac{t_m}{c_o} \right) \right] + 0.12 \frac{t^2}{chs} + \frac{t\, g\, h_s}{c\, v^2}$$

Again, the nomenclature is not explained. The total drag of a base vented nacelle (based on the wetted nacelle area) is given as

$$C_D = C_f \left[1 + 1.5 \left(\frac{d_m}{\ell_o} \right)^{1.5} \right] + \frac{2\, g\, h_N}{v^2} \frac{\pi\, r_m^2}{A_N}$$

where g is the acceleration due to gravity, h_N is the submergence, V is the speed, A_N the wetted area and Y_m the maximum radius ($= d_m/2$).

The strut drag in supercavitating flow is given as[18]

$$C_D\,(\sigma) = C_D\,(\sigma = 0)\,(1 + \sigma)$$

where

$$\sigma = \frac{p - p_{cav}}{\frac{1}{2} \rho V^2}$$

is the cavitation number, and $C_D(o)$ is the drag coefficient at zero cavitation number. The authors produce the following formula for the system drag coefficient for a supercavitating ram inlet

$$C_D = \sigma_N + \left[C_D\,(0)\,(1 + \sigma)\,\frac{h_s\,t_m}{A_i} \right]$$

where the first term is the nacelle cavitation number, and the second term represents strut drag based on inlet area.

For the purpose of internal loss analysis of waterjet inlets the inlet is broken into three components: the inlet diffuser, the transition elbow joining the strut and nacelle, and the strut diffuser section. A total head loss is obtained for the inlet by summing the component losses. Elevation losses are not considered in these calculations.

The inlet diffuser is a critical component of the waterjet duct system. Since the dynamic pressure is greatest at the diffuser entrance, an inefficient diffuser will seriously degrade overall propulsor performance at high speeds. Sherman and Lincoln's method of predicting diffuser losses is an approximate two-dimensional laminar and turbulent boundary layer calculation beginning at the inlet stagnation point and terminating at the maximum internal inlet diameter. The effects of axial symmetry and wall curvature on boundary layer development are not considered.

The Neumann problem is solved to obtain the potential flow. A step-by-step solution of the integral boundary layer equations is then used

to obtain the distribution of momentum thickness,displacement thickness and shape factor along the diffuser.

Transition is assumed to occur when a certain critical value of the displacement thickness[28] is reached. The turbulent portion of the boundary layer is calculated from Truckenbrodt's integral analysis. Starting with the value of momentum thickness at the transition point, the momentum thickness turbulent shape factor, and the displacement thickness are calculated along the wall. The value of the shape factor for which separation will occur is generally found to be between 1.8 and 2.4. However, a shape factor of 3.1 has been shown applicable to conical diffusers and is used as the upper limit in Sherman and Lincoln's analysis.

With subscripts 1 and 2 denoting the diffuser entrance and exit, respectively, the diffuser pressure recovery efficiency is calculated as follows. Once the displacement thickness is known, the effective area at the diffuser exit is given by

$$A_{2,eff} = \frac{\pi}{4} (d_2 - 2\delta)^2$$

The overall static pressure recovery is defined as

$$C_{pr} = \frac{p_2 - p_1}{q} \quad , \quad q = \tfrac{1}{2} \rho v_1^2$$

The ideal static pressure recovery for inviscid one dimensional flow is given by

$$C_{pr,i} = 1 - \left(\frac{A_1}{A_2}\right)^2$$

The diffuser efficiency or effectiveness is simply the ratio of overall to ideal pressure recovery.

$$\eta_D = \frac{C_{pr}}{C_{pr,i}} = \frac{p_2 - p_1}{q\left[1 - \left(\frac{A_1}{A_2}\right)^2\right]}$$

Assuming a one dimensional potential core flow outside the boundary layer, the diffuser efficiency becomes

$$\eta_D = \frac{1 - \left(\frac{A_1}{A_2}\right)^2_{eff}}{1 - \left(\frac{A_1}{A_2}\right)^2}$$

The total head loss in the nacelle elbow is expressed by an equation of the form

$$H_L = \left(K_T + 4\,\frac{L}{d_e}\,f\right)\frac{v^2}{2g}$$

where the friction factor f is obtained from circular pipe data using the equivalent hydraulic diameter d_e, and L is the elbow length. With complex geometries, component losses are assumed to be additive. The effect of channel curvature on the friction factor is, in the above equation, given by replacing f by

$$f_c = f\left[N_R \left(\frac{d_e}{2r}\right)^2\right]^{0.05}$$

where r is the turning radius. The straight duct friction factor f is

calculated from Nikuradse's formula

$$\frac{1}{\sqrt{f}} = 4 \log_{10} (N_R \sqrt{f}) - 0.40$$

The strut channel is treated as a rectangular diffuser with two convergent walls. Again using the upstream and downstream subscripts 1 and 2, respectively, strut losses are calculated using the following approximation for a truncated diffuser:

$$H_L = \left[C K_{T_1} + 4 \frac{L}{d_e} + K_{T_2} \left(\frac{A_1}{A_2}\right)^2 \right] \frac{v_1^2}{2g}$$

where the friction factors are given in Reference 34.

The Lockheed design method[2] also resorts to a formulary for the calculation of drag. In the subcavitating case, strut drag is composed of parasite and spray drag. Strut parasite drag is estimated by

$$C_D = 2 C_f \left[1 + 1.2 \left(\frac{t}{c}\right) + 60 \left(\frac{t}{c}\right)^4 \right]$$

where C_f is the Schoenherr friciton factor. Spray drag is obtained from

$$C_D = 0.24 \, q_\infty \, t^2$$

where $q_\infty = \frac{1}{2} V_o^2$ in the dynamic pressure.

Without further ceremony, the Lockheed report refers the reader to Hoerner[17] and "various NACA publications" for method of estimating strut, foil and nacelle interference drag. The drag coefficient for the nacelle is estimated by the following equation which is based on wetted area

$$C_D = C_f \left[1 + 1.5 \left(\frac{d_m}{L}\right)^{3/2} + 7 \left(\frac{d_m}{L}\right)^3 \right]$$

where d_m is the maximum external nacelle diameter and L is the maximum nacelle length.

The drag of base-vented nacelles is determined by the differences in pressure distribution between the base and the nose after deducting the internal momentum drag. The nose pressure is the sum of atmospheric and hydrostatic pressures. While the base pressure is atmospheric. The total base drag is then taken to be the product of hydrostatic pressure times the base area.

Interference drag of strut, nacelle and foil intersections resulting from flow separation along the afterbody intersections is considered negligible.

Internal pressure losses are caused by a) friction on the duct walls and b) form effects due to changes in the size, shape or direction of the duct and are, in general, proportional to the kinetic energy of the fluid for any duct configuration. For circular duct, the surface area is πLd (L = duct length, d = diameter) and the pressure loss can be expressed in terms of the Fanning friction factor F

$$\frac{\Delta p}{q} = 4 \frac{L}{d_h} F$$

where q is the dynamic pressure, d_h, the hydraulic diameter, is defined by

$$d_h = 4 \frac{\text{cross sectional area}}{\text{wetted perimeter}}$$

and F is given graphically in the Lockheed report as a function of Reynolds number and surface roughness. For all ducts associated with waterjet systems, Lockheed recommends that the smooth pipe curve be used.

Pressure losses due to changes in shape and direction of the duct are proportional to the dynamic pressure and can be expressed as

$$\frac{\Delta p}{q} = K_T$$

where K_T depends on the particular duct configuration. The total pressure loss for any component can be expressed by the sum

$$\frac{\Delta p}{q} = K_T + 4 F \frac{L}{d_h}$$

The purpose of diffuser is to convert kinetic energy at the entrance into pressure at the exit with a minimum loss in total pressure. The total pressure loss is directly related to the internal drag of the component while the exit flow distribution affects the operation of the duct components located downstream of the diffuser. It has been shown (although no reference is given in the Lockheed report) that for a given expansion angle and fixed inlet conditions, the total pressure loss of a diffuser is proportional to the theoretical value of total pressure loss for a sudden expansion of the same area ratio. The proportionality factor is defined as

$$K = \frac{(p_{t_1} - p_{t_2})/ q_1}{\left[(A_R - 1)/ A_R\right]^2}$$

where $A_R = A_2/A_1$, and the subscripts 1 and 2 define respectively the diffuser inlet and exit stations, P_t denotes the total pressure and q the dynamic pressure.

Two geometric variables are considered important in diffuser operation: area ratio and expansion angle. In general, Lockheed considers that the design of a good waterflow diffuser can be accomplished by having a uniform inlet velocity profile and keeping the expansion angle 2α between 8 and 12 degrees. It is also advantageous to prevent local flow separation due to wall roughness and sudden changes in flow direction. If possible, the diffuser axis should be straight. It is also claimed (again, no reference cited) that diffusers having an area variation such that the axial pressure change varies directly with the length achieves a better exit total pressure recovery than a conical diffuser of the same length and contraction ratio. A diffuser of this type has a so-called "trumpet" shape with an increasing rate of change of cross sectional area with distance from the inlet. (Interestingly, the trumpet shape is condemned by Sherman and Lincoln[3] as particularly susceptible to separation).

$$\frac{d_p/p}{d(x/L)} = \text{constant}$$

The loss coefficient for bends and elbows is a function of many variables: duct cross sectional shape, turning angle, turning radius, area variation and Reynolds number. The total loss coefficient for elbows is given by

$$\frac{\Delta p_t}{q} = C K_{t_{90}} + 4 F \frac{L}{d_h}$$

where $K_{t_{90}}$ is the loss factor for 90 degree bends and C is a correction factor for bends other than right angle. These quantities are presented

graphically in the Lockheed report. Losses in ducts may be reduced considerably by employing splitters or turning vanes which divide the flow in parallel channels, each having a larger radius to diameter ratio and aspect ratio than the original elbow. Care must be exercised to insure that the increased friction losses resulting from the splitters are not greater than the improvement in form loss.

REVIEW OF THE EXPERIMENTAL DATA

Presently attainable drag performance levels are indicated in Table 2. The drag coefficient (based on inlet area and cruise speed) of the Aerojet inlet is 0.45 and not inordinately out of line with the representative figure of 0.35 given by Etter.[14] Sobolewski's measurements[8] give 1.67 for the DSI model inlet system, but it must be remembered that this figure includes strut drag.

The predictive accuracy of existing drag prediction methods is described in Table 5.

In studying waterjet inlet technology, one becomes acutely aware of the deficiencies in a field which has not yet reached maturity. In the present situation, one faces a variety of experimental measurements of "inlet drag" by investigators who do not subscribe to the same definition of this important quantity. Although all drag measurements reported here were made on ram inlets, some data include foil drag and others contain the effects of internal ducting and even the exit nozzle. Strictly speaking,

Method	Investigator	% Error
Truckenbrodt	Hess (27)	4
Momentum Integral	Hess (27)	3
Young's Formula	Hess (27)	7
Truckenbrodt	White (32)	>50 (see text)
Granville	Kerney, White (33)	3-7
Hoerner	Moore (41)	≈10
Nakayama-Patel	Nakayama, Patel (42)	1
Cebeci	Cebeci et al. (47)	3

TABLE 5 - APPROXIMATE PREDICTIVE ACCURACY OF DRAG PREDICTION METHODS

each measurement is therefore valid only for the particular hardware on which it was performed. Fundamental differences between drag measurements performed on various inlet concepts preclude a direct comparison of their relative merits. Furthermore, one must regard the available data with a skeptical mind.

The effect of the variable area factor (the ratio of maximum to minimum inlet area) on inlet drag has been presented by Etter.[14] Smaller inlet drags are obtained with large variable area factors since less leading edge (lip) thickness is needed. In other words, by accommodating a demanding flowrate schedule with a variable area inlet, one no longer needs large and draggy lip thickness. The trade-off between lip

thickness and variable area factor is such that an overall lesser drag is obtained with variable area inlets. While Etter's conclusions are demonstrated for flush inlets, there is no reason to expect a different conclusion for strut pod inlets.

CONCLUSION AND RECOMMENDATION CONCERNING INLET DRAG

In reviewing drag prediction methods, it became clear that particular attention must be paid to the various flow regimes (laminar, turbulent, separated) in order to arrive at an accurate drag figure. Various approximate approaches have been developed to identify these regimes and to compute the resulting drag. The method of Nakayama and Patel[42] appears to be quite accurate (1% error) and utilizes only flow integral parameters, meaning that a detailed knowledge of the boundary layer structure is not needed. It must be said that this is an active field of research and that more literature on this subject is likely to be generated in the near future, but a drag prediction technique based on an integral flow analysis appears to be promising for inlet applications.

Sherman and Lincoln[3] have demonstrated the importance of internal losses in the design of strut-pod inlets. A reliable method of estimating these losses in strut pod structures is needed, and can be formulated from an empirical study of pressure profiles in such structures.

RECOMMENDATIONS FOR FURTHER WORK

In view of the eventual goal of establishing a reliable design method for strut-pod inlets, special efforts should be concentrated in the following areas.

1. It should be determined if the nacelle and inlet shapes proposed by Sherman and Lincoln are indeed optimal from a cavitation point of view. Systematic ways of producing cavitation free nacelle contours should be investigated.

2. There is an urgent need for a definitive report on inlet drag and losses. This would include analytical work aimed at clearly identifying the various components of drag and internal losses, their effect on inlet and craft performance, and would serve as a guide to experimenters in making measurements that can be meaningfully compared.

3. As previously mentioned, the Sherman-Lincoln design philosophy of minimizing overall losses in cavitation-free inlets should be coded as a modular program.

4. A review of optimization techniques should be made to find a rapid and efficient method of evaluating the many trade-offs encountered in inlet design. Specifically, a numerical optimization scheme should be recommended for inclusion in the modular design program.

5. A review of presently existing pressure data obtained from tests performed on actual inlets should be examined with the objective of formulating a reliable internal loss formula based on actual model tests. Such data already exist and if needed, further tests could be performed on the (suitably modified) DSI pod, a model of which already exists at DTNSRDC. Such a formula would inherently include interaction effects and would be specifically applicable to the strut-pod concept.

6. Another area in need of study is the vane system at the strut-pod elbow. This area is susceptible to cavitation and high losses. Several approaches are possible, from a multi-element vane system to the compartmentalization of the elbow into a few channels separated by flow dividers. A cavitation and loss analysis should be performed to develop an optimum flow turning geometry.

7. A simple momentum analysis of the flow in an around the inlet does not provide a satisfactory estimate of the drag, since no control volume can be specified with known velocities and pressures on all of its surfaces. An alternative method is needed, based on simple approximation, to yield the pre-entry drag and external pressure recovery. This could greatly help generate preliminary performance figures in a screening analysis of candidate inlet shapes.

REFERENCES

1. Wislicenus, George F., "Hydrodynamic Design Principles of Pumps and Ducting for Waterjet Propulsion," NSRDC Report 3990 (Jun 1973).

2. Lockheed California Company, "Waterjet Propulsion System Study," Report LR 17885-5.

3. Sherman, P.M. and Lincoln, F.W., "Ram Inlet Systems for Waterjet Propulsors," AIAA Paper No. 69-418 (1969).

4. Rockwell International, "Waterjet Technology Study Final Report," Report No. R77-175 (Jun 1977).

5. Lockheed Missile and Space Company, Inc., "Surface Effect Ships Propulsion Technology Design Manual," Vol. IV, "Waterjet Propulsion" (May 1974).

6. Developmental Sciences, Inc., "Theoretical Calculations of Pod inlets for Surface Effect Ships," Report No. 7210-F (Jan 1973).

7. Developmental Sciences, Inc., "Design of a Pod Inlet for a 200 Ton, 100 Knot Hydrofoil," Report No. 2024-FRD (Nov 1973).

8. Sobolewski, A.D., "Hydrodynamic Performance of a Variable Area Waterjet Inlet Designed for a 200 Ton, 100 Knot Hydrofoil Ship," SPD-735-01 (Feb 1977).

9. Küchemann, D. and Weber, J., "Aerodynamics of Propulsion," McGraw Hill, New York (1953).

10. Brandau, J.H., "Aspects of Performance Evaluation of Waterjet Propulsion Systems and a Critical Review of the State-of-the-Art, NSRDC Report 2550 (Oct 1967).

11. Barr, R.A. and Stark, N.R., "Current State-of-the-Art of Waterjet Inlet Systems for High Performance Naval Ships," Hydronautics, Inc. Report No. TR 7224-5 (Dec 1973).

12. Aerojet-General Corporation, "100 Ton SES Waterjet Testcraft Program Model Test Report," Report No. SES-E-E003-9 (May 1970).

13. Gyves, S.N. and Kirkman, K.L., "Developmental Tests of a Pod-Strut Ram Waterjet Inlet for a 100 Ton Surface Effect Ship Application," Hydronautics, Inc. Report No. 956-1 (Feb 1970).

14. Etter, R.J., "Waterjet Propulsion - an Overview," Marine Propulsion, ASME Press (1976).

15. Tsai, F.Y. and Ripken, J.F., "Hydraulic Studies of the Inlet-Duct Components for a Large Jet Propulsion System," St. Anthony Falls Hydraulic Laboratory, Univ. of Minnesota Memo. No. 106 (Apr 1966).

16. V.E. Johnson, et al., "Design and Performance of Diffusers, Fixed-Area Inlets and Variable-Area Inlets in Integrated Inlet-Diffuser Subsystems," Hydronautics, Inc., Technical Report 7152-1 (Aug 1972).

17. Hoerner, S.F., "Fluid-Dynamic Drag," published by the author (1958).

18. Eisenberg, P. and Tulin, M.P., "Cavitation," Section 12 of the Handbook of Fluid Dynamics, V.L. Streeter, Ed., McGraw-Hill, N.Y. (1961).

19. Wilson, M.B., "A Survey of Propulsion-Vehicle Interactions on High-Performance Marine Craft," presented at the 18th ATTC, Annapolis, MD (Aug 1977).

20. Hess, J.L. and Smith, A.M.O., "Calculation of Potential Flow About Arbitrary Bodies," Prog. Aero. Sci., Vol. 8, Pergamon Press (1966).

21. Cebeci, T., Smith, A.M.O. and Wang, L.C., "A Finite-Difference Method for Calculating Compressible Laminar and Turbulent Boundary Layers," Douglas Aircraft Co., Report DAC-67131 (Mar 1969).

22. Cebeci, T. and Smith, A.M.O., "A Finite-Difference Method for Calculating Compressible Laminar and Turbulent Boundary Layers," J. Basic Eng., 92, 523 (Sep 1970).

23. Keller, H.B. and Cebeci, T., "Accurate Numerical Methods for Boundary-Layer Flows, I. Two Dimensional Laminar Flows," Second International Conference on Numerical Methods in Fluid Dynamics, Univ. of California (Sep 1970).

24. Keller, H.B. and Cebeci, T., "Accurate Numerical Methods for Boundary-Layer Flows, II. Two Dimensional Turbulent Flows, " AIAA 9th Aerospace Sciences Meeting, AIAA paper No. 71-164, N.Y. (Jan 1971).

25. Brown, S.N. and Stewartson, "Laminar Separation," Annual Review of Fluid Mechanics, 1, 45 (1969).

26. Williams, J.C., "Incompressible Boundary-Layer Separation" Annual Review of Fluid Mechanics, 9, 113 (1977).

27. Hess, J.L., "On the Problem of Shaping an Axisymmetric Body to Obtain Low Drag at Large Reynolds Numbers," J. Ship Res., 20, 51 (1976).

28. Truckenbrodt, E., "A Method of Quadrature for Calculation of the Laminar and Turbulent Boundary Layer in Case of Plane and Rotationally Symmetrical Flow," NACA TM 1379, (May 1955).

29. Patel, V.C., "A Simple Integral Method for the Calculation of Thick Axisymmetric Turbulent Boundary Layers," Aero. Quart., 25, 47 (1974).

30. Granville, P.S., "The Calculation of Viscous Drag of Bodies of Revolution," DTMB Report No. 849 (1953).

31. Gertler, M., "Resistance Experiments on a Systematic Series of Streamlined Bodies of Revolution for Application to the Design of High-Speed Submarines," DTMB Report No. C-297 (Apr 1950) Unclassified.

32. White, N.M., "A Comparison Between a Simple Drag Formula and Experimental Drag Data for Bodies of Revolution," DTNSRDC Report No. 77-0028 (Jan 1977).

33. Kerney, K.P. and White, N.M., "Description and Evaluation of a Digital Computer Program for Calculating the Viscous Drag of Bodies of Revolution," DTNSRDC Report No. 4641 (Dec 1975).

34. Granville, P.S., "The Prediction of Transition from Laminar to Turbulent Flow in Boundary Layers on Bodies of Revolution," NSRDC Report No. 3900 (Sep 1974).

35. Carmichael, B.H., "Underwater Drag Reduction through Choice of Shape," AIAA paper No. 66-657 (1966).

36. Carmichael, B.H., "Underwater Drag Reduction through Optimum Shape," in "Underwater Missile Propulsion," Leonard Greiner, ed., Compass Publications, Arl., VA, pp 147-169 (1967).

37. Granville, P.S., "Similarity-Law Entrainment Method for Thick Axisymmetric Turbulent Boundary Layers in Pressure Gradients," DTNSRDC Report 4525 (Dec 1975).

38. Smith, A.M.O. and Cebeci, T., "Remarks on Methods for Predicting Viscous Drag," AGARD Conference Proceedings No. 124 on Aerodynamic Drag, Izmir, Turkey (Apr 1973).

39. Parsons, J.S., Goodson, R.E. and Goldschmied, F.R., "Shaping of Axisymmetric Bodies for Minimum Drag in Incompressible Flow," J. Hydronautics, 8, 100 (1974).

40. Young, A.D., "The Calculation of Total and Skin Friction Drags of Bodies of Revolution at Zero Incidence," Aeronautical Research Council R.&M. No. 1874, London (Apr 1939).

41. Moore, W.L., "Calculation of the Lift and Drag of Hydrofoils, Struts, and Pods in Various Configurations," NSRDC T&E Report No. 383-H-01 (Apr 1970).

42. Nakayama, A. and Patel, V.C., "Calculation of the Viscous Resistance of Bodies of Revolution," J. Hydronautics, 8, 154 (1974).

43. Thwaites, B., "Approximate Calculation of the Laminar Boundary Layer," Aero. Quart., 1, 245 (1949).

44. Michel, R., "Etude de la Transitions sur les Profiles d'Aile; Etablissement d'un Critere de Determination du Point de Transition et Calcul de la Trainee de Profile Incompressible," Report No. 1/1578A, ONERA, Chatillon (1951).

45. Crabtree, L.F., "Prediction of Transition in the Boundary Layer on Aerofoils," J. Aero. Sci., 62, 525 (1958).

46. van Driest, E.R. and Blumer, C.B., "Boundary-Layer Transition: Freestream Turbulence and Pressure Gradient Effects," AIAA J. 1, 1303 (1963).

47. Cebeci. T., Mosinskis, G.J. and Smith, A.M.O., "Calculation of Viscous Drag in Incompressible Flows," J. Aircraft 9, 691 (1972).

ACKNOWLEDGEMENT

It is a genuine pleasure to thank several individuals who have contributed to the development of this report; namely Dr. Michael B. Wilson, for sharing numerous enlightening thoughts on the subject of hydrodynamic drag; Mr. Alan D. Sobolewski, for his valuable assistance with the experimental literature; Mr. Gabor F. Dobay, my immediate supervisor, for several informative technical discussions; and Ms. Marjorie Reyes, whose patience, skills and assiduity ensured the timely publication of this report.

DTNSRDC ISSUES THREE TYPES OF REPORTS

1. DTNSRDC REPORTS, A FORMAL SERIES, CONTAIN INFORMATION OF PERMANENT TECHNICAL VALUE. THEY CARRY A CONSECUTIVE NUMERICAL IDENTIFICATION REGARDLESS OF THEIR CLASSIFICATION OR THE ORIGINATING DEPARTMENT.

2. DEPARTMENTAL REPORTS, A SEMIFORMAL SERIES, CONTAIN INFORMATION OF A PRELIMINARY, TEMPORARY, OR PROPRIETARY NATURE OR OF LIMITED INTEREST OR SIGNIFICANCE. THEY CARRY A DEPARTMENTAL ALPHANUMERICAL IDENTIFICATION.

3. TECHNICAL MEMORANDA, AN INFORMAL SERIES, CONTAIN TECHNICAL DOCUMENTATION OF LIMITED USE AND INTEREST. THEY ARE PRIMARILY WORKING PAPERS INTENDED FOR INTERNAL USE. THEY CARRY AN IDENTIFYING NUMBER WHICH INDICATES THEIR TYPE AND THE NUMERICAL CODE OF THE ORIGINATING DEPARTMENT. ANY DISTRIBUTION OUTSIDE DTNSRDC MUST BE APPROVED BY THE HEAD OF THE ORIGINATING DEPARTMENT ON A CASE-BY-CASE BASIS.